NASA/TP—2015–218464

Variable-Domain Displacement Transfer Functions for Converting Surface Strains into Deflections for Structural Deformed Shape Predictions

William L. Ko and Van Tran Fleischer
Armstrong Flight Research Center, Edwards, California

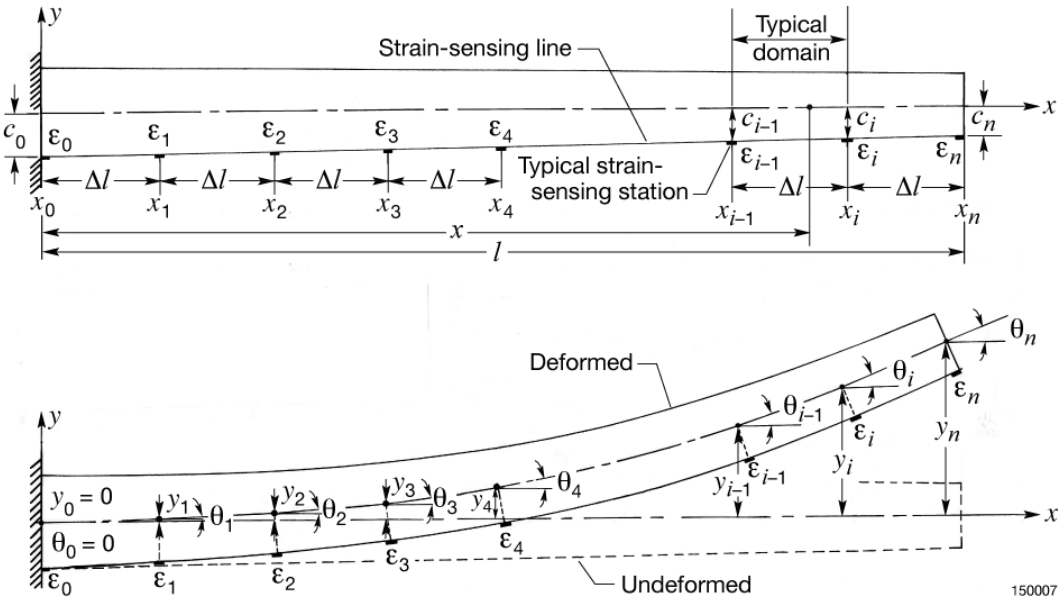

March 2015

NASA STI Program ... in Profile

Since its founding, NASA has been dedicated to the advancement of aeronautics and space science. The NASA scientific and technical information (STI) program plays a key part in helping NASA maintain this important role.

The NASA STI program operates under the auspices of the Agency Chief Information Officer. It collects, organizes, provides for archiving, and disseminates NASA's STI. The NASA STI program provides access to the NASA Aeronautics and Space Database and its public interface, the NASA Technical Reports Server, thus providing one of the largest collections of aeronautical and space science STI in the world. Results are published in both non-NASA channels and by NASA in the NASA STI Report Series, which includes the following report types:

- TECHNICAL PUBLICATION. Reports of completed research or a major significant phase of research that present the results of NASA Programs and include extensive data or theoretical analysis. Includes compilations of significant scientific and technical data and information deemed to be of continuing reference value. NASA counter-part of peer-reviewed formal professional papers but has less stringent limitations on manuscript length and extent of graphic presentations.

- TECHNICAL MEMORANDUM. Scientific and technical findings that are preliminary or of specialized interest, e.g., quick release reports, working papers, and bibliographies that contain minimal annotation. Does not contain extensive analysis.

- CONTRACTOR REPORT. Scientific and technical findings by NASA-sponsored contractors and grantees.

- CONFERENCE PUBLICATION. Collected papers from scientific and technical conferences, symposia, seminars, or other meetings sponsored or co-sponsored by NASA.

- SPECIAL PUBLICATION. Scientific, technical, or historical information from NASA programs, projects, and missions, often concerned with subjects having substantial public interest.

- TECHNICAL TRANSLATION. English-language translations of foreign scientific and technical material pertinent to NASA's mission.

Specialized services also include organizing and publishing research results, distributing specialized research announcements and feeds, providing information desk and personal search support, and enabling data exchange services.

For more information about the NASA STI program, see the following:

- Access the NASA STI program home page at http://www.sti.nasa.gov

- E-mail your question to help@sti.nasa.gov

- Fax your question to the NASA STI Information Desk at 757-864-6500

- Phone the NASA STI Information Desk at 757-864-9658

- Write to:
  NASA STI Program
  Mail Stop 148
  NASA Langley Research Center
  Hampton, VA 23681-2199

NASA/TP—2015–218464

Variable-Domain Displacement Transfer Functions for Converting Surface Strains into Deflections for Structural Deformed Shape Predictions

William L. Ko and Van Tran Fleischer
Armstrong Flight Research Center, Edwards, California

National Aeronautics and
Space Administration

Armstrong Flight Research Center
Edwards, CA 93523-0273

March 2015

Available from:

NASA STI Program
Service Mail Stop 148
NASA Langley Research Center
Hampton, VA 23681-2199

National Technical Information
5285 Port Royal Road
Springfield, VA 22161
703-605-6000

This report is also available in electronic form at http://www.sti.nasa.gov/ and http://ntrs.nasa.gov/

TABLE OF CONTENTS

ABSTRACT

Variable-Domain Displacement Transfer Functions were formulated for shape predictions of complex wing structures, for which surface strain-sensing stations must be properly distributed to avoid jointed junctures, and must be increased in the high strain gradient region. Each embedded beam (depth-wise cross section of structure along a surface strain-sensing line) was discretized into small variable domains. Thus, the surface strain distribution can be described with a piecewise linear or a piecewise nonlinear function. Through discretization, the embedded beam curvature equation can be piece-wisely integrated to obtain the Variable-Domain Displacement Transfer Functions (for each embedded beam), which are expressed in terms of geometrical parameters of the embedded beam and the surface strains along the strain-sensing line. By inputting the surface strain data into the Displacement Transfer Functions, slopes and deflections along each embedded beam can be calculated for mapping out overall structural deformed shapes. A long tapered cantilever tubular beam was chosen for shape prediction analysis. The input surface strains were analytically generated from finite-element analysis. The shape prediction accuracies of the Variable-Domain Displacement Transfer Functions were then determined in light of the finite-element generated slopes and deflections, and were found to be comparable to the accuracies of the constant-domain Displacement Transfer Functions.

NOMENCLATURE

a	coefficient of first term of quadratic function, $\varepsilon(\xi) = a + b\xi + e\xi^2$, in./in.
b	coefficient of second term of quadratic function, $\varepsilon(\xi) = a + b\xi + e\xi^2$, 1/in.
c	depth factor (vertical distance from neutral axis to lower surface of uniform embedded beam), in.
$c(x)$	depth factor (vertical distance from neutral axis to lower surface of nonuniform embedded beam at x), in.
c_i	$\equiv c(x_i)$, lower depth factor (vertical distance from neutral axis to lower surface of nonuniform embedded beam at $x = x_i$), in.
$\overline{c}_i$	upper depth factor (vertical distance from neutral axis to upper surface of nonuniform embedded beam at $x = x_i$), in.
c_0	value of c_i at fixed end (embedded beam root), $x = x_0 = 0$, in.
c_n	value of c_i at free end (embedded beam tip), $x = x_n = l$, in.
DLL	design limit load
e	coefficient of third term of quadratic function, $\varepsilon(\xi) = a + b\xi + e\xi^2$, 1/in^2
h_i	depth of embedded beam at $x = x_i$.
i	$= 0,1,2,3,....,n$, strain-sensing station identification number
j	dummy index
k	dummy index
l	length of embedded beam, in.
n	index for the last span-wise strain-sensing station (or number of strain-sensing domains)
R	radius of curvature, in.
RRF	rotated reference frame, aligned with wing's out-of-plane direction
	SPAR Structural Performance And Resizing
x, y	Cartesian coordinates (x in embedded beam axial direction, y in lateral direction), in.
x_i	axial coordinate (or symbol) associated with i-th strain-sensing station, in.

$y(x)$ embedded beam deflection at axial location *x*, in.

y_i $\equiv y(x_i)$, embedded beam deflection at axial location, $x = x_i$, in.

$(y_i)_{\text{Pred.}}$ predicted value of y_i, in.

$(y_i)_{\text{SPAR}}$ value of y_i calculated from SPAR program, in.

Δl $\equiv (x_i - x_{i-1}) = l/n$, constant-domain length (distance between two adjacent strain-sensing stations $\{x_{i-1}, x_i\}$, in.

$(\Delta l)_i$ $\equiv (x_i - x_{i-1})$, variable-domain length (distance between two adjacent strain-sensing stations $\{x_{i-1}, x_i\}$, in.

$\varepsilon(x)$ lower surface bending strain at axial location x, in/in

ε_i $\equiv \varepsilon(x_i)$, lower surface bending strain at strain-sensing station, x_i, in/in

$\overline{\varepsilon}_i$ upper surface bending strain at strain-sensing cross section, x_i, in/in

$\theta(x)$ embedded-beam slope in reference to *x*-system, deg

θ_i $\equiv \theta(x_i)$, slope at strain-sensing station, $x = x_i$, deg

$(\theta_i)_{\text{Pred.}}$ predicted values of θ_i, deg

$(\theta_i)_{\text{SPAR}}$ SPAR-calculated values of θ_i, deg

ξ $\equiv x - x_{i-1}$, local axial coordinate measured from strain-sensing station, x_{i-1}, in.

INTRODUCTION

For structural deformed shape predictions using distributed surface strains, the Displacement Transfer Functions (refs. 1−9) are needed to convert the surface strains into out-of-plane deflections for mapping out the overall structural deformed shapes. The surface strain data are to be obtained at the strain-sensing stations discretely distributed along the strain-sensing line lying on the surfaces of a planer structure (for example, an aircraft wing). The depth-wise cross section of the structure along the strain-sensing line can be considered as an embedded beam with width of the strain-sensing line (fig. 1).

In the formulations of earlier Displacement Transfer Functions (refs. 1–9), the embedded beam was first discretized evenly into multiple small domains (constant-domain lengths) with strain-sensing stations located at the domain junctures. Thus, within each small domain, the depth variation of the embedded beam could be described with a linear function, and the surface strain distribution could be described with either linear or nonlinear function. Such a piecewise approach enabled piecewise integrations of the embedded-beam curvature equation (second order differential equation) to yield beam slope and deflection equations in recursive forms. Each set of recursive slope and deflection equations were then combined into a summation-form deflection equation (called the Displacement Transfer Function) for each embedded beam. In the Displacement Transfer Function, the deflections are expressed explicitly in terms of geometrical parameters of the discretized embedded-beam and surface strains along the strain-sensing line. By inputting the surface strains into the Displacement Transfer Function, one can then calculate deflections along the embedded-beam for generating the elastic curve. By using multiple strain-sensing lines, one can then map out all the elastic curves of the multiple embedded beams to construct the overall structural deformed shapes (under bending and torsion) for visual display. The Displacement Transfer Functions combined with a strain-sensing system, thus created a revolutionary new structure-shape-sensing technology, "*Method for Real-Time Structure Shape-Sensing,*" (U.S. Patent Number 7,520,176, ref. 6), which is very attractive for application to the in-flight deformed shape monitoring of flexible wings and tails of unmanned flight vehicles by the ground-based pilot for maintaining safe flights. In addition, the real-time wing shape monitored could then be input to the aircraft control system for aero-elastic wing shape control.

The shape prediction accuracies of the earlier constant-domain Displacement Transfer Functions (based on piecewise-linear strain representations) (refs. 1−7) were successfully validated analytically using finite-element analyses of different sample structures such as cantilever tubular beams (uniform, tapered, slightly tapered, step-wisely tapered), two-point supported tapered tubular beams, flat panels, and tapered wing boxes (un-swept and swept).

Also, by using piecewise-nonlinear strain representations in the formulations (ref. 8), the shape prediction accuracies could be improved greatly, especially for highly tapered beam structures with rapidly changing strain gradients. The Displacement Transfer Functions were originally formulated for the straight embedded beams. However, with the introduction of empirically established curvature-effect correction terms, those Displacement Transfer Functions could be used for shape predictions of slender curved structures with different arc-angles up to 360 degrees, a complete circle (ref. 10). All the earlier Displacement Transfer Functions (refs. 1−9) were formulated based on uniform discretization of the embedded beam into multiple domains with equal domain lengths.

For the shape predictions of certain long complex wing structures consisting of multiple sections joined together, one must avoid locating the strain-sensing stations right at the jointed junctures, where the strain outputs could be erroneous. Also in the region where the strain gradient changes rapidly, shorter strain-sensing intervals (shorter domains) are needed to improve the shape prediction accuracies. Such situations demand the use of variable-domain lengths for properly locating the strain-sensing stations. Therefore, variable-domain Displacement Transfer Functions are needed for deformed shape calculations of a complex structure for which a non-uniform discretization approach is required.

This technical publication presents the formulations of the variable-domain Displacement Transfer Functions (unevenly distributed strain-sensing stations) by extending the previously developed constant-domain Displacement Transfer Functions (evenly distributed strain-sensing stations) (refs. 1−9) for structural deformed shape predictions.

A long tapered cantilever tubular beam was chosen for the shape prediction accuracy studies of the variable-domain Displacement Transfer Functions. Finite-element analysis was used to analytically calculate the input surface strains, and to generate reference yardsticks (slopes and deflections) for the shape prediction error analysis. The variable-domain Displacement Transfer Functions were found to provide highly accurate shape predictions, similar to the constant-domain Displacement Transfer Functions.

NONUNIFORM AND UNIFORM BEAMS

In the present technical publication, the term “beam” implies the embedded beam, which is defined as the depth-wise cross section of the structure along the strain-sensing line, and different from the isolated classical Euler-Bernoulli beam. The nonuniform beam implies the embedded beam with varying depth. The slightly tapered beam implies the embedded beam with slowly changing depth. The uniform beam implies the embedded beam with constant depth.

BASICS OF CONSTANT-DOMAIN DISPLACEMENT TRANSFER FUNCTIONS

This section reviews the basics of formulations of the earlier Displacement Transfer Functions for constant-domain lengths (refs. 1−9).

Curvature-Strain Equation

Formulations of the earlier constant-domain Displacement Transfer Functions for structure deformed shape predictions stemmed from the integrations of the following geometrically established shifted curvature-strain differential equation for the embedded beam (ref. 9):

$$\frac{d^2y}{dx^2} \approx \frac{\varepsilon(x)}{c(x)} = \frac{1}{R} \tag{1}$$

In equation (1), x is the undeformed axial coordinate, y is the lateral deflection, $\varepsilon(x)$ is bottom-surface bending strain, and $c(x)$ is the embedded beam depth factor, which is defined as the vertical distance from the neutral axis to the bottom surface of the embedded beam. Equation (1) is the simplified Lagrangian curvature equation, $1/R(x) = (d^2y/dx^2)\Big/\sqrt{1-(dy/dx)^2}$, with the term, $(dy/dx)^2$, neglected. Neglection of the $(dy/dx)^2$ term is equivalent to setting axial displacements to zero (called shifted Lagrangian formulation) (refs. 9, 11, and 12). Keep in mind that equation (1) is referred to as the undeformed x-coordinate, and is not the simplified form of the classical curvature equation, $1/R = (d^2y/dx^2)\Big/[1+(dy/dx)^2]^{3/2}$, which is referred to as the deformed x-coordinate (Eulerian formulation) (refs. 9, 11, and 12).

The seven types of constant-domain Displacement Transfer Functions formulated earlier, based on equation (1), were found to be quite accurate [0.0235~0.3852 percent error range at beam tip] in the shape predictions of a tapered cantilever tubular beam under both small and large bending deformations, even with the free-end deflection reaching as large as 94 percent of the structural length (ref. 9).

Discretizations

To integrate equation (1), the embedded beam of length, l, lying along the strain-sensing line (fig. 1), was first discretized evenly into n number of small domains, $x_{i-1} \le x \le x_i$ (i = 1,2,3,…..,n), with constant-domain lengths, $\Delta l = l/n\ [\equiv (x_i - x_{i-1})]$, so that within each small domain, $x_{i-1} \le x \le x_i$, the beam depth factor, $c(x)$ (vertical distance from neutral axis to lower surface of beam at axial location, x), could be described with linear functions, and the surface strain, $\varepsilon(x)$, could be described with either linear or nonlinear function as shown in equations (2)–(4a):

Piecewise-linear depth factor representations (refs. 1−7):

$$c(x) = c_{i-1} + (c_i - c_{i-1})\frac{x - x_{i-1}}{\Delta l} \quad ; \quad (x_{i-1} \le x \le x_i) \tag{2}$$

Piecewise-linear strain representations (refs. 1−7):

$$\varepsilon(x) = \varepsilon_{i-1} + (\varepsilon_i - \varepsilon_{i-1})\frac{x - x_{i-1}}{\Delta l} \quad ; \quad (x_{i-1} \le x \le x_i) \tag{3}$$

Piecewise-nonlinear strain representations (ref. 8):

$$\varepsilon(x) = \varepsilon_{i-1} - \frac{3\varepsilon_{i-1} - 4\varepsilon_i + \varepsilon_{i+1}}{2\Delta l}(x - x_{i-1}) + \frac{\varepsilon_{i-1} - 2\varepsilon_i + \varepsilon_{i+1}}{2(\Delta l)^2}(x - x_{i-1})^2 \qquad (4a)$$

$$(x_{i-1} \le x \le x_i)$$

Note that, when $i = n$, equation (4a) contains a nonexistence (fictitious) strain, ε_{n+1}, which can be estimated by using the following three-points extrapolation equation:

$$\varepsilon_{n+1} = \varepsilon_{n-2} - 3\varepsilon_{n-1} + 3\varepsilon_n \qquad (4b)$$

Equation (4b) was obtained from equation (4a) by setting $i = n - 1$ and setting the term $(x - x_{i-1})$ to $(x_{n+1} - x_{n-1}) = 3\Delta l$ in the region $(x_{n-1} \le x \le x_{n+1})$.

The piecewise approach enabled the piecewise integrations of the curvature-strain differential equation (1) to yield closed-form beam slope and deflection equations in recursive forms. The recursive slope and deflection equations were then combined into one deflection equation in dual summation forms (called the constant-domain Displacement Transfer Function), which are expressed in terms of embedded beam geometrical parameters and surface strains obtained at evenly spaced strain-sensing stations (at domain junctures) along the strain-sensing line. By inputting the surface strain data into the Displacement Transfer Function, one can then calculate the out-of-plane deflections along each embedded beam. By using multiple strain sensing lines, one can then map out the overall structural deformed shapes (under bending and torsion) for visual display.

LISTS OF CONSTANT-DOMAIN DISPLACEMENT TRANSFER FUNCTIONS

This section lists previously formulated key Displacement Transfer Functions for constant-domain lengths, $\Delta l = l/n$ (uniform discretization) (refs. 1–9). Those constant-domain Displacement Transfer Functions can then be used as a basis to formulate the variable-domain lengths Displacement Transfer Functions (nonuniform discretization) presented in the subsequent sections. Depending on the structural types, one can choose a suitable Displacement Transfer Function from the following list for shape predictions.

Based on Piecewise-Linear Strain Representations

The following two sets of slope and deflection equations were formulated using piecewise-linear functions [eqs. (2) and (3)] to describe the distributions of both depth factor and surface strain, $\{c(x), \varepsilon(x)\}$.

1. Nonuniform Embedded Beams (Linear Strain) $(c_{i-1} \ne c_i)$ (refs. 1, 3)

Slope equation:

$$\tan\theta_i = \Delta l\left[\frac{\varepsilon_{i-1} - \varepsilon_i}{c_{i-1} - c_i} + \frac{\varepsilon_{i-1}c_i - \varepsilon_i c_{i-1}}{(c_{i-1} - c_i)^2}\log\frac{c_i}{c_{i-1}}\right] + \tan\theta_{i-1} \qquad ; \quad (i = 1,2,3,\ldots..,n) \qquad (5a)$$

Deflection equations:
a. In recursive form:

$$y_i = (\Delta l)^2 \left\{ \frac{\varepsilon_{i-1} - \varepsilon_i}{2(c_{i-1} - c_i)} - \frac{\varepsilon_{i-1} c_i - \varepsilon_i c_{i-1}}{(c_{i-1} - c_i)^3} \left[c_i \log \frac{c_i}{c_{i-1}} + (c_{i-1} - c_i) \right] \right\} + y_{i-1} + \Delta l \tan \theta_{i-1} \qquad (5b)$$

(i = 1,2,3,…..,n)

b. In dual summation form:

$$y_i = \underbrace{(\Delta l)^2 \sum_{j=1}^{i} \left\{ \frac{\varepsilon_{j-1} - \varepsilon_j}{2(c_{j-1} - c_j)} - \frac{\varepsilon_{j-1} c_j - \varepsilon_j c_{j-1}}{(c_{j-1} - c_j)^3} \left[c_j \log_e \frac{c_j}{c_{j-1}} + (c_{j-1} - c_j) \right] \right\}}_{\text{Contributions from deflection terms}}$$
$$+ \underbrace{(\Delta l)^2 \sum_{j=1}^{i-1} \left\{ (i-j) \left[\frac{\varepsilon_{j-1} - \varepsilon_j}{c_{j-1} - c_j} + \frac{\varepsilon_{j-1} c_j - \varepsilon_j c_{j-1}}{(c_{j-1} - c_j)^2} \log_e \frac{c_j}{c_{j-1}} \right] \right\}}_{\text{Contribution from slope terms}} + \underbrace{y_0 + (i)\Delta l \tan \theta_0}_{\text{=0 for cantilever beams}} \qquad (5c)$$

(i = 1,2,3,…..,n)

Equations (5) are called the Constant-Domain Nonuniform Displacement Transfer Functions for a nonuniform embedded beam based on piecewise-linear strain representations. The term "Displacement Transfer Function" was used because equation (5c) transforms the surface strains into out-of-plane deflections for plotting the deformed shape of the embedded beam.

Note that equations (5) are not applicable to the limit case of uniform beam $(c_{i-1} = c_i = c)$ because of mathematical indeterminacy (0/0) caused by $\log(c_i / c_{i-1}) \to 0$ and $(c_i - c_{i-1}) \to 0$. However, by expanding the logarithmic terms in equations (5) in series forms in the neighborhood of $(c_{i-1} / c_i) \to 1$, the factor $(c_i - c_{i-1})$ in the denominators can be eliminated (refs. 1, 3). The resulting Log-expanded equations (6) listed below are for slightly nonuniform embedded beams $[(c_{i-1} / c_i) \to 1]$, and applicable to the limit case of uniform beams $(c_{i-1} = c_i = c)$.

2. Slightly Nonuniform Embedded Beams (Linear Strain) $[(c_{i-1} / c_i) \to 1]$ (refs. 1, 3)

Log-expanded slope equation:

$$\tan \theta_i = \frac{\Delta l}{2c_{i-1}} \left[\left(2 - \frac{c_i}{c_{i-1}} \right) \varepsilon_{i-1} + \varepsilon_i \right] + \tan \theta_{i-1} \quad ; \quad (i = 1,2,3,\ldots..,n) \qquad (6a)$$

Log-expanded deflection equations:
a. In recursive form:

$$y_i = \frac{(\Delta l)^2}{6c_{i-1}} \left[\left(3 - \frac{c_i}{c_{i-1}} \right) \varepsilon_{i-1} + \varepsilon_i \right] + y_{i-1} + \Delta l \tan \theta_{i-1} \quad ; \quad (i = 1,2,3,\ldots..,n) \qquad (6b)$$

b. In dual summation form:

$$y_i = \underbrace{\frac{(\Delta l)^2}{6}\sum_{j=1}^{i}\left\{\frac{1}{c_{j-1}}\left[\left(3-\frac{c_j}{c_{j-1}}\right)\varepsilon_{j-1}+\varepsilon_j\right]\right\}+y_0}_{\text{Contribution from deflection terms}}$$
$$+\underbrace{\frac{(\Delta l)^2}{2}\sum_{j=1}^{i-1}\left\{\frac{(i-j)}{c_{j-1}}\left[\left(2-\frac{c_j}{c_{j-1}}\right)\varepsilon_{j-1}+\varepsilon_j\right]\right\}+(i)\Delta l\tan\theta_0}_{\text{Contributions from slope terms}} \tag{6c}$$

Equations (6) are called the Constant-Domain Log-expanded Displacement Transfer Functions for slightly nonlinear (including uniform) embedded beams based on piecewise-linear strain representations.

Based on Piecewise-Nonlinear Strain Representations

The following two sets of slope and deflection equations were formulated by using the piecewise-linear function [eq. (2)] to describe the actual distribution of the depth factor, $c(x)$, and the piecewise-nonlinear function [eq. (4)] to describe the actual distribution of the surface strain, $\varepsilon(x)$.

1. Nonuniform Beams (Nonlinear Strain) $(c_{i-1} \neq c_i)$ (ref. 8)

Improved slope equation:

$$\tan\theta_i = \frac{\Delta l}{2(c_i-c_{i-1})^3}\left[(2c_i-c_{i-1})(c_i\varepsilon_{i-1}-2c_{i-1}\varepsilon_i)+c_ic_{i-1}\varepsilon_{i+1}\right]\log_e\frac{c_i}{c_{i-1}}$$
$$-\frac{\Delta l}{4(c_i-c_{i-1})^2}\left[(5c_i-3c_{i-1})\varepsilon_{i-1}-2(3c_i-c_{i-1})\varepsilon_i+(c_i+c_{i-1})\varepsilon_{i+1}\right]+\tan\theta_{i-1} \tag{7a}$$
$$(i=1,2,3,....,n)$$

Improved deflection equations:

a. In recursive form:

$$y_i = \frac{(\Delta l)^2}{2(c_i-c_{i-1})^4}\left[(2c_i-c_{i-1})(c_i\varepsilon_{i-1}-2c_{i-1}\varepsilon_i)+c_ic_{i-1}\varepsilon_{i+1}\right]\left[c_i\log_e\frac{c_i}{c_{i-1}}-(c_i-c_{i-1})\right]$$
$$-\frac{(\Delta l)^2}{12(c_i-c_{i-1})^2}\left[(8c_i-5c_{i-1})\varepsilon_{i-1}-2(5c_i-2c_{i-1})\varepsilon_i+(2c_i+c_{i-1})\varepsilon_{i+1}\right]+y_{i-1}+\Delta l\tan\theta_{i-1} \tag{7b}$$
$$(i=1,2,3,....,n)$$

b. In dual summation form:

$$y_i = (\Delta l)^2 \sum_{j=1}^{i} \underbrace{\left\{ \begin{array}{l} \dfrac{1}{2(c_j - c_{j-1})^4}\Big[(2c_j - c_{j-1})(c_j\varepsilon_{j-1} - 2c_{j-1}\varepsilon_j) + c_j c_{j-1}\varepsilon_{j+1}\Big] \times \\ \qquad\qquad \times \left[c_j \log_e \dfrac{c_j}{c_{j-1}} - (c_j - c_{j-1}) \right] \\ -\dfrac{1}{12(c_j - c_{j-1})^2}\Big[(8c_j - 5c_{j-1})\varepsilon_{j-1} - 2(5c_j - 2c_{j-1})\varepsilon_j + (2c_j + c_{j-1})\varepsilon_{j+1}\Big] \end{array} \right\}}_{\text{Contribution from deflection terms}} + \mathrm{y}_0$$

$$+(\Delta l)^2 \sum_{j=1}^{i-1} (i-j) \underbrace{\left\{ \begin{array}{l} \dfrac{1}{2(c_j - c_{j-1})^3}\Big[(2c_j - c_{j-1})(c_j\varepsilon_{j-1} - 2c_{j-1}\varepsilon_j) + c_j c_{j-1}\varepsilon_{j+1}\Big]\log_e \dfrac{c_j}{c_{j-1}} \\ -\dfrac{1}{4(c_j - c_{j-1})^2}\Big[(5c_j - 3c_{j-1})\varepsilon_{j-1} - 2(3c_j - c_{j-1})\varepsilon_j + (c_j + c_{j-1})\varepsilon_{j+1}\Big] \end{array} \right\}}_{+(i)\Delta l \tan\theta_0 \quad \text{Contributions from slope terms}} \qquad (7c)$$

$(i = 1,2,3,\ldots..,n)$

Equations (7) are called the Constant-Domain Improved Displacement Transfer Functions for nonuniform embedded beams based on piecewise-nonlinear strain representations.

Equations (7) are not applicable to the limit case of uniform beam ($c_{i-1} = c_i = c$) because of mathematical indeterminacy (that is, 0/0). To handle the limit case of uniform beams $(c_{i-1} = c_i = c)$, the logarithmic terms in equations (7) could be expanded in series forms in the neighborhood of $(c_{i-1}/c_i) \to 1$ (ref. 8), and obtain the following Log-expanded equations (8a), (8b), and (8c) for slightly nonuniform beams, and which are applicable to the limit case of uniform embedded beams $(c_{i-1} = c_i = c)$.

2. Slightly Nonuniform Embedded Beams (Nonlinear Strain) $[(c_{i-1}/c_i) \to 1]$ (ref. 8)

Log-expanded slope equation:

$$\tan\theta_i = \frac{\Delta l}{12c_{i-1}^3}\Big\{\Big[5c_{i-1}^2 + 4(c_i - c_{i-1})^2\Big]\varepsilon_{i-1} - 8c_{i-1}(c_i - 2c_{i-1})\varepsilon_i + c_{i-1}(2c_i - 3c_{i-1})\varepsilon_{i+1}\Big\} + \tan\theta_{i-1} \qquad (8a)$$

$(i = 1,2,3,....,n)$

Log-expanded deflection equations:
a. In recursive form:

$$y_i = \frac{(\Delta l)^2}{24c_{i-1}^4}\left\{ \begin{array}{l} \Big[7c_{i-1}^3 + (c_i - c_{i-1})(8c_i c_{i-1} - 3c_i^2) - 3(c_i^3 - c_{i-1}^3)\Big]\varepsilon_{i-1} \\ +2c_{i-1}\Big[(3c_i^2 + (c_i - c_{i-1})(3c_i - 8c_{i-1})\Big]\varepsilon_i - c_{i-1}\Big[c_i^2 + 2(c_i - c_{i-1})^2\Big]\varepsilon_{i+1} \end{array} \right\} \qquad (8b)$$
$$+ y_{i-1} + \Delta l \tan\theta_{i-1}$$

$(i = 1,2,3,....,n)$

b. In dual summation form:

$$y_i = \underbrace{\frac{(\Delta l)^2}{24}\sum_{j=1}^{i}\frac{1}{c_{j-1}^4}\begin{Bmatrix}\left[7c_{j-1}^3+(c_j-c_{j-1})(8c_jc_{j-1}-3c_j^2)-3(c_j^3-c_{j-1}^3)\right]\varepsilon_{j-1}\\+2c_{j-1}\left[(3c_j^2+(c_j-c_{j-1})(3c_j-8c_{j-1})\right]\varepsilon_j\\-c_{j-1}\left[c_j^2+2(c_j-c_{j-1})^2\right]\varepsilon_{j+1}\end{Bmatrix}+y_0}_{\text{Contributions from deflection terms}}$$

$$+\underbrace{\frac{(\Delta l)^2}{12}\sum_{j=1}^{i-1}\frac{(i-j)}{c_{j-1}^3}\begin{Bmatrix}\left[5c_{j-1}^2+4(c_j-c_{j-1})^2\right]\varepsilon_{j-1}-8c_{j-1}(c_j-2c_{j-1})\varepsilon_j\\+c_{j-1}(2c_j-3c_{j-1})\varepsilon_{j+1}\end{Bmatrix}+(i)\Delta l\tan\theta_0}_{\text{Contributions from slope terms}} \qquad (8c)$$

$$(i=1,2,3,....,n)$$

Equations (8) are called the Constant-Domain Log-expanded Displacement Transfer Functions for slightly nonuniform (including uniform) embedded beams based on piecewise-nonlinear strain representations.

FORMULATION OF VARIABLE-DOMAIN DISPLACEMENT TRANSFER FUNCTIONS

This section describes the formulations of the Displacement Transfer Functions for variable-domain lengths (nonuniform discretization cases). Let the embedded beam be discretized into *n* domains with variable-domain length, $(\Delta l)_i (\equiv x_i - x_{i-1})$ $(i=1,2,3,....,n)$ [Δl in figure 1 replaced with $(\Delta l)_i$], then the beam depth factor, $c(x)$, within each small domain, $x_{i-1} \le x \le x_i$, between the two adjacent strain-sensing stations, $\{x_{i-1}, x_i\}$, can be represented with the piecewise-linear function, and the surface strain, $\varepsilon(x)$, represented with either the piecewise-linear or the piecewise-nonlinear function (quadratic function).

Piecewise-linear depth factor representation as shown in equation (9):

$$c(x) = c_{i-1} + (c_i - c_{i-1})\frac{x - x_{i-1}}{(\Delta l)_i} \quad ; \quad (x_{i-1} \le x \le x_i) \qquad (9)$$

Piecewise-linear strain representation as shown in equation (10):

$$\varepsilon(x) = \varepsilon_{i-1} + (\varepsilon_i - \varepsilon_{i-1})\frac{x - x_{i-1}}{(\Delta l)_i} \quad ; \quad (x_{i-1} \le x \le x_i) \qquad (10)$$

Piecewise-nonlinear strain representations (fig. 2) (see Appendix A for derivation):

$$\varepsilon(x) = \varepsilon_{i-1} - \frac{(\Delta l)_{i+1}[2(\Delta l)_i + (\Delta l)_{i+1}]\varepsilon_{i-1} - [(\Delta l)_i + (\Delta l)_{i+1}]^2 \varepsilon_i + (\Delta l)_i^2 \varepsilon_{i+1}}{(\Delta l)_i (\Delta l)_{i+1}[(\Delta l)_i + (\Delta l)_{i+1}]}(x - x_{i-1})$$
$$+ \frac{(\Delta l)_{i+1}\varepsilon_{i-1} - [(\Delta l)_i + (\Delta l)_{i+1}]\varepsilon_i + (\Delta l)_i \varepsilon_{i+1}}{(\Delta l)_i (\Delta l)_{i+1}[(\Delta l)_i + (\Delta l)_{i+1}]}(x - x_{i-1})^2 \qquad (11)$$
$$(x_{i-1} \le x \le x_i)$$

When $i = n$, equation (11) contains a nonexistence (fictitious) strain, ε_{n+1}. By setting $i = n-1$ and setting the term $(x - x_{i-1})$ to $(x_{n+1} - x_{n-1}) = [(\Delta l)_{n-1} + (\Delta l)_n + (\Delta l)_{n+1}]$ in the region $(x_{n-1} \le x \le x_{n+1})$, equation (11) becomes the following three-points extrapolation formula for the calculation of the fictitious strain, ε_{n+1}:

$$\varepsilon_{n+1} = \varepsilon_{n-2} - \frac{(\Delta l)_n[2(\Delta l)_{n-1} + (\Delta l)_n]\varepsilon_{n-2} - [(\Delta l)_{n-1} + (\Delta l)_n]^2 \varepsilon_{n-1} + (\Delta l)_{n-1}^2 \varepsilon_n}{(\Delta l)_{n-1}(\Delta l)_n[(\Delta l)_{n-1} + (\Delta l)_n]} \times$$
$$\times [(\Delta l)_{n-1} + (\Delta l)_n + (\Delta l)_{n+1}] \qquad (12)$$
$$+ \frac{(\Delta l)_n \varepsilon_{n-2} - [(\Delta l)_{n-1} + (\Delta l)_n]\varepsilon_{n-1} + (\Delta l)_{n-1}\varepsilon_n}{(\Delta l)_{n-1}(\Delta l)_n[(\Delta l)_{n-1} + (\Delta l)_n]}[(\Delta l)_{n-1} + (\Delta l)_n + (\Delta l)_{n+1}]^2$$

For a special case of constant-domain lengths, $(\Delta l)_1 = (\Delta l)_2 = (\Delta l)_3 = ... = \Delta l$, it is easy to show that equations [(11), and (12)] will degenerate respectively into equations [(4a), and (4b)] (see Appendix A).

LISTS OF VARIABLE-DOMAIN DISPLACEMENT TRANSFER FUNCTIONS

The variable-domain slope and deflection equations in recursive forms can be obtained from the constant-domain recursion slope and deflection equations [(5a), and (5b)−(8a), and (8b)] by simply changing the constant-domain length, $\Delta l (\equiv l/n)$, into variable-domain lengths, $(\Delta l)_i (\equiv x_i - x_{i-1})$. However, the derivations of the variable-domain Displacement Transfer Functions (recursive slope and deflection equations combined into dual summation forms) require considerable mathematical manipulations (see Appendix B).

Based on Piecewise-Linear Strain Representations

The following two sets of variable-domain slope and deflection equations were formulated by using piecewise-linear functions to describe the piecewise variations of the depth factor and surface strain, $\{c(x)$ $\varepsilon(x)\}$, [eqs. (9), and (10)].

1. Nonuniform Beams (Linear Strain) $[(\Delta l)_{i-1} \neq (\Delta l)_i ; (c_{i-1} \neq c_i)]$

Slope equation [see eq. (5a)]:

$$\tan\theta_i = (\Delta l)_i \left[\frac{\varepsilon_{i-1} - \varepsilon_i}{c_{i-1} - c_i} + \frac{\varepsilon_{i-1} c_i - \varepsilon_i c_{i-1}}{(c_{i-1} - c_i)^2} \log \frac{c_i}{c_{i-1}} \right] + \tan\theta_{i-1} \qquad (13a)$$

$$(i = 1,2,3,....,n)$$

Deflection equations:
a. In recursive form [see eq. (5b)]:

$$y_i = (\Delta l)_i^2 \left\{ \frac{\varepsilon_{i-1} - \varepsilon_i}{2(c_{i-1} - c_i)} - \frac{\varepsilon_{i-1} c_i - \varepsilon_i c_{i-1}}{(c_{i-1} - c_i)^3} \left[c_i \log \frac{c_i}{c_{i-1}} + (c_{i-1} - c_i) \right] \right\} + y_{i-1} + (\Delta l)_i \tan\theta_{i-1} \qquad (13b)$$

$$(i = 1,2,3,....,n)$$

b. In dual summation form (see Appendix B for derivation):

$$y_i = \underbrace{\sum_{j=1}^{i} \left\{ (\Delta l)_j^2 \left[\frac{\varepsilon_{j-1} - \varepsilon_j}{2(c_{j-1} - c_j)} - \frac{\varepsilon_{j-1} c_j - \varepsilon_j c_{j-1}}{(c_{j-1} - c_j)^3} \left\langle c_j \log_e \frac{c_j}{c_{j-1}} + (c_{j-1} - c_j) \right\rangle \right] \right\}}_{\text{Contributions from deflection terms}} + y_0$$

$$+ \underbrace{\sum_{j=1}^{i-1} \left\{ \left[\sum_{k=j+1}^{i} (\Delta l)_k \right] (\Delta l)_j \left[\frac{\varepsilon_{j-1} - \varepsilon_j}{c_{j-1} - c_j} + \frac{\varepsilon_{j-1} c_j - \varepsilon_j c_{j-1}}{(c_{j-1} - c_j)^2} \log_e \frac{c_j}{c_{j-1}} \right] \right\} + \left[\sum_{j=1}^{i} (\Delta l)_j \right] \tan\theta_0}_{\text{Contributions from slope terms}} \qquad (13c)$$

$$(i = 1,2,3,....,n)$$

Equations (13) are called the Variable-Domain Nonuniform Displacement Transfer Functions for nonuniform embedded beams based on piecewise-linear strain representations. For constant-domain lengths, $(\Delta l)_1 = (\Delta l)_2 = (\Delta l)_3 = ... = \Delta l$, equation (13c) degenerates into equation (5c). Equations (13) are not applicable to the limit case of uniform beam $(c_{i-1} = c_i = c)$ because of mathematical indeterminacy (that is, $0/0$). However, by expanding the logarithmic terms in equations (13) in series forms in the neighborhood of $(c_{i-1}/c_i) \to 1$ (refs. 1, and 3), one can obtain the following Log-expanded equations (14) for slightly nonuniform embedded beams $[(c_{i-1}/c_i) \to 1]$, which are applicable to the limit case of uniform beams $(c_{i-1} = c_i = c)$.

2. Slightly Nonuniform Embedded Beams (Linear Strain) $[(\Delta l)_{i-1} \neq (\Delta l)_i ; (c_i / c_{i-1}) \to 1]$

Slope equations:

$$\tan\theta_i = \frac{(\Delta l)_i}{2c_{i-1}} \left[\left(2 - \frac{c_i}{c_{i-1}} \right) \varepsilon_{i-1} + \varepsilon_i \right] + \tan\theta_{i-1} \qquad ; \qquad (i = 1,2,3,....,n) \qquad (14a)$$

Deflection equations:
a. In recursive form:

$$y_i = \frac{(\Delta l)_i^2}{6c_{i-1}}\left[\left(3-\frac{c_i}{c_{i-1}}\right)\varepsilon_{i-1}+\varepsilon_i\right]+y_{i-1}+\Delta l\tan\theta_{i-1} \quad ; \quad (i=1,2,3,....,n) \tag{14b}$$

b. In dual summation form:

$$\begin{aligned} y_i = & \underbrace{\frac{1}{6}\sum_{j=1}^{i}\left\{\frac{(\Delta l)_j^2}{c_{j-1}}\left[\left(3-\frac{c_j}{c_{j-1}}\right)\varepsilon_{j-1}+\varepsilon_j\right]\right\}+y_0}_{\text{Contributions from deflection terms}} \\ & \underbrace{+\frac{1}{2}\sum_{j=1}^{i-1}\left\{\left[\sum_{k=j+1}^{i}(\Delta l)_k\right]\frac{(\Delta l)_j}{c_{j-1}}\left[\left(2-\frac{c_j}{c_{j-1}}\right)\varepsilon_{j-1}+\varepsilon_j\right]\right\}+\left[\sum_{j=1}^{i}(\Delta l)_j\right]\tan\theta_0}_{\text{Contributions from slope terms}} \end{aligned} \tag{14c}$$

(i = 1,2,3,…..,n)

Equations (14) are the Variable-Domain Log-expanded Displacement Transfer Function for slightly nonuniform (including uniform) embedded beams based on piecewise-linear strain representations. The derivation of equation (14c) is similar to that of equation (13c) (see Appendix B). For constant-domain lengths, $(\Delta l)_1 = (\Delta l)_2 = (\Delta l)_3 = ... = \Delta l$, equation (14c) degenerates into equation (6c). It must be mentioned that the shape prediction accuracy of equation (14a), (14b), and (14c) was experimentally validated (see section: Experimental Validations of Shape-Prediction Accuracies).

Based on Piecewise-Nonlinear Strain Representations

The following two sets of slope and deflection equations were formulated by using the piecewise-nonlinear function to describe the variation of the surface strain, $\varepsilon(x)$ [eq. (11)], but the piecewise-linear function was used to describe the variation of the depth factor, $c(x)$ [eq. (9)]. For simplifications, let the coefficients of the second and third terms of equation (11) be represented respectively with symbols A_i and B_i as shown in equations (15) and (16) respectively:

$$A_i \equiv -\frac{(\Delta l)_{i+1}[2(\Delta l)_i+(\Delta l)_{i+1}]\varepsilon_{i-1}-[(\Delta l)_i+(\Delta l)_{i+1}]^2\varepsilon_i+(\Delta l)_i^2\varepsilon_{i+1}}{(\Delta l)_i(\Delta l)_{i+1}[(\Delta l)_i+(\Delta l)_{i+1}]} \tag{15}$$

$$B_i \equiv \frac{(\Delta l)_{i+1}\varepsilon_{i-1}-[(\Delta l)_i+(\Delta l)_{i+1}]\varepsilon_i+(\Delta l)_i\varepsilon_{i+1}}{(\Delta l)_i(\Delta l)_{i+1}[(\Delta l)_i+(\Delta l)_{i+1}]} \tag{16}$$

Then, the improved slope and deflection equations can be written as (see Appendix C for derivations):

1. Nonuniform Embedded Beams (Nonlinear Strain) $[(\Delta l)_{i-1} \neq (\Delta l)_i ; (c_{i-1} \neq c_i)]$

Improved slope equation:

$$\tan\theta_i = \frac{(\Delta l)_i}{(c_i - c_{i-1})^3}\left[(c_i - c_{i-1})^2 \varepsilon_{i-1} - A_i(\Delta l)_i c_{i-1}(c_i - c_{i-1}) + B_i(\Delta l)_i^2 c_{i-1}^2\right]\log_e \frac{c_i}{c_{i-1}} + \frac{(\Delta l)_i}{2(c_i - c_{i-1})^2}\left[2A_i(\Delta l)_i(c_i - c_{i-1}) + B_i(\Delta l)_i^2(c_i - 3c_{i-1})\right] + \tan\theta_{i-1} \qquad (i = 1,2,3,....,n) \tag{17a}$$

Improved deflection equations:
a. In recursive form:

$$y_i = \frac{(\Delta l)_i^2}{(c_i - c_{i-1})^4}\left[(c_i - c_{i-1})^2 \varepsilon_{i-1} - A_i(\Delta l)_i(c_i - c_{i-1})c_{i-1} + B_i(\Delta l)_i^2 c_{i-1}^2\right]\left[c_i \log_e \frac{c_i}{c_{i-1}} - (c_i - c_{i-1})\right] + \frac{(\Delta l)_i^2}{6(c_i - c_{i-1})^2}\left[3A(\Delta l)_i(c_i - c_{i-1}) + B_i(\Delta l)_i^2(c_i - 4c_{i-1})_i\right] + y_{i-1} + (\Delta l)_i \tan\theta_{i-1} \qquad (i = 1,2,3,....,n) \tag{17b}$$

b. In dual summation form:

$$y_i = \underbrace{\sum_{j=1}^{i}\left\{\begin{array}{l}\dfrac{(\Delta l)_j^2}{(c_j - c_{j-1})^4}\left[(c_j - c_{j-1})^2 \varepsilon_{j-1} - A_j(\Delta l)_j(c_j - c_{j-1})c_{j-1} + B_j(\Delta l)_j^2 c_{j-1}^2\right]\times \\ \qquad\qquad \times\left[c_j \log_e \dfrac{c_j}{c_{j-1}} - (c_j - c_{j-1})\right] \\ + \dfrac{(\Delta l)_j^2}{6(c_j - c_{j-1})^2}\left[3A_j(\Delta l)_j(c_j - c_{j-1}) + B_j(\Delta l)_j^2(c_j - 4c_{j-1})\right]\end{array}\right\}}_{\text{Contribution from deflection terms}} + y_0$$

$$+ \underbrace{\sum_{j=1}^{i-1}\left\{\left[\sum_{k=j+1}^{i}(\Delta l)_k\right]\left[\begin{array}{l}\dfrac{(\Delta l)_j}{(c_j - c_{j-1})^3}\left\langle\begin{array}{l}(c_j - c_{j-1})^2 \varepsilon_{j-1} - A_j(\Delta l)_j c_{j-1}(c_j - c_{j-1}) \\ + B_j(\Delta l)_j^2 c_{j-1}^2\end{array}\right\rangle \log_e \dfrac{c_j}{c_{j-1}} \\ + \dfrac{(\Delta l)_j^2}{2(c_j - c_{j-1})^2}\left\langle 2A_j(\Delta l)_j(c_j - c_{j-1}) + B_j(\Delta l)_j^2(c_j - 3c_{j-1})\right\rangle\end{array}\right]\right\}}_{\text{Contributions from slope terms}}$$

$$+ \underbrace{\left[\sum_{j=1}^{i}(\Delta l)_j\right]\tan\theta_0}_{\text{Contributions from slope terms}} \qquad (i = 1,2,3,\ldots..,n) \tag{17c}$$

Equations (17) are called the Variable-Domain Improved Displacement Transfer Functions for non-uniform embedded beams based on piecewise-nonlinear strain representations. Derivation of equation (17c) is similar to that of equation (13c) (see Appendix B). For the constant-domain lengths, $(\Delta l)_1 = (\Delta l)_2 = (\Delta l)_3 = ... = \Delta l$, equations (17) will degenerate into equations (7) (see Appendix C).

Equations (17) are not applicable to the limit case of uniform embedded beam ($c_{i-1} = c_i = c$) because of mathematical indeterminacy (that is, 0/0). Therefore, the logarithmic terms in equations (17) were expanded in series forms in the neighborhood of $(c_{i-1}/c_i) \to 1$, to yield the following Log-expanded equations (18) for slightly nonuniform embedded beams [$(c_{i-1}/c_i) \to 1$], applicable to the limit case of uniform beams $(c_{i-1} = c_i = c)$ (see derivations in Appendix D).

2. Slightly Nonuniform Embedded Beams (Nonlinear Strain) $[(\Delta l)_{i-1} \neq (\Delta l)_i ; (c_i / c_{i-1}) \to 1]$

Log-expanded slope equation:

$$\tan\theta_i = \frac{(\Delta l)_i}{6c_{i-1}^3}\begin{bmatrix} \left\langle 6c_{i-1}^2 + (c_i - c_{i-1})(2c_i - 5c_{i-1}) \right\rangle \varepsilon_{i-1} \\ -A_i(\Delta l)_i c_{i-1}(2c_i - 5c_{i-1}) + 2B_i(\Delta l)_i^2 c_{i-1}^2 \end{bmatrix} + \tan\theta_{i-1} \qquad (18a)$$

$$(i = 1,2,3,....,n)$$

Log-expanded deflection equations:
a. In recursive form:

$$y_i = \frac{(\Delta l)_i^2}{12c_{i-1}^4}\begin{Bmatrix} \left[6c_{i-1}^3 + c_{i-1}(10c_i - 3c_{i-1})(c_i - c_{i-1}) - 3(c_i^3 - c_{i-1}^3) \right] \varepsilon_{i-1} \\ +A_i(\Delta l)_i c_{i-1}\left[2c_{i-1}^2 + (3c_i - 4c_{i-1})(c_i - c_{i-1}) \right] \\ +B_i(\Delta l)_i^2 c_{i-1}^2 \left[c_{i-1} - 3(c_i - c_{i-1}) \right] \end{Bmatrix} + y_{i-1} + (\Delta l)_i \tan\theta_{i-1} \qquad (18b)$$

$$(i = 1,2,3,....,n)$$

b. In dual summation form:

$$y_i = \underbrace{\frac{1}{12}\sum_{j=1}^{i} \frac{(\Delta l)_j^2}{c_{j-1}^4}\begin{Bmatrix} \left[6c_{j-1}^3 + c_{j-1}(10c_j - 3c_{i-1})(c_j - c_{j-1}) - 3(c_j^3 - c_{j-1}^3) \right] \varepsilon_{j-1} \\ +A_j(\Delta l)_j \left[2c_{j-1}^2 + c_{i-1}(c_j - c_{j-1})(3c_j - 4c_{j-1}) \right] \\ +B_j(\Delta l)_j^2 c_{i-1}^2 \left[c_{j-1} - 3(c_j - c_{j-1}) \right] \end{Bmatrix}}_{\text{Contributions from deflection terms}} + y_0$$

$$+ \underbrace{\frac{1}{6}\sum_{j=1}^{i-1}\left\{ \left[\sum_{k=j+1}^{i} (\Delta l)_k \right] \frac{(\Delta l)_j}{c_{j-1}^3} \begin{bmatrix} \left\langle 6c_{j-1}^2 + (c_j - c_{j-1})(2c_j - 5c_{j-1}) \right\rangle \varepsilon_{j-1} \\ -A_j(\Delta l)_j c_{j-1}(2c_j - 5c_{j-1}) + 2B_j(\Delta l)_j^2 c_{j-1}^2 \end{bmatrix} + \left[\sum_{j=1}^{i} (\Delta l)_j \right] \tan\theta_0 \right\}}_{\text{Contributions from slope terms}} \qquad (18c)$$

$$(i = 1,2,3,....,n)$$

Equation (18) are called the Variable-Domain Log-expanded Displacement Transfer Functions for slightly nonuniform (including uniform) embedded beams based on piecewise-nonlinear strain representations. Derivation of equation (18c) is similar to that of equation (13c) (see Appendix B). For constant-domain lengths, $(\Delta l)_1 = (\Delta l)_2 = (\Delta l)_3 = ... = \Delta l$, equation (18c) degenerates into equation (8c) (see Appendices D, and E).

CHARACTERISTICS OF DISPLACEMENT TRANSFER FUNCTIONS

The Displacement Transfer Functions listed above are purely geometrical in nature, relating surface strains and depth factors to out-of-plane deflections, and contain no material/structural properties. Thus, in the shape predictions using the Displacement Transfer Functions, no knowledge of material/structural properties is required. In fact, the effects of material/structural properties are felt only by the surface strains and influence their outputs.

Another key characteristic of the Displacement Transfer Functions is that the deflection, y_i, at the strain-sensing station, x_i, is expressed in terms of the inboard surface strains, $(\varepsilon_0, \varepsilon_1, \varepsilon_2, ..., \varepsilon_i)$, obtained at all the inboard strain-sensing stations, $(x_0, x_1, x_2, ..., x_i)$, including the strain, ε_i, at the current strain-sensing station, x_i, where y_i is calculated. The outboard surface strains, $(\varepsilon_{i+1}, \varepsilon_{i+2}, \varepsilon_{i+3}, ..., \varepsilon_n)$, are not needed in the calculations of y_i.

DETERMINATIONS OF DEPTH FACTORS

To use the Displacement Transfer Functions to convert surface strains into deflections, the depth factors, $c_i\,(i = 1,2,3,....,n)$, of the embedded beam are needed in the deflection calculations. To determine the depth factors, c_i (that is, locating the neutral axis), one can use two strain-sensing lines, each of which are lying respectively on the lower and upper surfaces of the embedded beam. The lower and upper surface strains, $\{\varepsilon_i,\ \overline{\varepsilon}_i\}\,(i = 1,2,3,....,n)$, can then be used to determine the lower and upper depth factors, $\{c_i,\ \overline{c}_i\}$.

As shown in figure 3, *R* is the radius of curvature of the neutral axis of the embedded beam under upward bending; A_0B_0 is the undeformed segment length along the neutral axis; *CD* is the elongation of the lower surface from un-deformed length, $AB(= A_0B_0)$ to deformed length, *AC*; $-\bar{C}\bar{D}$ is the contraction of the upper surface from undeformed length, $\bar{A}\bar{B}(= A_0B_0)$ to deformed length, $\bar{A}\bar{C}$. Then, through geometrical similarities of the curved triangles, $\Delta OAC, \Delta B_0BC, \Delta B_0\bar{B}\bar{C}$ (fig. 3), the lower and upper surface strains, $\{\varepsilon_i,\ \overline{\varepsilon}_i\}$, can be related respectively to the lower and upper depth factors, $\{c_i,\ \overline{c}_i\}$, as:

$$\varepsilon_i = \frac{BC}{AB} = \frac{BC}{A_0B_0} = \frac{c_i}{R}\ \text{(tension)} \quad ; \quad \overline{\varepsilon}_i = \frac{-\bar{B}\bar{C}}{\bar{A}\bar{B}} = \frac{-\bar{B}\bar{C}}{A_0B_0} = -\frac{\overline{c}_i}{R}\ \text{(compression)} \tag{19}$$

Keep in mind that in upward or downward bending, the signs of the lower and upper surface strains, $\{\varepsilon_i,\ \overline{\varepsilon}_i\}$, are always opposite. By eliminating *R* in equation (19), the two depth factors, $\{c_i, \overline{c}_i\}$, can be related as:

$$\overline{c}_i = -\frac{\overline{\varepsilon}_i}{\varepsilon_i} c_i \qquad ; \qquad (i = 1,2,3,....,n) \tag{20}$$

The depth of the embedded beam, h_i, at strain-sensing station, x_i, is given by:

$$h_i = c_i + \overline{c}_i \qquad ; \qquad (i = 1,2,3,....,n) \qquad (21)$$

In view of equations (20) and (21), one can establish the depth factor equations in the forms:

$$c_i = \frac{\varepsilon_i}{\varepsilon_i - \overline{\varepsilon}_i} h_i \quad ; \quad \overline{c}_i = \frac{-\overline{\varepsilon}_i}{\varepsilon_i - \overline{\varepsilon}_i} h_i \qquad ; \qquad (i = 1,2,3,....,n) \qquad (22)$$

Equation (22) can also be used for downward bending, and is applicable to both solid beam cross sections, and hollow beam cross sections (for example, aircraft wing cross sections).

If $\{\varepsilon_i, \overline{\varepsilon}_i\}$ have the same magnitudes (opposite signs), then equation (22) gives $c_i = \bar{c}_i = h_i/2$, indicating that the neutral axis is located at the beam half depth. Equation (22) was used with great success in the shape predictions of both Ikhana (General Atomics Aeronautical Systems Inc., San Diego, California) composite wings (66-ft wingspan) (ref. 3) and Global Observer (AeroVironment Inc., Monrovia, California) composite wings (175-ft wingspan) (ref. 13), for which the locations of neutral axes were unknown. Therefore, equation (22) had to be used to calculate the depth factors, $\{c_i, \overline{c}_i\}$, for each embedded beam using the associated surface strains, $\{\varepsilon_i, \overline{\varepsilon}_i\}$.

STRUCTURE USED FOR SHAPE PREDICTION ACCURACY STUDIES

To compare the shape-prediction accuracies of the newly formulated variable-domain Displacement Transfer Function with the earlier constant-domain Displacement Transfer Functions, a sample structure was needed. The structure chosen for the prediction accuracy analysis was an aluminum tapered cantilever tubular beam with geometries listed in table 1.

Table 1. Geometries of aluminum tapered cantilever tubular beam.

l, in. (Length)	t, in. (Wall thickness)	c_0, in. (Root depth factor)	c_n, in. (Tip depth factor)	$\alpha\{=\tan^{-1}[(c_0 - c_n)/l]\}$, deg. (Taper angle)
300	0.02296	4	1	0.5729

The embedded beam (depth-wise structural cross section along the strain-sensing line) shown in figure 1 can also represent the embedded beam of the tapered cantilever tubular beam. The embedded beam for the tubular beam is defined as the span-wise vertical cross section along the strain-sensing line which is coincidental with the bottom generatrix (a straight line for generating tubular surface through sidewise circular motion). Because the depth factor, $c_i (i = 1,2,3,\ldots..,n)$ (fig. 1), is the known local radius, only one strain-sensing line is needed to obtain surface strains, $\varepsilon_i (i = 1,2,3,\ldots..,n)$ (fig. 1) for shape predictions. An upward point load of P = 300 lb (or P = 600 lb) was applied at the beam free end.

In the present technical publication, sixteen (n = 16) strain-sensing domains (distance between two adjacent strain-sensing stations) were used for the constant-domain cases with equal domain lengths of $\Delta l = l/n = 300/16 = 18.75$ in. To create variable-domain cases, the strain-sensing stations at $i = 4$, 8, and 12 of constant-domain cases were removed to double the domain length to $(\Delta l)_i = 2 \times 18.75 = 37.5$ in. in those three regions. The rest of the domain lengths remain unchanged [that is, $(\Delta l)_i = 18.75$ in.]

ANALYTICAL SHAPE PREDICTIONS

The shape prediction analysis in the present technical publication report is called analytical shape prediction analysis. Namely, instead of using experimentally measured surface strains, the Structural Performance And Resizing (SPAR) finite-element computer program (ref. 14) was used to analytically calculate the surface strains for input to the Displacement Transfer Functions for shape calculations. Also, for estimations of shape prediction errors of different Displacement Transfer Functions, the SPAR-generated slopes and deflections were used as reference yardsticks.

FINITE ELEMENT ANALYSIS

The purpose of the finite-element analysis is to generate input surface strains, and to calculate the slopes and deflections, which were used as the reference yardsticks in the shape prediction error analysis.

Finite-Element Model

The SPAR finite-element model generated for the tapered cantilever tubular beam has the following numbers of nodes and elements:

3673 nodes = 3636 nodes for the tube wall (101 axial nodes $\times$ 36 circumferential nodes) +
37 nodes on the beam-tip disk

3636 four-node elements = 3600 elements for the tube wall +
36 elements for beam-tip disk outer region

36 three-node elements for beam-tip disk central region

The upward point load of $P = 300$ lb (or $P = 600$ lb) was applied at the beam-tip disk central node of the SPAR model.

Figure 4 shows the undeformed and deformed shapes of the SPAR model generated for the tapered cantilever tubular beam subjected to beam-tip load of $P = 300$ lb (or $P = 600$ lb). Note that for the loading case of $P = 300$ lb, the beam-tip deflection reached $y_n \approx 141.6$ in., and the beam-tip slope reached as large as $\theta_n \approx 48$ deg. For the doubled loading case of $P = 600$ lb, the beam-tip deflection was doubled to $y_n \approx$ 283.2 in. (because of linear elasticity), however, the beam-tip slope was not doubled, but only increased by 1.375 times to $\theta_n \approx 66$ deg ($=1.375 \times 48$ deg).

It must be mentioned that the SPAR model has 100 elements in the axial direction (fig. 3). For $n = 16$ strain-sensing domains, the even number of strain sensing stations can be either coincidental with SPAR nodes or at the midpoints between two adjacent SPAR axial nodes. However, the odd numbers of strain-sensing stations are not precisely at the SPAR nodes. Therefore, the shape prediction errors were based on the actual prediction errors at the even numbers of strain-sensing stations.

Analytical Surface Strains

In the present paper, the surface strains, ε_i $(i = 0,1,2,3,....,n)$, for inputs to the Displacement Transfer Functions were calculated analytically (not actually measured) by using the SPAR program. Namely, finite elements were used to simulate actual strain gages. The surface bending strains, ε_i $(i = 0,1,2,3,....,n)$, at the *i*-th strain-sensing stations (fig. 1) were generated by converting the nodal or element axial stresses into axial strains, ε_i (bending strains), through stress-strain relationship.

It must be mentioned that the surface strain, ε_i, can also be obtained from the span-wise nodal displacement differentials of the SPAR elements. However, it was found that in the beam-tip regions of the highly bent tapered beams (large deformations), the axial strains became negative because the output nodal displacements were the projected displacements along the original beam axis, and not along the deformed beam axis to reflect true span-wise displacements. Therefore, this displacement method was not used.

Figure 5 shows the plots of SPAR-generated surface strains for the two loading cases, $P = \{300, 600\}$ lb. Note that the strain level doubled when the applied load was increased from $P = 300$ lb to $P = 600$ lb because of linear elasticity used in the SPAR program. Note that the surface strains for the two loading cases increased practically linearly from the fixed ends and reached their respective peaks in the outboard region, and then decreased rapidly toward the beam tip (because of decreasing depth factor), and finally reached small nonzero values at the beam tip. Theoretically the beam-tip strains should be zero. Because of finite length, the beam-tip finite element (simulated strain gage), which has one end at the beam tip, but the other end is slightly off from the beam tip, gave small nonzero strains. By reducing the element sizes, the small nonzero beam-tip strains could be reduced. Keep in mind that if an actual strain gage is installed at the beam tip, the strain output could also be nonzero because of finite length of the strain gage.

Criteria of Prediction Errors

The SPAR-calculated surface strain data of figure 5 were then input to the Displacement Transfer Functions (constant-domain and variable-domain cases) to calculate the slopes and deflections. The shape prediction errors of the Displacement Transfer Functions were estimated by comparison with the SPAR-calculated slopes and deflections, which were used as reference yardsticks. The prediction errors are then defined as the percent of normalized differences (signs neglected) between the predicted slopes and deflections, $\{(\theta)_{\text{Pred.}}, (y_i)_{\text{Pred.}}\}$, and the corresponding SPAR-generated slopes and deflections, $\{(\theta)_{\text{SPAR.}}, (y_i)_{\text{SPAR}}\}$. Namely,

$$\text{Slope } (\theta_i) \text{ prediction error} \equiv \left| \frac{(\theta_i)_{\text{Pred.}} - (\theta_i)_{\text{SPAR}}}{(\theta_i)_{\text{SPAR}}} \right| \times 100\% \quad ; \quad (i = 1,2,3,\ldots..,n) \tag{23}$$

$$\text{Deflection } (y_i) \text{ prediction error} \equiv \left| \frac{(y_i)_{\text{Pred.}} - (y_i)_{\text{SPAR}}}{(y_i)_{\text{SPAR}}} \right| \times 100\% \quad ; \quad (i = 1,2,3,\ldots..,n) \tag{24}$$

SELECTED DISPLACEMENT TRANSFER FUNCTIONS

Because the cantilever tubular beam is highly tapered, the following four Displacement Transfer Functions for nonuniform beams were chosen in the prediction accuracy analysis.

Based on piecewise-linear strain representations:

1. Equations (5) — constant-domain Nonuniform Displacement Transfer Functions formulated for nonuniform beams based on piecewise-linear strain representations.
2. Equations (13) — variable-domain Nonuniform Displacement Transfer Functions formulated for nonuniform beams based on piecewise-linear strain representations.

Based on piecewise-nonlinear strain representations:

3. Equations (7) — constant-domain Improved Displacement Transfer Functions formulated for nonuniform beams based on piecewise-nonlinear strain representations.
4. Equations (17) — variable-domain Improved Displacement Transfer Functions formulated for nonuniform beams based on piecewise-nonlinear strain representations.

The above four Displacement Transfer Functions were used to calculate both slopes and deflections for comparison with the corresponding SPAR-calculated values.

NUMERICAL RESULTS

The SPAR-generated surface strain data of figure 5 were then input into equations (5a), (5b), (5c), (13a), (13b), and (13c) (piecewise-linear strain representations), and equations (7a), (7b), (7c), (17a), (17b), and (17c) (piecewise-nonlinear strain representations) for the calculations of both slopes and deflections. The slope and deflection prediction errors were then calculated respectively from the prediction error equations (23), and (24).

Calculated Slope Data

The slopes, θ_i , calculated from the slope equations (5a), and (13a) (based on piecewise-linear strain representations) and slope equations (7a), and (17a) (based on piecewise-nonlinear strain representations for the two loading cases, $P = \{300, 600\}$ lb, are listed below. The percent slope prediction errors were calculated from the slope prediction error equation (23).

For Piecewise-Linear Strain Representations:

The slope prediction errors based on piecewise-linear strain representations are listed in tables 2 and 3 for loading cases of $P = \{300, 600\}$ lb.

Table 2. Comparisons of slopes, θ_i, calculated from SPAR and from constant and variable-domain slope equations [(5a), (13a)] (piecewise-linear strain representations); tapered cantilever tubular beam ($l = 300$ in., $c_0 = 4$ in., $c_n = 1$ in.) subjected to tip load of $P = 300$ lb; $n = 16$, $\Delta l = 18.75$ in., fine $(\Delta l)_i = 18.75$ in., coarse $(\Delta l)_i = 37.50$ in.

	SPAR	Constant-domain [eq. (5a)]		Variable-domains [eq. (13a)]	
i	θ_i, deg	θ_i, deg	Percent error	θ_i, deg	Percent error
0	0.0000	0.0000	0.0000	0.0000	0.0000
1	2.1815	2.0895	4.2174	2.0895	4.2174
2	4.3526	4.3460	0.1502	4.3460	0.1502
3	7.0977	6.7873	4.3742	6.7873	4.3742
4	9.4255	9.4213	0.0447	----------	----------
5	12.3764	12.2534	0.9943	12.2542	0.9876
6	15.2999	15.2918	0.0525	15.2926	0.0473
7	18.9492	18.5395	2.1623	18.5403	2.1582
8	21.9903	21.9831	0.0326	----------	----------
9	25.1656	25.5988	1.7214	25.5937	1.7013
10	29.3683	29.3544	0.0474	29.3497	0.0634
11	33.0596	33.1950	0.4097	33.1907	0.3966
12	37.0656	37.0367	0.0780	----------	----------
13	40.9426	40.7621	0.4409	40.6960	0.6024
14	44.2216	44.1650	0.1278	44.1057	0.2620
15	46.8926	46.8405	0.1112	46.7865	0.2262
16	48.2679	48.0961	0.3559	48.0446	0.4625*

* 30-percent increase from constant-domain case.

Table 3. Comparisons of slopes, θ_i , calculated from SPAR and from constant and variable-domain non-uniform slope equations [(5a), (13a)] (piecewise-linear strain representations); long tapered cantilever tubular beam ($l = 300$ in., $c_0 = 4$ in., $c_n = 1$ in.) subjected to tip load of $P = 600$ lb, $n = 16$, $\Delta l = 18.75$ in.; fine $(\Delta l)_i = 18.75$ in., coarse $(\Delta l)_i = 37.50$ in.

	SPAR	Constant-domain [eq. (5a)]		Variable-domains [eq. (13a)]	
i	θ_i , deg	θ_i , deg	Percent error	θ_i , deg	Percent error
0	0.0000	0.0000	0.0000	0.0000	0.0000
1	4.0121	4.1735	4.0242	4.1735	4.0242
2	8.6553	8.6426	0.1463	8.6426	0.1463
3	13.5897	13.3892	1.4750	13.3892	1.4750
4	18.3669	18.3591	0.0424	--------	--------
5	23.2829	23.4785	0.8400	23.4800	0.8462
6	28.6842	28.6712	0.0453	28.6726	0.0407
7	34.0679	33.8507	0.6375	33.8519	0.6340
8	38.9263	38.9162	0.0260	--------	--------
9	43.6006	43.7767	0.4039	43.7703	0.3891
10	48.3787	48.3626	0.0332	48.3571	0.0446
11	52.7958	52.6120	0.3481	52.6075	0.3567
12	56.4976	56.4700	0.0490	--------	--------
13	59.7895	59.8850	0.1597	59.8269	0.0626
14	62.8071	62.7611	0.0732	62.7127	0.1502
15	65.0539	64.8797	0.2679	64.8381	0.3318
16	65.9637	65.8349	0.1954	65.7962	0.2540*

* 30-percent increase from constant-domain case.

Note from tables 2, and 3 (piecewise-linear strain representations) that, by removing three strain-sensing stations at i = 4, 8, 12 to change the constant-domain cases into variable-domain cases, the beam-tip slope (θ_n) prediction errors increased from 0.3559 percent to 0.4625 percent (30-percent increase) for loading case of $P = 300$ lb (table 2), and from 0.1954 percent to 0.2540 percent (also a 30-percent increase) for loading cases of $P = 600$ lb (table 3). However, the slope prediction errors are still in the negligible levels. Note also that by increasing the load from $P = 300$ lb to $P = 600$ lb, the beam-tip slope (θ_n) prediction errors decreased from 0.3559 percent (table 2) down to 0.1954% (table 3) (45-percent reduction) for the constant-domain cases, and decreased from 0.4625 percent (table 2) down to 0.2540 percent (table 3) (also a 45-percent reduction) for the variable-domain cases.

For Piecewise-Nonlinear Strain Representations:

The slope prediction errors based on piecewise-nonlinear strain representations are listed in tables 4 and 5 for loading cases of P = {300, 600} lb.

Table 4. Comparisons of slopes, θ_i, calculated from SPAR and from constant and variable-domain slope equations [(7a), (17a)] (piecewise-nonlinear strain representations); tapered cantilever tubular beam ($l = 300$ in., $c_0 = 4$ in., $c_n = 1$ in.) subjected to tip load of $P = 300$ lb; $n = 16$, $\Delta l = 18.75$ in., fine $(\Delta l)_i = 18.75$ in., coarse $(\Delta l)_i = 37.50$ in.

	SPAR	Constant-domain [eq. (7a)]		Variable-domains [eq. (17a)]	
i	θ_i, deg	θ_i, deg	Percent error	θ_i, deg	Percent error
0	0.0000	0.0000	0.0000	0.0000	0.0000
1	2.1815	2.0884	4.2683	2.0884	4.2683
2	4.3526	4.3447	0.1813	4.3447	0.1813
3	7.0977	6.7862	4.3890	6.7862	4.3890
4	9.4255	9.4201	0.0571	--------	--------
5	12.3764	12.2516	1.0089	12.2655	0.8964
6	15.2999	15.2903	0.0629	15.3038	0.0258
7	18.9492	18.5391	2.1644	18.5522	2.0953
8	21.9903	21.9837	0.0300	--------	--------
9	25.1656	25.6010	1.7301	25.6218	1.8130
10	29.3683	29.3606	0.0262	29.3801	0.0400
11	33.0596	33.2072	0.4467	33.2252	0.5010
12	37.0656	37.0587	0.0184	--------	--------
13	40.9426	40.8057	0.3343	40.7581	0.4506
14	44.2216	44.2497	0.0636	44.2071	0.0328
15	46.8926	46.9762	0.1784	46.9376	0.0959
16	48.2679	48.2910	0.0479	48.2543	0.0283*

* 41-percent reduction from constant-domain case.

Table 5. Comparisons of slopes, θ_i, calculated from SPAR and from constant and variable-domain slope equations [(7a), (17a)] (piecewise-nonlinear strain representations); tapered cantilever tubular beam ($l = 300$ in., $c_0 = 4$ in., $c_n = 1$ in.) subjected to tip load of $P = 600$ lb; $n = 16$, $\Delta l = 18.75$ in., fine $(\Delta l)_i = 18.75$ in., coarse $(\Delta l)_i = 37.50$ in.

	SPAR	Constant-domain [eq. (7a)]		Variable-domains [eq. (17a)]	
i	θ_i, deg	θ_i, deg	Percent error	θ_i, deg	Percent error
0	0.0000	0.0000	0.0000	0.0000	0.0000
1	4.0121	4.1713	3.9690	4.1713	3.9690
2	8.6553	8.6400	0.1771	8.6400	0.1771
3	13.5897	13.3872	1.4898	13.3872	1.4898
4	18.3669	18.3569	0.0542	--------	--------
5	23.2829	23.4753	0.8263	23.4999	0.9317
6	28.6842	28.6686	0.0545	28.6911	0.0238
7	34.0679	33.8501	0.6393	33.8702	0.5803
8	38.9263	38.9170	0.0238	--------	--------
9	43.6006	43.7796	0.4104	43.8063	0.4716
10	48.3787	48.3698	0.0183	48.3924	0.0284
11	52.7958	52.6249	0.3237	52.6438	0.2879
12	56.4976	56.4911	0.0116	--------	--------
13	59.7895	59.9232	0.2237	59.8815	0.1538
14	62.8071	62.8299	0.0364	62.7953	0.0188
15	65.0539	64.9841	0.1073	64.9544	0.1530
16	65.9637	65.9811	0.0263	65.9536	0.0154*

* 41-percent deduction from constant-domain case.

Note from tables 4, and 5 (piecewise-nonlinear strain representations) that, by removing three strain-sensing stations at i = 4, 8, 12 to change the constant-domain cases into variable-domain cases, the beam-tip slope (θ_n) prediction errors decreased from 0.0479 percent down to 0.0283 percent (41-percent reduction) for the loading case of $P = 300$ lb (table 4), and from 0.0263 percent down to 0.0154 percent (also a 41-percent reduction) for loading case of $P = 600$ lb (table 5) [remember, 30-percent increase for stepwise linear strain representations (tables 2, and 3)].

Also note that by increasing the load from $P = 300$ lb to $P = 600$ lb, the beam-tip slope (θ_n) prediction errors decreased from 0.0479 percent (table 4) down to 0.0263 percent (table 5) (45-percent reduction) for the constant-domain cases, and decreased from 0.0283 percent (table 4) down to 0.0154 percent (table 5) (also a 45-percent reduction) for the variable-domain cases.

It is important to mention that by changing the piecewise-linear strain representations (tables 2, and 3) into piecewise-nonlinear strain representations (tables 4, and 5), the beam-tip slope (θ_n) prediction errors for both loading cases, $P = \{300, 600\}$ lb, were reduced by as large as 87 percent for the constant-domain cases, and by 94 percent for the variable-domain cases. Note from tables 4 and 5 that nonlinear strain representations reducing the number of domains (that is, increasing domain lengths) could somewhat improve the beam-tip slope (θ_n) prediction accuracies. Such domain-length-dependent shape prediction

accuracies of the Displacement Transfer Functions were also observed in the experimental shape-prediction accuracy studies (ref. 13).

Calculated Slope Curves

Figures 6 and 7 respectively show the slope (θ_i) curves generated using the slope data of tables 2 and 3 (piecewise-linear strain representations), and tables 4 and 5 (piecewise-nonlinear strain representations). Note from figures 6 and 7 that the slope-curves are slightly s-shaped, and the values of θ_i did not double when the load was increased from $P = 300$ lb to $P = 600$ lb. Namely, θ_i is not a linear function of P. Because of infinitesimal slope prediction errors, the predicted slope curves for all the constant and variable-domain cases pictorially fell on top of the corresponding SPAR slope curves, showing remarkable accuracies of the Displacement Transfer Functions formulated based on piecewise approaches.

Calculated Deflection Data

The deflections, y_i, calculated from the deflection equations (5b), (5c), (13b), and (13c) (based on piecewise-linear strain representations) and deflection equations (7b), (7c), (17b), and (17c) (based on piecewise-nonlinear strain representations) for the two loading cases, $P = \{300, 600\}$ lb are listed below. The percent deflection prediction errors were calculated from the deflection prediction error equation (24).

For Piecewise-Linear Strain Representations:

The deflections, y_i, calculated from the deflection equations (5b), (5c) (13b), and (13c)] (based on piecewise-linear strain representations) for the loading cases, $P = \{300, 600\}$ lb are listed respectively in tables 6, and 7.

Table 6. Comparisons of deflections, y_i, calculated from SPAR and from constant and variable-domain deflection equations [(5b, 5c), (13b, 13c)] (piecewise-linear strain representations); tapered cantilever tubular beam ($l = 300$ in., $c_0 = 4$ in., $c_n = 1$ in.) subjected to tip load of $P = 300$ lb, $n = 16$, $\Delta l = 18.75$ in., fine $(\Delta l)_i = 18.75$ in., coarse $(\Delta l)_i = 37.50$ in.

i	SPAR	Constant domain [eqs. (5b,5c)]		Variable domains [eqs. (13b,13c)]	
	y_i, in.	y_i, in.	Percent error	y_i, in.	Percent error
0	0.0000	0.0000	0.0000	0.0000	0.0000
1	0.3223	0.3377	4.7845	0.3377	4.7845
2	1.4029	1.3871	1.1270	1.3871	1.1269
3	3.3148	3.2096	3.1741	3.2096	3.1741
4	5.8910	5.8746	0.2789	---------	--------
5	9.3147	9.4591	1.5503	9.4594	1.5533
6	14.0737	14.0501	0.1678	14.0506	0.1638
7	20.0231	19.7479	1.3747	19.7487	1.3705
8	26.6907	26.6659	0.0928	--------	--------
9	34.5995	34.9302	0.9558	34.9294	0.9533
10	44.7190	44.6814	0.0841	44.6785	0.0906
11	56.6063	56.0742	0.9399	56.0693	0.9486
12	69.3198	69.2690	0.0734	--------	--------
13	83.8382	84.4150	0.6880	84.3710	0.6355
14	101.7093	101.6065	0.1010	101.5248	0.1813
15	121.7164	120.7512	0.7930	120.6318	0.8910
16	141.6016	141.3056	0.2090	141.1485	0.3199*

* 53-percent increase from constant-domain case.

Table 7. Comparisons of deflections, y_i, calculated from SPAR and from constant and variable-domain deflection equations [(5b, 5c), (13b, 13c)] (piecewise-linear strain representations); tapered cantilever tubular beam ($l = 300$ in., $c_0 = 4$ in., $c_n = 1$ in.) subjected to tip load of $P = 600$ lb, $n = 16$, $\Delta l = 18.75$ in., fine $(\Delta l)_i = 18.75$ in., coarse $(\Delta l)_i = 37.50$ in.

i	SPAR	Constant domain [eqs. (5b,5c)]		Variable domains [eqs. (13b,13c)]	
	y_i, in.	y_i, in.	Percent error	y_i, in.	Percent error
0	0.0000	0.0000	0.0000	0.0000	0.0000
1	0.6446	0.6755	4.7845	0.6755	4.7845
2	2.8058	2.7742	1.1270	2.7742	1.1270
3	6.6296	6.4192	3.1741	6.4192	3.1741
4	11.7821	11.7492	0.2789	--------	--------
5	18.6294	18.9182	1.5503	18.9187	1.5533
6	28.1474	28.1001	0.1678	28.1013	0.1638
7	40.0463	39.4957	1.3747	39.4974	1.3705
8	53.3814	53.3319	0.0928	--------	--------
9	69.1991	69.8605	0.9558	69.8587	0.9533
10	89.4381	89.3628	0.0841	89.3570	0.0906
11	113.2126	112.1485	0.9399	112.1386	0.9486
12	138.6397	138.5379	0.0734	--------	--------
13	167.6765	168.8301	0.6880	168.7421	0.6355
14	203.4186	203.2131	0.1010	203.0497	0.1813
15	243.4327	241.5024	0.7930	241.2637	0.8910
16	283.2032	282.6112	0.2090	282.2971	0.3199*

* 53-percent increase from constant-domain case.

Note from tables 6, and 7 (piecewise-linear strain representations) that deflections (y_i) were doubled when the load was doubled from $P = 300$ lb to $P = 600$ lb because y_i are linear functions of P. Note also that the y_i-prediction percent errors under the two loading cases, $P = \{300, 600\}$ lb, (tables 6, and 7) are identical for both constant and variable-domain cases, and are independent of the loading magnitude of P.

As shown in tables 6, and 7, by removing three strain-sensing stations at $i = 4, 8, 12$, to change the constant-domain cases to variable-domain cases, the beam-tip deflection (y_n) prediction errors increased from 0.2090 percent (constant-domain cases) to 0.3199 percent (variable-domain cases) (53-percent increase) for both loading cases, $P = \{300, 600\}$ lb.

For Piecewise-Nonlinear Strain Representations:

The deflections, y_i, calculated from the deflection equations (7b), (7c) (17b), and (17c) (based on piecewise-nonlinear strain representations) for the loading cases, $P = \{300, 600\}$ lb are listed respectively in tables 8, and 9.

Table 8. Comparisons of deflections, y_i, calculated from SPAR and from constant and variable-domain deflection equations [(7b, 7c), (17b, 17c)] (piecewise-nonlinear strain representations); tapered cantilever tubular beam ($l = 300$ in., $c_0 = 4$ in., $c_n = 1$ in.) subjected to tip load of $P = 300$ lb, n = 16, fine $(\Delta l)_i = 18.75$ in., coarse $(\Delta l)_i = 37.50$ in.

	SPAR	Constant domain [eqs. (7b,7c)]		Variable domains [eqs. (17b,17c)]	
i	y_i, in.	y_i, in.	Percent error	y_i, in.	Percent error
0	0.0000	0.0000	0.0000	0.0000	0.0000
1	0.3223	0.3376	4.7284	0.3376	4.7284
2	1.4029	1.3865	1.1688	1.3865	1.1688
3	3.3148	3.2086	3.2038	3.2086	3.2038
4	5.8910	5.8732	0.3019	--------	--------
5	9.3147	9.4572	1.5303	9.4619	1.5800
6	14.0737	14.0476	0.1853	14.0570	0.1184
7	20.0231	19.7451	1.3887	19.7592	1.3179
8	26.6907	26.6632	0.1032	--------	--------
9	34.5995	34.9280	0.9494	34.9554	1.0286
10	44.7190	44.6810	0.0851	44.7168	0.0051
11	56.6063	56.0780	0.9333	56.1222	0.8552
12	69.3198	69.2812	0.0557	--------	--------
13	83.8382	84.4453	0.7241	84.4750	0.7595
14	101.7093	101.6760	0.0327	101.6786	0.0302
15	121.7164	120.8950	0.6749	120.8703	0.6951
16	141.6016	141.5683	0.0235	141.5165	0.0601*

* 156-percent increase from constant-domain case.

Table 9. Comparisons of deflections, y_i, calculated from SPAR and from constant and variable-domain deflection equations [(7b, 7c), (17b, 17c)] (piecewise-nonlinear strain representations); tapered cantilever tubular beam ($l = 300$ in., $c_0 = 4$ in., $c_n = 1$ in.) subjected to tip load of $P = 600$ lb, $n = 16$, fine $(\Delta l)_i = 18.75$ in., coarse $(\Delta l)_i = 37.50$ in.

	SPAR	Constant domain [eqs. (7b,7c)]		Variable domains [eqs. (17b,17c)]	
i	y_i, in.	y_i, in.	Percent error	y_i, in.	Percent error
0	0.0000	0.0000	0.0000	0.0000	0.0000
1	0.6446	0.6751	4.7282	0.6751	4.7282
2	2.8058	2.7730	1.1688	2.7730	1.1688
3	6.6296	6.4172	3.2038	6.4172	3.2038
4	11.7821	11.7465	0.3019	--------	--------
5	18.6294	18.9145	1.5303	18.9237	1.5800
6	28.1474	28.0952	0.1853	28.1140	0.1184
7	40.0463	39.4901	1.3887	39.5185	1.3179
8	53.3814	53.3264	0.1032	--------	--------
9	69.1991	69.8560	0.9494	69.9109	1.0286
10	89.4381	89.3619	0.0851	89.4335	0.0051
11	113.2126	112.1560	0.9333	112.2443	0.8552
12	138.6397	138.5624	0.0557	--------	--------
13	167.6765	168.8907	0.7241	168.9500	0.7595
14	203.4186	203.3521	0.0327	203.3571	0.0302
15	243.4327	241.7899	0.6749	241.7406	0.6951
16	283.2032	283.1367	0.0235	283.0330	0.0601*

* 156-percent increase from constant-domain case.

Note from tables 8 and 9 (piecewise-nonlinear strain representations) that deflections (y_i) were doubled when the load was doubled from $P = 300$ lb to $P = 600$ lb because y_i are linear functions of P. It is important to note that the y_i-prediction errors are identical under the two loading cases, $P = \{300, 600\}$ lb, (tables 8 and 9) for both constant and variable-domain cases and are, therefore, invariant to the loading magnitude of P.

By removing three strain-sensing stations at i = 4, 8, 12, to convert the constant-domain cases to variable-domain cases, the beam-tip deflection (y_n) prediction errors increased from 0.0235 percent (constant-domain cases) to 0.0601 percent (156-percent increase) for both loading cases, $P = \{300, 600\}$ lb. [Remember, there is only a 53-percent increase for piecewise-linear strain representations (tables 6, and 7)].

Calculated Deflection Curves

Figures 8 and 9 respectively show the deflection (y_i) curves generated using the deflection data of tables 6, and 7 (piecewise-linear strain representations) and tables 8, and 9 (piecewise-nonlinear strain representations). Note from figures 8 and 9 that the y_i -curves are shallow bow-shaped, and the values of y_i were doubled when the load was increased from $P = 300$ lb to $P = 600$ lb. Namely, y_i is a linear

function of *P*. Because of infinitesimal deflection prediction errors, the predicted deflection curves for all the constant and variable-domain cases practically fell on top of the corresponding SPAR deflection curves, showing amazing high accuracies of the Displacement Transfer Functions formulated based on piecewise formulations.

SHAPE PREDICTION ERROR ANALYSIS

This section compares the shape prediction errors of constant and variable-domain Displacement Transfer Functions formulated using linear or nonlinear strain representations. The slope and deflection prediction errors were calculated respectively from the shape prediction error equations (23) and (24).

Slope Prediction Error Curves

Figures 10 and 11 respectively show the slope (θ_i) prediction error curves for loading cases of $P = \{300, 600\}$ lb based on the slope data listed in tables 2 and 3 (piecewise-linear strain representations). The beam-tip slope (θ_n) prediction errors (in percent) are also indicated in figures 10 and 11. Those θ_i -error curves were plotted by using only the actual prediction error data at the even strain-sensing stations which are either coincidental with SPAR nodes or at the midpoints between two adjacent SPAR axial nodes. The larger prediction errors at the odd strain-sensing stations (tables 2 and 3) cannot represent the true prediction errors because the odd strain-sensing stations are not precisely at the SPAR nodes and, therefore, were not plotted in figures 10 and 11.

The constant-domain cases and variable-domain cases are shown respectively with solid curves (with solid circular symbols), and dashed curves (with open square symbols). The larger errors near the inboard regions are due to small numbers divided by other small numbers. The variable-domain cases have slightly larger errors in the outboard regions (figs. 10 and 11).

Note from figures 10 and 11 that, doubling the load from $P = 300$ lb to $P = 600$ lb, the θ_i -prediction errors in the outboard regions came down considerably (45-percent error reduction at the beam tip for both constant-domain and variable-domain cases).

Figures 12 and 13 respectively show the predicted slope (θ_i) error curves for loading cases of $P = \{300, 600\}$ lb based on the slope data listed in tables 4 and 5 (piecewise-nonlinear strain representations). The constant-domain cases and variable-domain cases are shown respectively with solid curves (with solid circular symbols), and dashed curves (with open square symbols). The amounts of the beam-tip slope (θ_n) prediction errors are also shown in figures 12 and 13.

Note from figures 12 and 13 that, doubling the load from $P = 300$ lb to $P = 600$ lb, the θ_i -prediction errors in the outboard regions came down considerably, and at the beam tip, the prediction errors also decreased by 45 percent for both constant-domain and variable-domain cases.

It is very important to mention that by changing the piecewise-linear strain representations (figs. 10 and 11) into piecewise-nonlinear strain representations (figs. 12 and 13), the beam-tip slope (θ_n) prediction errors for both loading cases, $P = \{300, 600\}$ lb could be reduced remarkably. Namely, reducing from {0.3559 percent, 0.1954 percent} (figs. 10 and 11) down respectively to {0.0479 percent, 0.0263 percent} (87-percent error reduction) (figs. 12 and 13) for the constant-domain cases, and reducing from {0.4625 percent, 0.2540 percent} (figs. 10 and 11) down respectively to {0.0283 percent, 0.0154 percent} (94-percent error reduction) (figs. 12 and 13) for the variable-domain cases.

Deflection Prediction Error Curves

Figures 14 and 15 respectively show the predicted deflection (y_i) error curves based on the deflection error data at even strain-sensing stations listed in tables 6 and 7 (piecewise-linear strain representations) and tables 8 and 9 (piecewise-nonlinear strain representations). The predicted deflection (y_i) error curves are identical for both loading cases, P = {300, 600} lb. The constant-domain cases and variable-domain cases are shown respectively with solid curves (with solid circular symbols), and dashed curves (with open square symbols). Again, the large errors (figs. 14 and 15) near the fixed end are due to a small number divided by another small number.

As shown in figures 14 and 15, changing from piecewise-linear strain representations into piecewise-nonlinear strain representations, the y_i -prediction errors could be reduced considerably in the outboard region. For example, the beam-tip deflections (y_n) prediction errors for both loading cases, P = {300, 600} lb could be reduced from 0.2090 percent down to 0.0235 percent (89 percent error reduction) for the constant-domain cases, and from 0.3199 percent down to 0.0601 percent (81 percent error deduction) for the variable-domain cases.

EXPERIMENTAL VALIDATIONS OF SHAPE-PREDICTION ACCURACIES

In the process of writing the present report, large-scale ground loads tests of the Global Observer wing (175-ft. wingspan) were carried out at NASA Dryden (now Armstrong) Flight Research Center Flight Loads Laboratory (Edwards, California) (ref. 14). The experimentally measured strains obtained from the ground tests were then used to validate the Displacement Transfer Functions accuracies. The Global Observer wing is slightly tapered and consisted of several sections joined together. Therefore, the strain-sensing stations had to be properly distributed in order to avoid positioning them at the connection junctures, and thus creating the variable-domain case. The surface strains were measured by using four fiber-optic strain-sensing lines, with two lines on the wing upper surface, and another two lines on the wing lower surface. The whole wing was loaded from 0 percent up to 100 percent Design Limit Load (DLL) at which the wing-tip slope exceeded 20 degrees, and wing-tip deflection reached nearly 14 ft. The variable-domain Displacement Transfer Function (14c), developed for the slightly nonuniform beam, was used for the wing shape calculations. Using the measured surface strain data, the wing deflections were calculated from equation (14c), and were compared with the photogrammetry data, which were used as yardsticks to estimate the shape prediction errors.

Figures 16, and 17 (duplications of figures 11 and 12 of ref. 14) respectively show the plots of the predicted and measured wing deflections along the strain-sensing lines Number 3 and Number 4. Note that the strain data points are not uniformly distributed because of variable-domains. Amazingly, the measured data points practically fell on top of the corresponding predicted deflection curves for the whole range of loading levels (0−100-percent DLL). The wing-tip deflection prediction errors based on Number 3 and Number 4 strain-sensing lines are respectively in the small ranges of (0.09−1.72 percent) and (0.25−1.45 percent) at 100-percent DLL, depending on the strain-sensing domain distances used (ref. 14).

In this ground test, it was found that by increasing the domain length from $(\Delta l)_i = 1$ in. to $(\Delta l)_i = 12$ in., the averaged wing-tip deflection prediction errors at 100-percent DLL could be reduced from 1.92 percent down to 0.27 percent (a remarkable 86-percent error reduction). This particular case certainly violates the principle that reducing the strain-sensing domains (that is, increasing the number of strain-sensing stations) can improve the shape prediction accuracies. Because of noisy strain data, increasing the number of strain-sensing stations caused more errors to be accumulated (fig. 10 of ref. 14).

This large-scale ground test results thus reinforced the previous finite-element analytical validation results (refs. 1–9), and give confidence in the shape prediction accuracies of the Variable-Domains Displacement Transfer Functions.

FACTORS AFFECTING SHAPE PREDICTION ACCURACIES

The surprising high accuracies of analytical deformed shape predictions could be attributed to the piecewise (or recursive) formulations of the Displacement Transfer Functions. The major factors affecting the shape prediction accuracies of the Displacement Transfer Functions can be listed as:

1. Domain lengths (that is, intervals of strain-sensing stations along each strain-sensing line),
2. Accuracies of piecewise-linear representations of depth-factor distributions,
3. Accuracies of piecewise-linear or piecewise-nonlinear representations of strain distributions,
4. Accuracies of the input surface strains,
5. Accuracies of depth factors determined from surface strains.

CONCLUDING REMARKS

The variable-domain Displacement Transfer Functions were formulated through piecewise integrations of the shifted curvature-strain differential equation. Using a long tapered cantilever tubular beam, the shape prediction accuracies of the variable-domain Displacement Transfer Functions were compared with the shape prediction accuracies of the constant-domain Displacement Transfer Functions formulated earlier.

Finite-element analysis was used to analytically generate surface strains. Also, the finite-element calculated slopes and deflections were used as reference yardsticks in the shape prediction error estimations. Some key results are listed below:

1. The slope and deflection equations in recursive forms developed for the constant-domain cases could be converted to those for the variable-domain cases by simply replacing the constant-domain lengths with variable-domain lengths.

2. The variable-domain Displacement Transfer Functions are highly accurate like the constant-domain Displacement Transfer Functions in shape predictions.

3. The shape prediction errors (slopes and deflections) are in the negligible ranges, with beam-tip slope (θ_n) prediction errors in the ranges of {(0.0263−0.3559 percent) and (0.0154−0.4625 percent)} respectively for the constant-domain and variable-domain cases; and the beam-tip deflection (y_n) prediction errors in the ranges of {(0.0253−0.2090 percent) and (0.0601−0.3199 percent)} respectively for the constant-domain and variable-domain cases.

4. Based on either piecewise-linear or piecewise-nonlinear strain representations, the deflection prediction errors of the constant-domain and variable-domain Displacement Transfer Functions are invariant to the loading magnitudes. However, the slope prediction errors decreased with increasing loading magnitude.

5. For piecewise-linear strain representations, changing from constant-domain cases into variable-domain cases, the beam-tip slope and deflection $\{\theta_n, y_n\}$ prediction errors increased by {30 percent and 53 percent} respectively, regardless of loading magnitude.

6. For piecewise-nonlinear strain representations, changing from constant-domain cases into variable-domain cases, regardless of loading magnitude, the beam-tip slope (θ_n) prediction errors decreased by 41 percent, however, the beam-tip deflection (y_n) prediction errors increased by 156 percent.

7. By changing from the piecewise-linear strain representations to piecewise-nonlinear strain representations, the beam-tip slope (θ_n) prediction errors could be reduced by 87 percent for the constant-domain cases, and reduced by 94 percent for the variable-domain cases.

8. By changing from the piecewise-linear strain representations to piecewise-nonlinear strain representations, the beam-tip deflection (y_n) prediction errors could be reduced by 89 percent for the constant-domain cases, and reduced by 81 percent for the variable-domain cases.

FIGURES

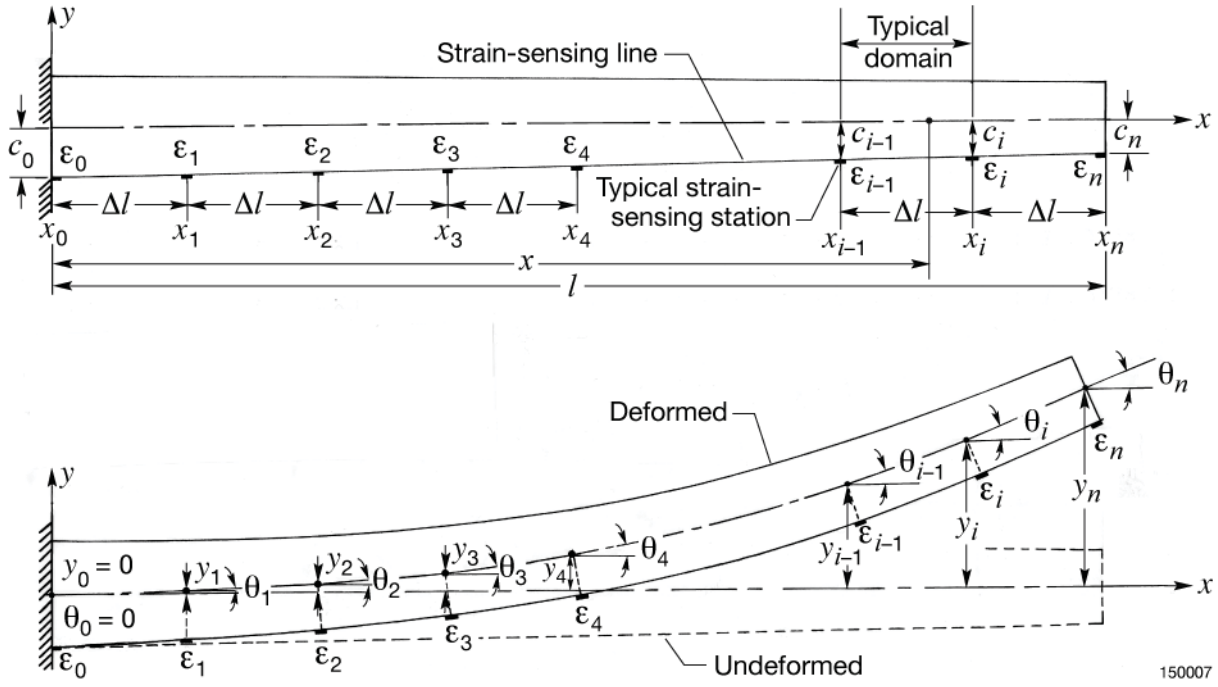

Figure 1. Embedded beam (cross section of structure, including a tubular beam) along strain-sensing line with evenly distributed strain-sensing stations.

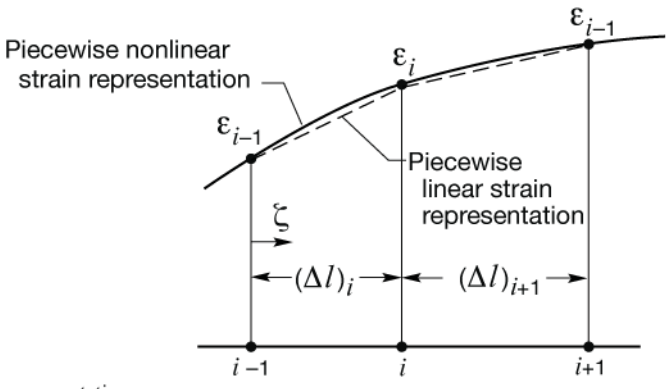

Piecewise linear strain representation:

$$\varepsilon(x) = \varepsilon_{i-1} + (\varepsilon_i - \varepsilon_{i-1})\frac{x - x_{i-1}}{(\Delta l)} \quad ; \quad (x_{i+1} \le x \le x_i)$$

Piecewise nonlinear strain representation:

$$\varepsilon(x) = \varepsilon_{i-1} - \frac{(\Delta l)_{i+1}\,[2(\Delta l)_i + (\Delta l)_{i+1}]\varepsilon_{i-1} - [(\Delta l)_i + (\Delta l)_{i+1}]^2\varepsilon_i + (\Delta l)_i^2\,\varepsilon_{i+1}}{(\Delta l)_i(\Delta l)_{i+1}\,[(\Delta l)_i + (\Delta l)_{i+1}]}\,(x - x_{i-1})$$

$$+ \frac{(\Delta l)_{i+1}\varepsilon_{i-1} - [(\Delta l)_i + (\Delta l)_{i+1}]\varepsilon_i + (\Delta l)_i\,\varepsilon_{i+1}}{(\Delta l)_i(\Delta l)_{i+1}\,[(\Delta l)_i + (\Delta l)_{i+1}]}\,(x - x_{i-1})^2$$

$$(x_{i-1} \le x \le x_i)$$

Figure 2. Piecewise linear and piecewise nonlinear representations of variable domain surface strain distribution.

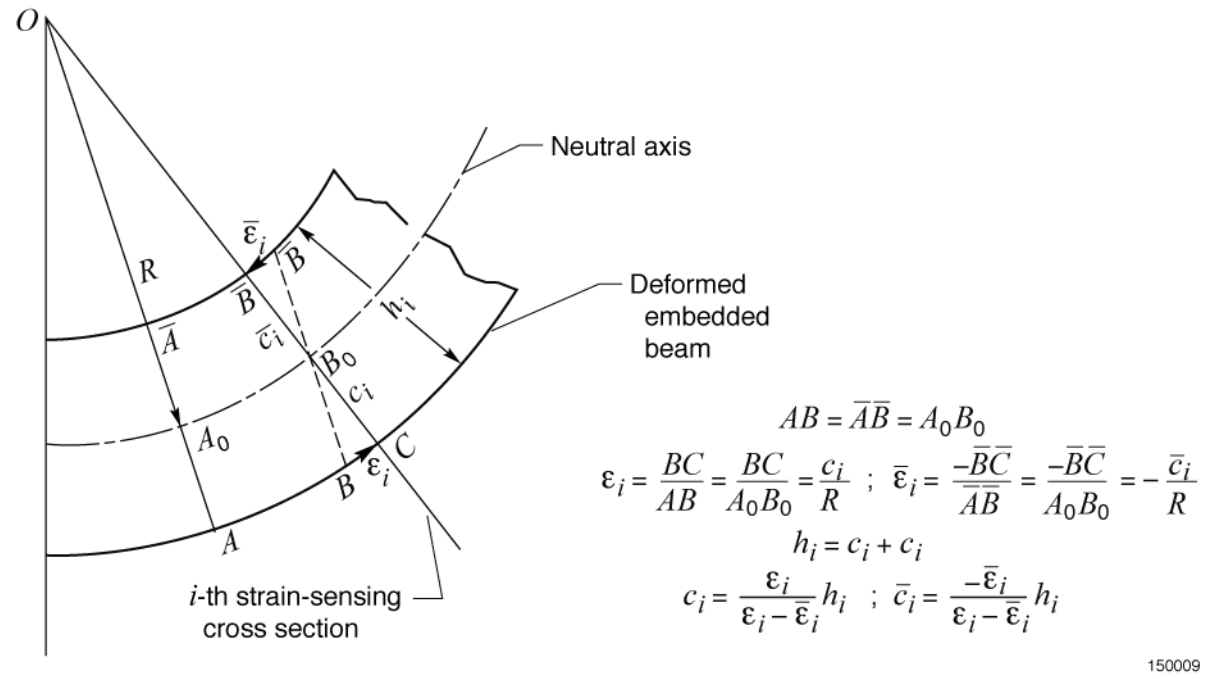

$$AB = \overline{A}\overline{B} = A_0B_0$$

$$\varepsilon_i = \frac{BC}{AB} = \frac{BC}{A_0B_0} = \frac{c_i}{R} \;\; ; \;\; \bar{\varepsilon}_i = \frac{-\overline{B}\overline{C}}{\overline{A}\overline{B}} = \frac{-\overline{B}\overline{C}}{A_0B_0} = -\frac{\bar{c}_i}{R}$$

$$h_i = c_i + \bar{c}_i$$

$$c_i = \frac{\varepsilon_i}{\varepsilon_i - \bar{\varepsilon}_i} h_i \;\; ; \;\; \bar{c}_i = \frac{-\bar{\varepsilon}_i}{\varepsilon_i - \bar{\varepsilon}_i} h_i$$

Figure 3. Segment of deformed embedded beam used for geometrically relate lower and upper surface strains, $\{\varepsilon_i, \bar{\varepsilon}_i\}$, to lower and upper depth factors, $\{c_i, \bar{c}_i\}$.

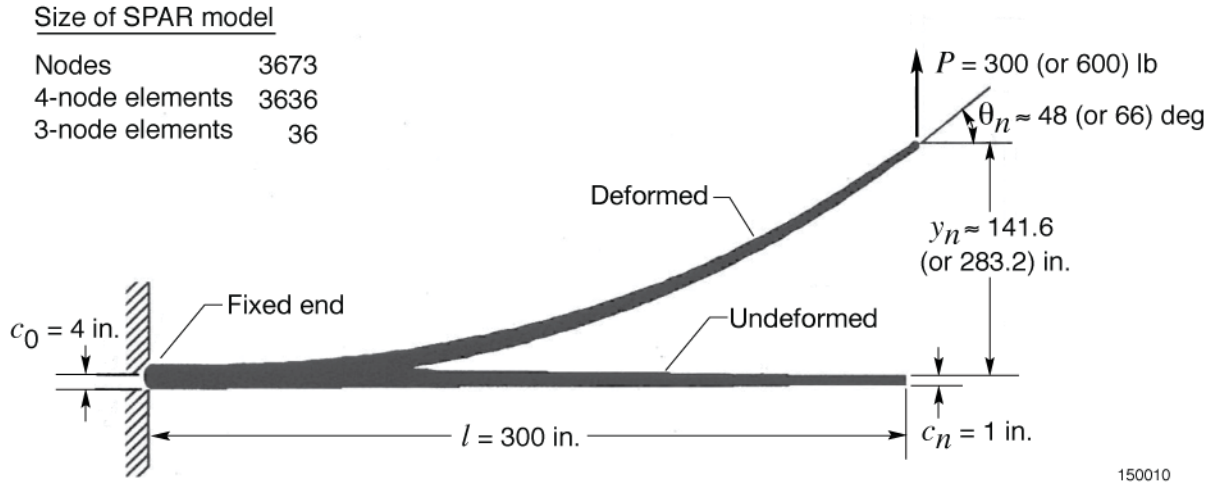

Figure 4. Large deformations of tapered cantilever tubular beam (SPAR finite-element model) subjected to upward tip load of P = 300 lb (or P = 600 lb); l = 300 in., c_0 = 4 in., c_n = 1 in.

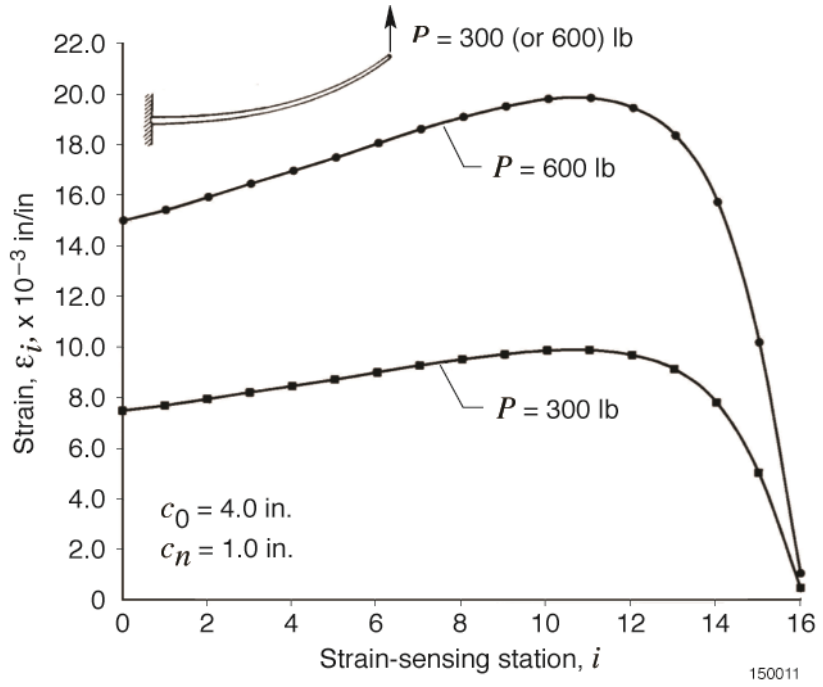

Figure 5. SPAR-generated surface strain curves for tapered cantilever tubular beam subjected to to upward tip load of P = 300 lb (or P = 600 lb); l = 300 in., c_0 = 4 in., c_n = 1 in.

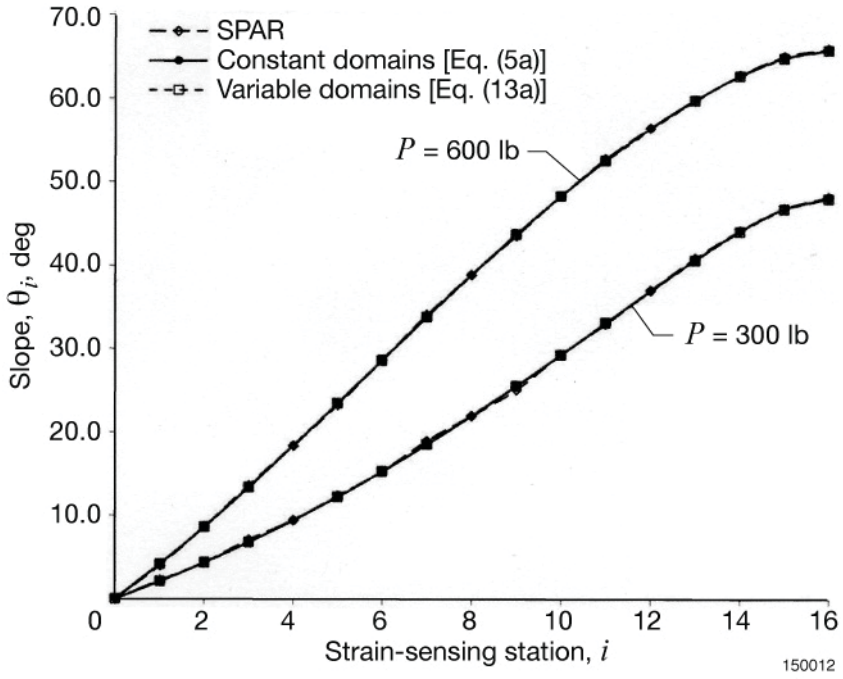

Figure 6. Slopes, θ_i, of tapered cantilever tubular beam calculated from constant domain and variable domain slope equations [(5a), and (13a)] (piecewise linear strain representations); l = 300 in., c_0 = 4 in., c_n = 1 in.; P = {300, 600} lb.

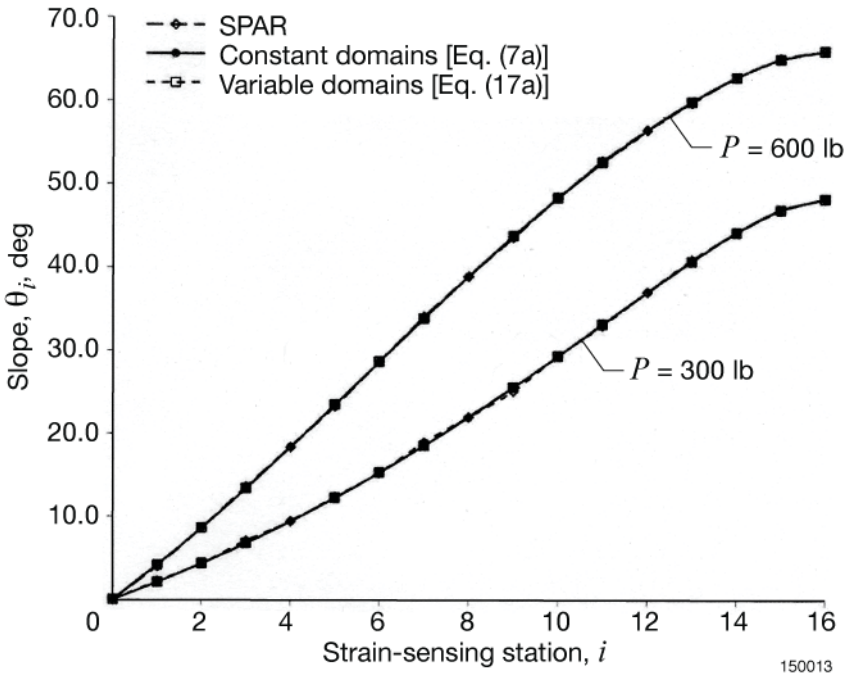

Figure 7. Slopes, θ_i, of tapered cantilever tubular beam calculated from constant domain and variable domain slope equations [(7a), and (17a)] (piecewise nonlinear strain representations); l = 300 in., c_0 = 4 in., c_n = 1 in.; P = {300, 600} lb.

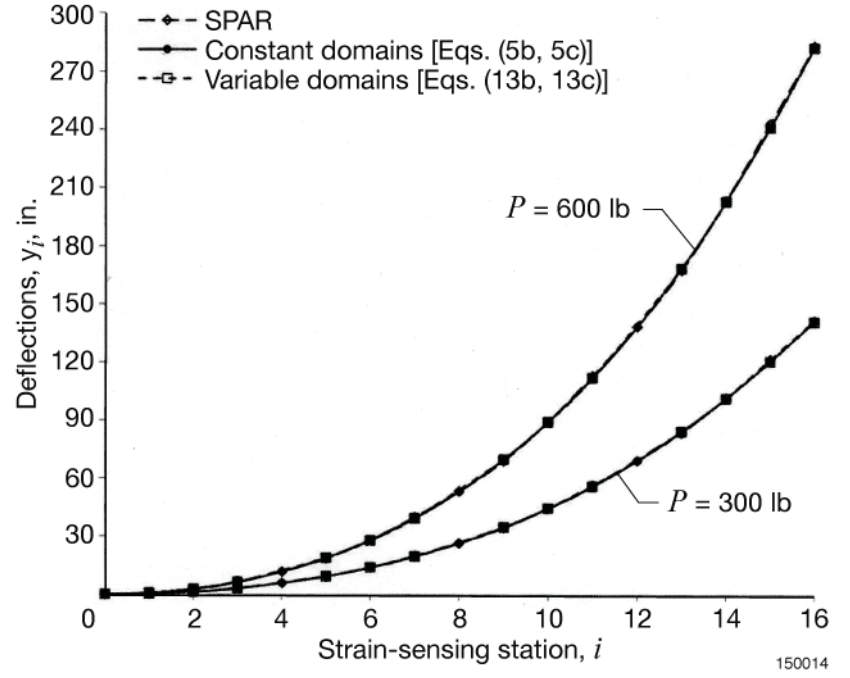

Figure 8. Deflections, y_i, of tapered cantilever tubular beam calculated from constant domain and variable domain deflection equations [(5b, (5c), (13b), and (13c)] (piecewise linear strain representations); l = 300 in., c_0 = 4 in., c_n = 1 in.; P = {300, 600} lb.

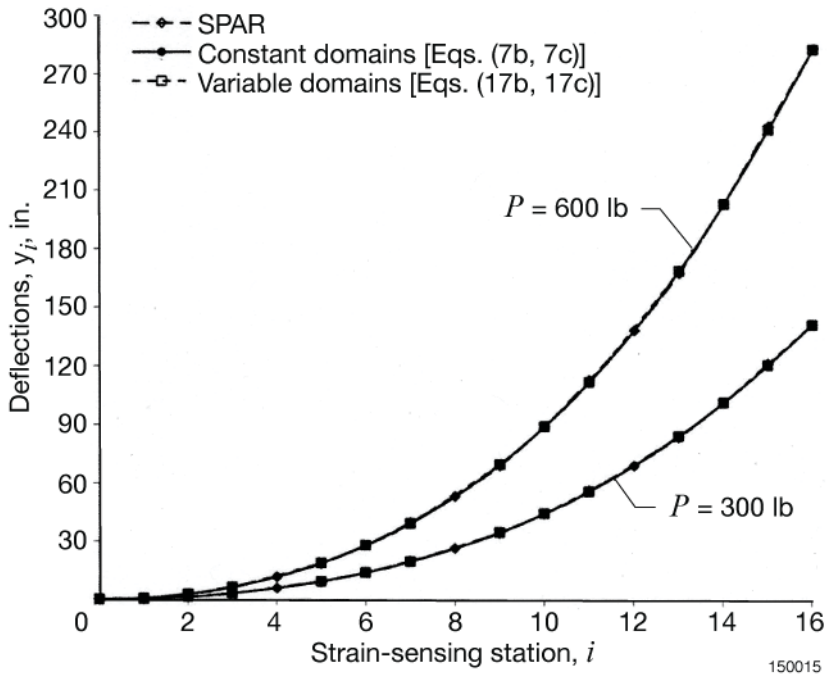

Figure 9. Deflections, y_i, of tapered cantilever tubular beam calculated from constant domain and variable domain deflection equations [(7b), (7c), (17b), and (17c)] (piecewise nonlinear strain representations); l = 300 in., c_0 = 4 in., c_n = 1 in.; P = {300, 600} lb.

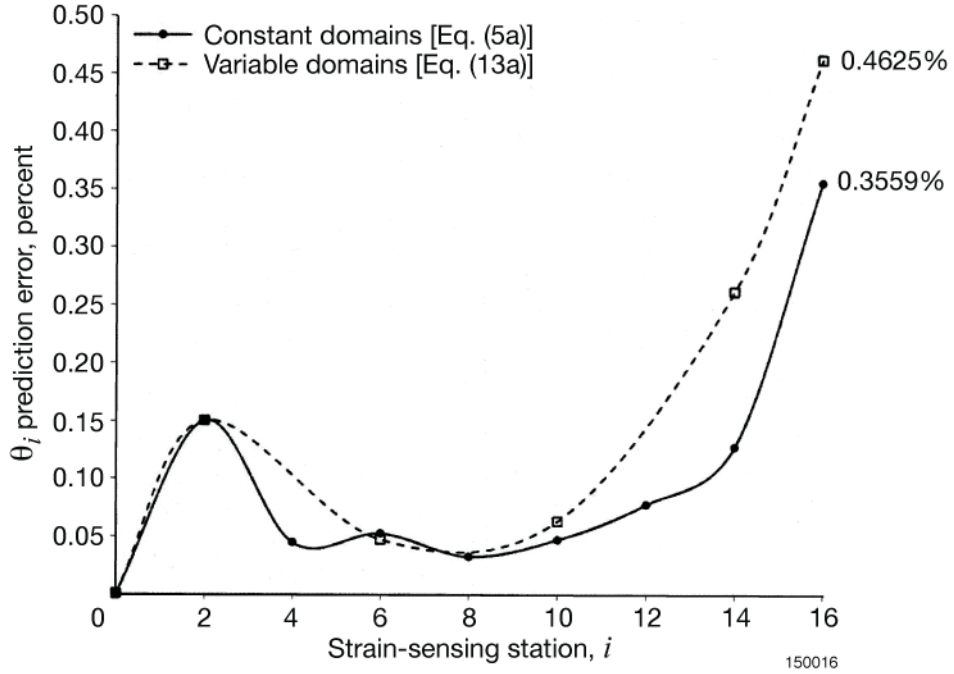

Figure 10. Comparison of slope (θ_i) prediction errors of constant domain and variable domain slope equations [(5a), and (13a)] (piecewise linear strain representations); tapered cantilever tubular beam; l = 300 in, c_0 = 4 in., c_n = 1 in.; P = 300 lb.

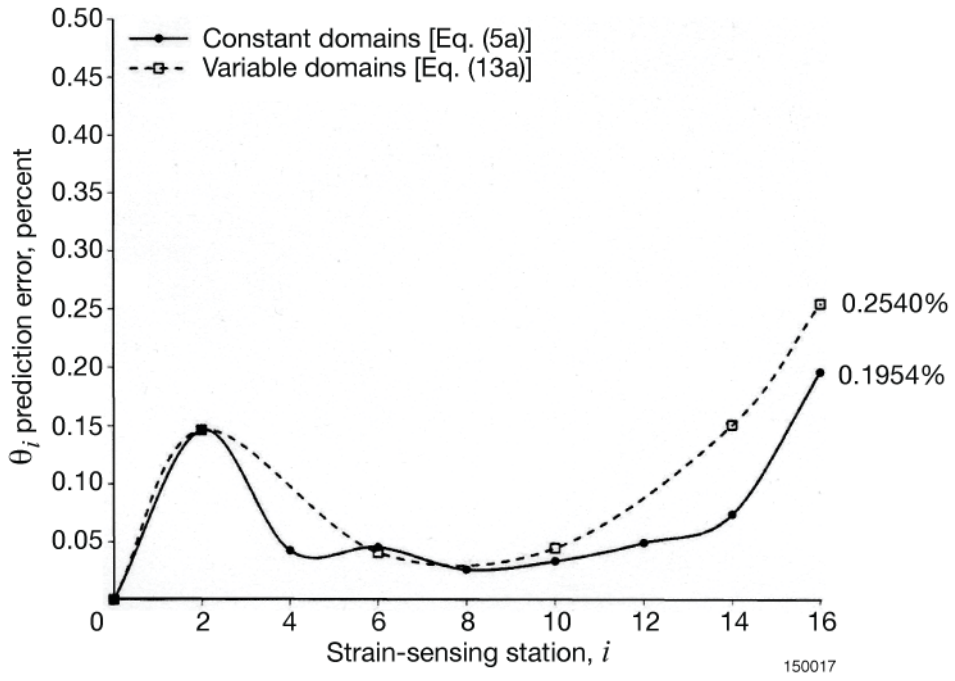

Figure 11. Comparison of slope (θ_i) prediction errors of constant domain and variable domain slope equations [(5a), and (13a)] (piecewise linear strain representations); tapered cantilever tubular beam; l = 300 in, c_0 = 4 in., c_n = 1 in.; P = 600 lb.

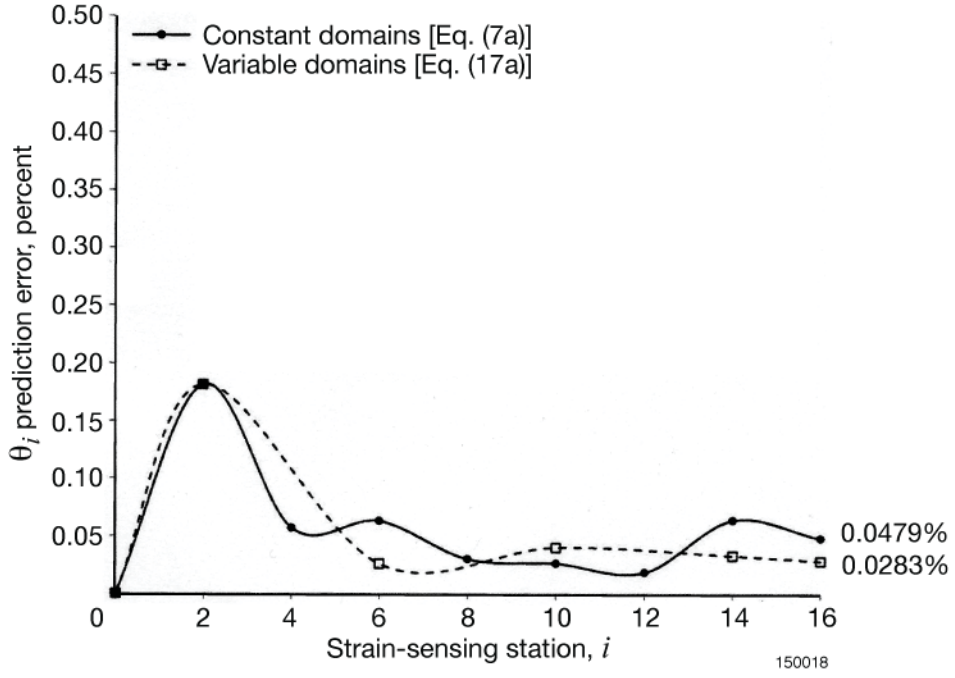

Figure 12. Comparison of slope (θ_i) prediction errors of constant domain and variable domain slope equations [(7a), and (17a)] (piecewise nonlinear strain representations); tapered cantilever tubular beam; l = 300 in, c_0 = 4 in., c_n = 1 in.; P = 300 lb.

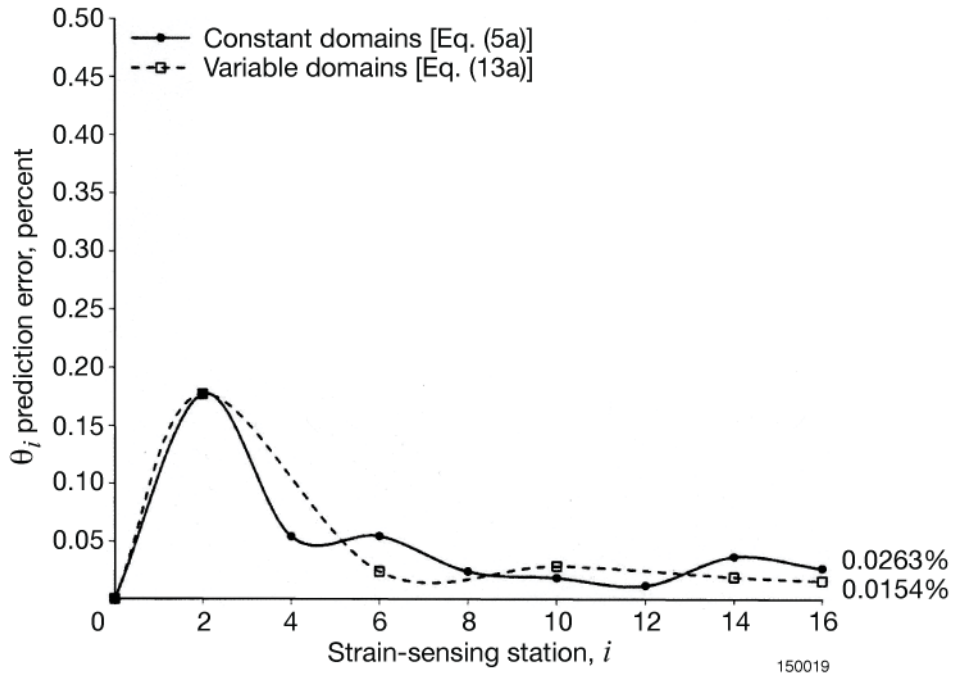

Figure 13. Comparison of slope (θ_i) prediction errors of constant domain and variable domain slope equations [(7a), and (17a)] (piecewise nonlinear strain representations); tapered cantilever tubular beam; l = 300 in, c_0 = 4 in., c_n = 1 in.; P = 600 lb.

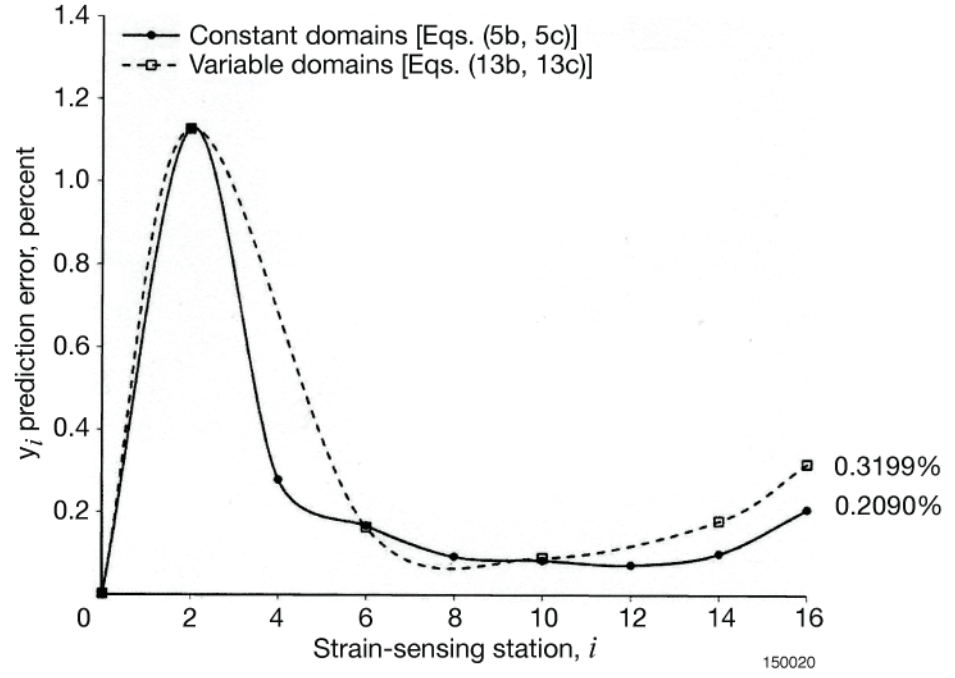

Figure 14. Comparisons of deflection (y_i) prediction errors of constant domain and variable domain deflection equations [(5b), (5c), (13b), and (13c))] (piecewise linear strain representations); tapered cantilever tubular beam; l = 300 in, c_0 = 4 in., c_n = 1 in.; P = {300, 600} lb.

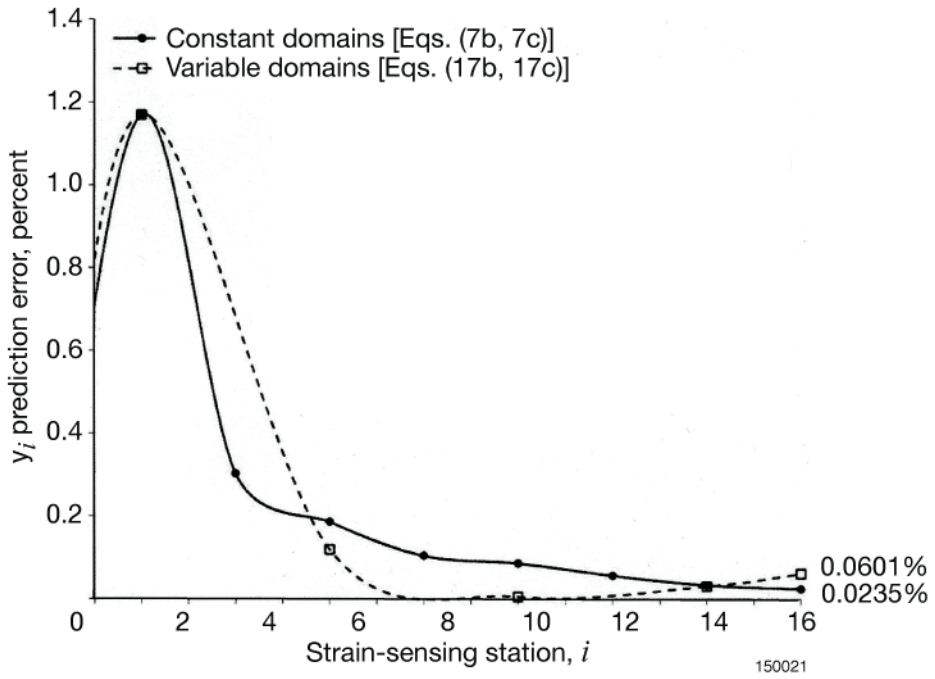

Figure 15. Comparisons of deflection (y_i) prediction errors of constant domain and variable domain deflection equations [(7b), (7c)), (17b), and (17c)] (piecewise linear strain representations); tapered cantilever tubular beam; l = 300 in, c_0 = 4 in., c_n = 1 in.; P = {300, 600} lb.

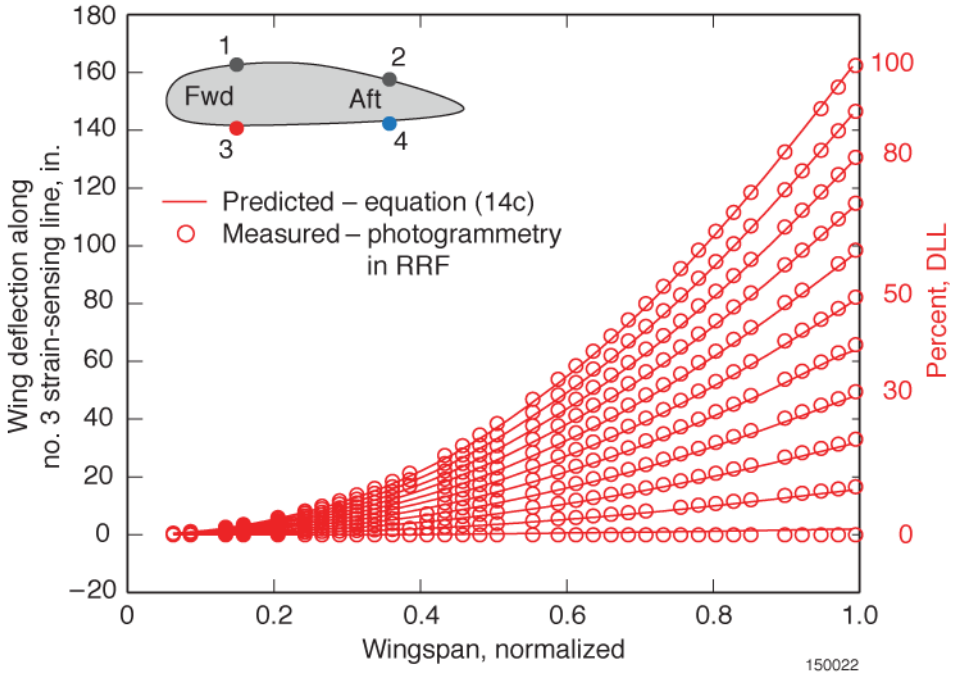

Figure 16. Comparison of predicted and measured wing deflections along No. 3 strain-sensing line for different loading levels (duplication of figure 11, ref. 14).

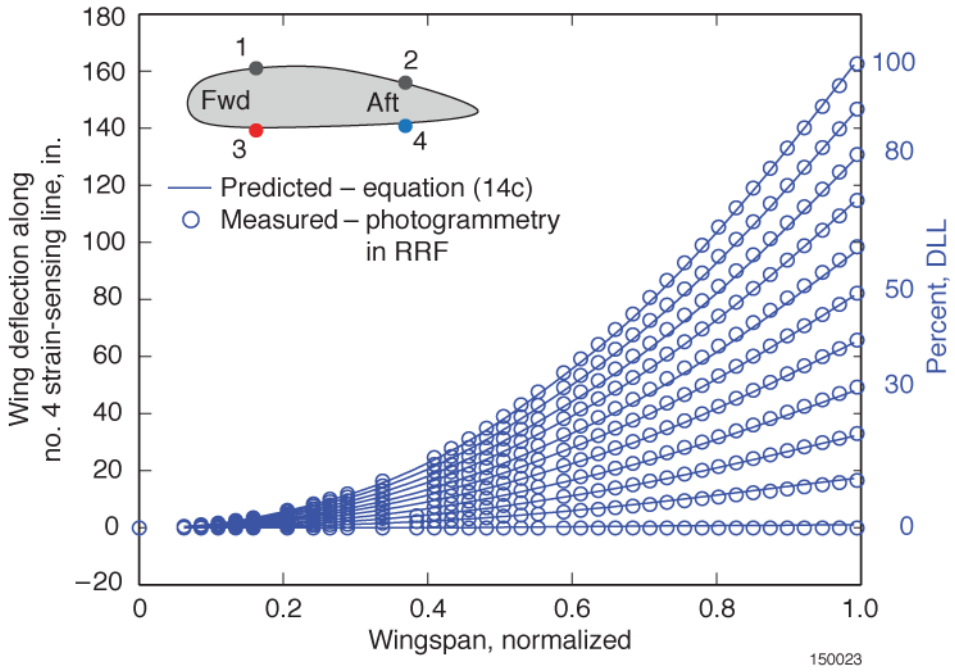

Figure 17. Comparison of predicted and measured wing deflections along No. 4 strain-sensing line for different loading levels (duplication of figure 12, ref. 14).

APPENDIX A
DERIVATION OF STRAIN FUNCTION FOR VARIABLE DOMAIN PIECEWISE-NONLINEAR STRAIN REPRESENTATIONS

Let $\xi(\equiv x - x_{i-1})$ be the local axial coordinate measured from the strain-sensing station, x_{i-1} (fig. 2), and let the distribution of strain, $\varepsilon(\xi)$, within the two adjacent domains, $x_{i-1} \le x \le x_i$ and $x_i \le x \le x_{i+1}$, be presented by the following nonlinear function (quadratic equation) (fig. 2):

$$\varepsilon(\xi) = a + b\xi + e\xi^2 \quad ; \quad \xi \equiv x - x_{i-1} \tag{A1}$$

where *a*, *b*, and *e* are coefficients, which are to be determined in terms of three strains, $\{\varepsilon_{i-1}, \varepsilon_i, \varepsilon_{i+1}\}$ respectively at three strain-sensing stations, $\{x_{i-1}, x_i, x_{i+1}\}$.

At $\xi \equiv 0$ (i.e., at strain-sensing station, x_{i-1}), we have $\varepsilon(0) = \varepsilon_{i-1}$, and equation (A1) gives:

$$a = \varepsilon_{i-1} \tag{A2}$$

At $\xi \equiv (\Delta l)_i$ (that is, at strain-sensing station, x_i), we have $\varepsilon[(\Delta l)_i] = \varepsilon_i$, then in view of equation (A2), equation (A1) can be written as equation (A3):

$$\varepsilon_i = \varepsilon_{i-1} + b(\Delta l)_i + e(\Delta l)_i^2 \tag{A3}$$

which can be rewritten as equation (A4):

$$b + e(\Delta l)_i = \frac{\varepsilon_i - \varepsilon_{i-1}}{(\Delta l)_i} \tag{A4}$$

At $\xi \equiv (\Delta l)_i + (\Delta l)_{i+1}$ (that is, at strain-sensing station, x_{i+1}), we have $\varepsilon[(\Delta l)_i + (\Delta l)_{i+1}] = \varepsilon_{i+1}$. Then in view of equation (A2), equation (A1) can be written as equation (A5):

$$\varepsilon_{i+1} = \varepsilon_{i-1} + b[(\Delta l)_i + (\Delta l)_{i+1}] + e[(\Delta l)_i + (\Delta l)_{i+1}]^2 \tag{A5}$$

which can be rewritten as equation (A6):

$$b + e[(\Delta l)_i + (\Delta l)_{i+1}] = \frac{\varepsilon_{i+1} - \varepsilon_{i-1}}{(\Delta l)_i + (\Delta l)_{i+1}} \tag{A6}$$

Subtracting equation (A4) from (A6), one can eliminate *b* and obtain the expression for *e* as equation (A7):

$$\begin{aligned} e(\Delta l)_{i+1} &= \frac{\varepsilon_{i+1} - \varepsilon_{i-1}}{(\Delta l)_i + (\Delta l)_{i+1}} - \frac{\varepsilon_i - \varepsilon_{i-1}}{(\Delta l)_i} \\ &= \frac{(\Delta l)_i(\varepsilon_{i+1} - \varepsilon_{i-1}) - [(\Delta l)_i + (\Delta l)_{i+1}](\varepsilon_i - \varepsilon_{i-1})}{(\Delta l)_i[(\Delta l)_i + (\Delta l)_{i+1}]} \end{aligned}$$

$$= \frac{(\Delta l)_i \varepsilon_{i+1} - (\Delta l)_i \varepsilon_{i-1} - [(\Delta l)_i + (\Delta l)_{i+1}]\varepsilon_i + [(\Delta l)_i + (\Delta l)_{i+1}]\varepsilon_{i-1}}{(\Delta l)_i[(\Delta l)_i + (\Delta l)_{i+1}]} \tag{A7}$$

From equation (A7), e can be written as:

$$e = \frac{(\Delta l)_{i+1} \varepsilon_{i-1} - [(\Delta l)_i + (\Delta l)_{i+1}]\varepsilon_i + (\Delta l)_i \varepsilon_{i+1}}{(\Delta l)_i (\Delta l)_{i+1}[(\Delta l)_i + (\Delta l)_{i+1}]} \tag{A8}$$

Substitution of equation (A8) into equation (A4) yields equation (A9):

$$\begin{aligned} b &= \frac{\varepsilon_i - \varepsilon_{i-1}}{(\Delta l)_i} - \frac{(\Delta l)_{i+1} \varepsilon_{i-1} - [(\Delta l)_i + (\Delta l)_{i+1}]\varepsilon_i + (\Delta l)_i \varepsilon_{i+1}}{(\Delta l)_i (\Delta l)_{i+1}[(\Delta l)_i + (\Delta l)_{i+1}]} (\Delta l)_i \\ &= \frac{(\Delta l)_{i+1}[(\Delta l)_i + (\Delta l)_{i+1}](\varepsilon_i - \varepsilon_{i-1}) - (\Delta l)_i (\Delta l)_{i+1} \varepsilon_{i-1} + (\Delta l)_i [(\Delta l)_i + (\Delta l)_{i+1}]\varepsilon_i - (\Delta l)_i^2 \varepsilon_{i+1}}{(\Delta l)_i (\Delta l)_{i+1}[(\Delta l)_i + (\Delta l)_{i+1}]} \\ &= \frac{1}{(\Delta l)_i (\Delta l)_{i+1}[(\Delta l)_i + (\Delta l)_{i+1}]} \begin{bmatrix} -(\Delta l)_{i+1}[(\Delta l)_i + (\Delta l)_{i+1}]\varepsilon_{i-1} + (\Delta l)_{i+1}[(\Delta l)_i + (\Delta l)_{i+1}]\varepsilon_i \\ -(\Delta l)_i (\Delta l)_{i+1} \varepsilon_{i-1} + (\Delta l)_i [(\Delta l)_i + (\Delta l)_{i+1}]\varepsilon_i - (\Delta l)_i^2 \varepsilon_{i+1} \end{bmatrix} \end{aligned} \tag{A9}$$

After grouping terms, one obtains the expression for b as equation (A10):

$$b = -\frac{(\Delta l)_{i+1}[2(\Delta l)_i + (\Delta l)_{i+1}]\varepsilon_{i-1} - [(\Delta l)_i + (\Delta l)_{i+1}]^2 \varepsilon_i + (\Delta l)_i^2 \varepsilon_{i+1}}{(\Delta l)_i (\Delta l)_{i+1}[(\Delta l)_i + (\Delta l)_{i+1}]} \tag{A10}$$

In view of equations (A2), (A8), and (A10), equation (A1) can be written as equation (A11):

$$\begin{aligned} \varepsilon(x) = \varepsilon_{i-1} &- \frac{(\Delta l)_{i+1}[2(\Delta l)_i + (\Delta l)_{i+1}]\varepsilon_{i-1} - [(\Delta l)_i + (\Delta l)_{i+1}]^2 \varepsilon_i + (\Delta l)_i^2 \varepsilon_{i+1}}{(\Delta l)_i (\Delta l)_{i+1}[(\Delta l)_i + (\Delta l)_{i+1}]} (x - x_{i-1}) \\ &+ \frac{(\Delta l)_{i+1} \varepsilon_{i-1} - [(\Delta l)_i + (\Delta l)_{i+1}]\varepsilon_i + (\Delta l)_i \varepsilon_{i+1}}{(\Delta l)_i (\Delta l)_{i+1}[(\Delta l)_i + (\Delta l)_{i+1}]} (x - x_{i-1})^2 \end{aligned} \tag{A11}$$

which is equation (11) in the text.

For the constant-domain case, $(\Delta l)_{i-1} = (\Delta l)_i = (\Delta l)_{i+1} = \Delta l$, equation (A11) can be simplified as equation (A12):

$$\varepsilon(x) = \varepsilon_{i-1} - \frac{3\varepsilon_{i-1} - 4\varepsilon_i + \varepsilon_{i+1}}{2\Delta l}(x - x_{i-1}) + \frac{\varepsilon_{i-1} - 2\varepsilon_i + \varepsilon_{i+1}}{2(\Delta l)^2}(x - x_{i-1})^2 \tag{A12}$$

Equation (A12) is identical to equation (4a) in the text.

APPENDIX B
DERIVATION OF VARIABLE-DOMAIN DISPLACEMENT TRANSFER FUNCTIONS FOR NONUNIFORM EMBEDDED BEAMS

(Based on Piecewise-Linear Strain Representations)

The slope equation (13a) and the deflection equation (13b) for nonuniform beams, based on piecewise-linear representations of both depth factors and surface strains, are duplicated below as equations (B1) and (B2).

Slope equation:

$$\tan\theta_i = (\Delta l)_i \left[\frac{\varepsilon_{i-1} - \varepsilon_i}{c_{i-1} - c_i} + \frac{\varepsilon_{i-1} c_i - \varepsilon_i c_{i-1}}{(c_{i-1} - c_i)^2} \log_e \frac{c_i}{c_{i-1}} \right] + \tan\theta_{i-1} \qquad (B1)$$

$$(i = 1,2,3,....,n)$$

Deflection equation:

$$y_i = (\Delta l)_i^2 \left\{ \frac{\varepsilon_{i-1} - \varepsilon_i}{2(c_{i-1} - c_i)} - \frac{\varepsilon_{i-1} c_i - \varepsilon_i c_{i-1}}{(c_{i-1} - c_i)^3} \left[c_i \log_e \frac{c_i}{c_{i-1}} + (c_{i-1} - c_i) \right] \right\} + y_{i-1} + (\Delta l)_i \tan\theta_{i-1} \qquad (B2)$$

$$(i = 1,2,3,....,n)$$

Writing out equation (B2) for different indices, $i\ (=1,2,3,....,n)$, and considering the indicial relationships expressed in equations (B1) and (B2), one obtains equation (B3):

For $i = 1$:

$$y_1 = (\Delta l)_1^2 \left\{ \frac{\varepsilon_0 - \varepsilon_1}{2(c_0 - c_1)} - \frac{\varepsilon_0 c_1 - \varepsilon_1 c_0}{(c_0 - c_1)^3} \left[c_1 \log_e \frac{c_1}{c_0} + (c_0 - c_1) \right] \right\} + y_0 + (\Delta l)_1 \tan\theta_0 \qquad (B3)$$

For $i = 2$:

$$
\begin{aligned}
y_2 &= (\Delta l)_2^2 \left\{ \frac{\varepsilon_1 - \varepsilon_2}{2(c_1 - c_2)} - \frac{\varepsilon_1 c_2 - \varepsilon_2 c_1}{(c_1 - c_2)^3} \left[c_2 \log_e \frac{c_2}{c_1} + (c_1 - c_2) \right] \right\} + y_1 + (\Delta l)_2 \tan\theta_1 \\
&= (\Delta l)_2^2 \left\{ \frac{\varepsilon_1 - \varepsilon_2}{2(c_1 - c_2)} - \frac{\varepsilon_1 c_2 - \varepsilon_2 c_1}{(c_1 - c_2)^3} \left[c_2 \log_e \frac{c_2}{c_1} + (c_1 - c_2) \right] \right\} \\
&\quad \overbrace{+ (\Delta l)_1^2 \left\{ \frac{\varepsilon_0 - \varepsilon_1}{2(c_0 - c_1)} - \frac{\varepsilon_0 c_1 - \varepsilon_1 c_0}{(c_0 - c_1)^3} \left[c_1 \log_e \frac{c_1}{c_0} + (c_0 - c_1) \right] \right\}}^{y_1} + y_0 + (\Delta l)_1 \tan\theta_0 \\
&\quad + (\Delta l)_2 \overbrace{\left\{ (\Delta l)_1\left[\frac{\varepsilon_0 - \varepsilon_1}{c_0 - c_1} + \frac{\varepsilon_0 c_1 - \varepsilon_1 c_0}{(c_0 - c_1)^2} \log_e \frac{c_1}{c_0} \right] + \tan\theta_0 \right\}}^{\tan\theta_1}
\end{aligned}
\tag{B4}
$$

After grouping terms, equation (B4) becomes:

$$
\begin{aligned}
y_2 &= (\Delta l)_2^2 \left\{ \frac{\varepsilon_1 - \varepsilon_2}{2(c_1 - c_2)} - \frac{\varepsilon_1 c_2 - \varepsilon_2 c_1}{(c_1 - c_2)^3} \left[c_2 \log_e \frac{c_2}{c_1} + (c_1 - c_2) \right] \right\} \\
&\quad + (\Delta l)_1^2 \left\{ \frac{\varepsilon_0 - \varepsilon_1}{2(c_0 - c_1)} - \frac{\varepsilon_0 c_1 - \varepsilon_1 c_0}{(c_0 - c_1)^3} \left[c_1 \log_e \frac{c_1}{c_0} + (c_0 - c_1) \right] \right\} \\
&\quad + (\Delta l)_2 \left\{ (\Delta l)_1 \left[\frac{\varepsilon_0 - \varepsilon_1}{c_0 - c_1} + \frac{\varepsilon_0 c_1 - \varepsilon_1 c_0}{(c_0 - c_1)^2} \log_e \frac{c_1}{c_0} \right] \right\} + y_0 + \left[(\Delta l)_1 + (\Delta l)_2 \right] \tan\theta_0
\end{aligned}
\tag{B5}
$$

For $i = 3$:

$$y_3 = (\Delta l)_3^2 \left\{ \frac{\varepsilon_2 - \varepsilon_3}{2(c_2 - c_3)} - \frac{\varepsilon_2 c_3 - \varepsilon_3 c_2}{(c_2 - c_3)^3} \left[c_3 \log_e \frac{c_3}{c_2} + (c_2 - c_3) \right] \right\} + y_2 + (\Delta l)_3 \tan\theta_2$$

$$= (\Delta l)_3^2 \left\{ \frac{\varepsilon_2 - \varepsilon_3}{2(c_2 - c_3)} - \frac{\varepsilon_2 c_3 - \varepsilon_3 c_2}{(c_2 - c_3)^3} \left[c_3 \log_e \frac{c_3}{c_2} + (c_2 - c_3) \right] \right\}$$

$$+ \overbrace{\left\{ \begin{array}{l} (\Delta l)_2^2 \left\{ \frac{\varepsilon_1 - \varepsilon_2}{2(c_1 - c_2)} - \frac{\varepsilon_1 c_2 - \varepsilon_2 c_1}{(c_1 - c_2)^3} \left[c_2 \log_e \frac{c_2}{c_1} + (c_1 - c_2) \right] \right\} \\ + (\Delta l)_1^2 \left\{ \frac{\varepsilon_0 - \varepsilon_1}{2(c_0 - c_1)} - \frac{\varepsilon_0 c_1 - \varepsilon_1 c_0}{(c_0 - c_1)^3} \left[c_1 \log_e \frac{c_1}{c_0} + (c_0 - c_1) \right] \right\} \\ + (\Delta l)_2 (\Delta l)_1 \left[\frac{\varepsilon_0 - \varepsilon_1}{c_0 - c_1} + \frac{\varepsilon_0 c_1 - \varepsilon_1 c_0}{(c_0 - c_1)^2} \log_e \frac{c_1}{c_0} \right] + y_0 + \left[(\Delta l)_1 + (\Delta l)_2 \right] \tan\theta_0 \end{array} \right\}}^{y_2} \quad \text{(B6)}$$

$$+ (\Delta l)_3 \overbrace{\left\{ (\Delta l)_2 \left[\frac{\varepsilon_1 - \varepsilon_2}{c_1 - c_2} + \frac{\varepsilon_1 c_2 - \varepsilon_2 c_1}{(c_1 - c_2)^2} \log_e \frac{c_2}{c_1} \right] + (\Delta l)_1 \left[\frac{\varepsilon_0 - \varepsilon_1}{c_0 - c_1} + \frac{\varepsilon_0 c_1 - \varepsilon_1 c_0}{(c_0 - c_1)^2} \log_e \frac{c_1}{c_0} \right] + \tan\theta_0 \right\}}^{\tan\theta_2}$$

After grouping terms, equation (B6) becomes equation (B7):

$$\begin{aligned} y_3 = {} & (\Delta l)_3^2 \left\{ \frac{\varepsilon_2 - \varepsilon_3}{2(c_2 - c_3)} - \frac{\varepsilon_2 c_3 - \varepsilon_3 c_2}{(c_2 - c_3)^3} \left[c_3 \log_e \frac{c_3}{c_2} + (c_2 - c_3) \right] \right\} \\ & + (\Delta l)_2^2 \left\{ \frac{\varepsilon_1 - \varepsilon_2}{2(c_1 - c_2)} - \frac{\varepsilon_1 c_2 - \varepsilon_2 c_1}{(c_1 - c_2)^3} \left[c_2 \log_e \frac{c_2}{c_1} + (c_1 - c_2) \right] \right\} \\ & + (\Delta l)_1^2 \left\{ \frac{\varepsilon_0 - \varepsilon_1}{2(c_0 - c_1)} - \frac{\varepsilon_0 c_1 - \varepsilon_1 c_0}{(c_0 - c_1)^3} \left[c_1 \log_e \frac{c_1}{c_0} + (c_0 - c_1) \right] \right\} \\ & + (\Delta l)_3 \left\{ (\Delta l)_2 \left[\frac{\varepsilon_1 - \varepsilon_2}{c_1 - c_2} + \frac{\varepsilon_1 c_2 - \varepsilon_2 c_1}{(c_1 - c_2)^2} \log_e \frac{c_2}{c_1} \right] \right\} \\ & + \left[(\Delta l)_3 + (\Delta l)_2 \right] \left\{ (\Delta l)_1 \left[\frac{\varepsilon_0 - \varepsilon_1}{c_0 - c_1} + \frac{\varepsilon_0 c_1 - \varepsilon_1 c_0}{(c_0 - c_1)^2} \log_e \frac{c_1}{c_0} \right] \right\} \\ & + y_0 + \left[(\Delta l)_1 + (\Delta l)_2 + (\Delta l)_3 \right] \tan\theta_0 \end{aligned} \quad \text{(B7)}$$

For $i = 4$:

$$
\begin{aligned}
y_4 &= (\Delta l)_4^2 \left\{ \frac{\varepsilon_3 - \varepsilon_4}{2(c_3 - c_4)} - \frac{\varepsilon_3 c_4 - \varepsilon_4 c_3}{(c_3 - c_4)^3} \left[c_4 \log_e \frac{c_4}{c_3} + (c_3 - c_4) \right] \right\} + y_3 + (\Delta l)_4 \tan\theta_3 \\
&= (\Delta l)_4^2 \left\{ \frac{\varepsilon_3 - \varepsilon_4}{2(c_3 - c_4)} - \frac{\varepsilon_3 c_4 - \varepsilon_4 c_3}{(c_3 - c_4)^3} \left[c_4 \log_e \frac{c_4}{c_3} + (c_3 - c_4) \right] \right\} \\
&\quad \overbrace{\left\{ \begin{aligned}
&(\Delta l)_3^2 \left\{ \frac{\varepsilon_2 - \varepsilon_3}{2(c_2 - c_3)} - \frac{\varepsilon_2 c_3 - \varepsilon_3 c_2}{(c_2 - c_3)^3} \left[c_3 \log_e \frac{c_3}{c_2} + (c_2 - c_3) \right] \right\} \\
&+ (\Delta l)_2^2 \left\{ \frac{\varepsilon_1 - \varepsilon_2}{2(c_1 - c_2)} - \frac{\varepsilon_1 c_2 - \varepsilon_2 c_1}{(c_1 - c_2)^3} \left[c_2 \log_e \frac{c_2}{c_1} + (c_1 - c_2) \right] \right\} \\
&+ (\Delta l)_1^2 \left\{ \frac{\varepsilon_0 - \varepsilon_1}{2(c_0 - c_1)} - \frac{\varepsilon_0 c_1 - \varepsilon_1 c_0}{(c_0 - c_1)^3} \left[c_1 \log_e \frac{c_1}{c_0} + (c_0 - c_1) \right] \right\} \\
&+ (\Delta l)_3 \left\{ (\Delta l)_2 \left[\frac{\varepsilon_1 - \varepsilon_2}{c_1 - c_2} + \frac{\varepsilon_1 c_2 - \varepsilon_2 c_1}{(c_1 - c_2)^2} \log_e \frac{c_2}{c_1} \right] \right\} \\
&+ \left[(\Delta l)_3 + (\Delta l)_2 \right] \left\{ (\Delta l)_1 \left[\frac{\varepsilon_0 - \varepsilon_1}{c_0 - c_1} + \frac{\varepsilon_0 c_1 - \varepsilon_1 c_0}{(c_0 - c_1)^2} \log_e \frac{c_1}{c_0} \right] \right\} \\
&+ y_0 + \left[(\Delta l)_1 + (\Delta l)_2 + (\Delta l)_3 \right] \tan\theta_0
\end{aligned} \right.}^{y_3} \\
&+ (\Delta l)_4 \overbrace{\left\{ \begin{aligned}
&(\Delta l)_3 \left[\frac{\varepsilon_2 - \varepsilon_3}{c_2 - c_3} + \frac{\varepsilon_2 c_3 - \varepsilon_3 c_2}{(c_2 - c_3)^2} \log_e \frac{c_3}{c_2} \right] + (\Delta l)_2 \left[\frac{\varepsilon_1 - \varepsilon_2}{c_1 - c_2} + \frac{\varepsilon_1 c_2 - \varepsilon_2 c_1}{(c_1 - c_2)^2} \log_e \frac{c_2}{c_1} \right] \\
&+ (\Delta l)_1 \left[\frac{\varepsilon_0 - \varepsilon_1}{c_0 - c_1} + \frac{\varepsilon_0 c_1 - \varepsilon_1 c_0}{(c_0 - c_1)^2} \log_e \frac{c_1}{c_0} \right] + \tan\theta_0
\end{aligned} \right\}}^{\tan\theta_3}
\end{aligned}
\tag{B8}
$$

After grouping terms, equation (B8) becomes equation (B9):

$$
\begin{aligned}
y_4 = {} & (\Delta l)_4^2 \left\{ \frac{\varepsilon_3 - \varepsilon_4}{2(c_3 - c_4)} - \frac{\varepsilon_3 c_4 - \varepsilon_4 c_3}{(c_3 - c_4)^3} \left[c_4 \log_e \frac{c_4}{c_3} + (c_3 - c_4) \right] \right\} \\
& + (\Delta l)_3^2 \left\{ \frac{\varepsilon_2 - \varepsilon_3}{2(c_2 - c_3)} - \frac{\varepsilon_2 c_3 - \varepsilon_3 c_2}{(c_2 - c_3)^3} \left[c_3 \log_e \frac{c_3}{c_2} + (c_2 - c_3) \right] \right\} \\
& + (\Delta l)_2^2 \left\{ \frac{\varepsilon_1 - \varepsilon_2}{2(c_1 - c_2)} - \frac{\varepsilon_1 c_2 - \varepsilon_2 c_1}{(c_1 - c_2)^3} \left[c_2 \log_e \frac{c_2}{c_1} + (c_1 - c_2) \right] \right\} \\
& + (\Delta l)_1^2 \left\{ \frac{\varepsilon_0 - \varepsilon_1}{2(c_0 - c_1)} - \frac{\varepsilon_0 c_1 - \varepsilon_1 c_0}{(c_0 - c_1)^3} \left[c_1 \log_e \frac{c_1}{c_0} + (c_0 - c_1) \right] \right\} \\
& + (\Delta l)_4 \left\{ (\Delta l)_3 \left[\frac{\varepsilon_2 - \varepsilon_3}{c_2 - c_3} + \frac{\varepsilon_2 c_3 - \varepsilon_3 c_2}{(c_2 - c_3)^2} \log_e \frac{c_3}{c_2} \right] \right\} \\
& + \left[(\Delta l)_4 + (\Delta l)_3 \right] \left\{ (\Delta l)_2 \left[\frac{\varepsilon_1 - \varepsilon_2}{c_1 - c_2} + \frac{\varepsilon_1 c_2 - \varepsilon_2 c_1}{(c_1 - c_2)^2} \log_e \frac{c_2}{c_1} \right] \right\} \\
& + \left[(\Delta l)_4 + (\Delta l)_3 + (\Delta l)_2 \right] \left\{ (\Delta l)_1 \left[\frac{\varepsilon_0 - \varepsilon_1}{c_0 - c_1} + \frac{\varepsilon_0 c_1 - \varepsilon_1 c_0}{(c_0 - c_1)^2} \log_e \frac{c_1}{c_0} \right] \right\} \\
& + y_0 + \left[(\Delta l)_1 + (\Delta l)_2 + (\Delta l)_3 + (\Delta l)_4 \right] \tan \theta_0
\end{aligned}
\tag{B9}
$$

Based on the indicial progression patterns in equations (B3), (B5), (B7), and (B9), the generalized form of the deflection equation can be written in dual summation forms (with different summation limits) as:

$$
\begin{aligned}
y_i = {} & \underbrace{\sum_{j=1}^{i} \left\{ (\Delta l)_j^2 \left[\frac{\varepsilon_{j-1} - \varepsilon_j}{2(c_{j-1} - c_j)} - \frac{\varepsilon_{j-1} c_j - \varepsilon_j c_{j-1}}{(c_{j-1} - c_j)^3} \left\langle c_j \log_e \frac{c_j}{c_{j-1}} + (c_{j-1} - c_j) \right\rangle \right] \right\} + y_0}_{\text{Contributions from deflection terms}} \\
& \underbrace{+ \sum_{j=1}^{i-1} \left\{ \left[(\Delta l)_{j+1} + (\Delta l)_{j+2} + \ldots + (\Delta l)_i \right] (\Delta l)_j \left[\frac{\varepsilon_{j-1} - \varepsilon_j}{c_{j-1} - c_j} + \frac{\varepsilon_{j-1} c_j - \varepsilon_j c_{j-1}}{(c_{j-1} - c_j)^2} \log_e \frac{c_j}{c_{j-1}} \right] \right\} + \left[\sum_{j=1}^{i} (\Delta l)_j \right] \tan \theta_0}_{\text{Contributions from slope terms}}
\end{aligned}
\tag{B10}
$$

Equation (B10) can be rewritten in a more compact form as:

$$y_i = \underbrace{\sum_{j=1}^{i}\left\{(\Delta l)_j^2\left[\frac{\varepsilon_{j-1}-\varepsilon_j}{2(c_{j-1}-c_j)}-\frac{\varepsilon_{j-1}c_j-\varepsilon_j c_{j-1}}{(c_{j-1}-c_j)^3}\left\langle c_j\log_e\frac{c_j}{c_{j-1}}+(c_{j-1}-c_j)\right\rangle\right]\right\}+y_0}_{\text{Contributions from deflection terms}}$$
$$+\underbrace{\sum_{j=1}^{i-1}\left\{\left[\sum_{k=j+1}^{i}(\Delta l)_k\right](\Delta l)_j\left[\frac{\varepsilon_{j-1}-\varepsilon_j}{c_{j-1}-c_j}+\frac{\varepsilon_{j-1}c_j-\varepsilon_j c_{j-1}}{(c_{j-1}-c_j)^2}\log_e\frac{c_j}{c_{j-1}}\right]\right\}+\left[\sum_{j=1}^{i}(\Delta l)_j\right]\tan\theta_0}_{\text{Contributions from slope terms}} \qquad (B11)$$

$$(i=1,2,3,....,n)$$

Equation (B11) is identical to equation (13c) in the text, and is called the Variable-Domain Nonuniform Displacement Transfer Function in dual summation form for nonuniform embedded beams based on piecewise-linear strain representations.

For constant-domain lengths, $(\Delta l)_1=(\Delta l)_2=(\Delta l)_3=.....=\Delta l$, equation (B11) degenerates into:

$$y_i = \underbrace{(\Delta l)^2\sum_{j=1}^{i}\left\{\frac{\varepsilon_{j-1}-\varepsilon_j}{2(c_{j-1}-c_j)}-\frac{\varepsilon_{j-1}c_j-\varepsilon_j c_{j-1}}{(c_{j-1}-c_j)^3}\left[c_j\log_e\frac{c_j}{c_{j-1}}+(c_{j-1}-c_j)\right]\right\}+y_0}_{\text{Contributions from deflection terms}}$$
$$+\underbrace{(\Delta l)^2\sum_{j=1}^{i-1}\left\{(i-j)\left[\frac{\varepsilon_{j-1}-\varepsilon_j}{c_{j-1}-c_j}+\frac{\varepsilon_{j-1}c_j-\varepsilon_j c_{j-1}}{(c_{j-1}-c_j)^2}\log_e\frac{c_j}{c_{j-1}}\right]\right\}+(i)\Delta l\tan\theta_0}_{\text{Contribution from slope terms}} \qquad (B12)$$

$$(i=1,2,3,....,n)$$

Equation (B12) is identical to equation (5c) in the text, and is called the Constant-Domain Nonuniform Displacement Transfer Function in dual summation form for nonuniform embedded beams based on piecewise-linear strain representations.

APPENDIX C
DERIVATIONS OF VARIABLE-DOMAIN IMPROVED DISPLACEMENT TRANSFER FUNCTION FOR NONUNIFORM EMBEDDED BEAMS

(Based on Piecewise-Nonlinear Strain Representations)

Appendix C presents the details of integrations of the beam curvature equation (1) to obtain the improved slope and deflection equations for the formulation of variable-domain Improved Displacement Transfer Functions for nonuniform embedded beams based on piecewise-nonlinear strain representations.

Improved Slope Equations

The slope, $\tan\theta(x)$, of the nonuniform beam in the small domain, $x_{i-1} \le x \le x_i$, between the two adjacent strain-sensing stations, $\{x_{i-1}, x_i\}$, can be obtained by integrating equation (1) as equation (C1):

$$\int_{x_{i-1}}^{x} \frac{d^2y}{dx^2}dx = \frac{dy}{dx} - \underbrace{\left(\frac{dy}{dx}\right)_{i-1}}_{\text{Slope at } x_{i-1}} \equiv \tan\theta(x) - \underbrace{\tan\theta_{i-1}}_{\text{Slope at } x_{i-1}} = \int_{x_{i-1}}^{x} \frac{\varepsilon(x)}{c(x)}dx \quad ; \quad (x_{i-1} \le x \le x_i) \tag{C1}$$

The distributions of the beam depth factor, $c(x)$ [eq. (9)], and bending strain, $\varepsilon(x)$ [eq. (11)], in the small domain, $x_{i-1} \le x \le x_i$, between the two adjacent strain-sensing stations, $\{x_{i-1}, x_i\}$, are respectively duplicated below as equations (C-2) and (C-3).

$$c(x) = c_{i-1} + (c_i - c_{i-1})\frac{x - x_{i-1}}{(\Delta l)_i} \quad ; \quad (x_{i-1} \le x \le x_i) \tag{C2}$$

$$\begin{aligned}\varepsilon(x) = \varepsilon_{i-1} &- \frac{(\Delta l)_{i+1}[2(\Delta l)_i + (\Delta l)_{i+1}]\varepsilon_{i-1} - [(\Delta l)_i + (\Delta l)_{i+1}]^2\varepsilon_i + (\Delta l)_i^2\varepsilon_{i+1}}{(\Delta l)_i(\Delta l)_{i+1}[(\Delta l)_i + (\Delta l)_{i+1}]}(x - x_{i-1}) \\ &+ \frac{(\Delta l)_{i+1}\varepsilon_{i-1} - [(\Delta l)_i + (\Delta l)_{i+1}]\varepsilon_i + (\Delta l)_i\varepsilon_{i+1}}{(\Delta l)_i(\Delta l)_{i+1}[(\Delta l)_i + (\Delta l)_{i+1}]}(x - x_{i-1})^2 \\ &\qquad\qquad (x_{i-1} \le x \le x_i)\end{aligned} \tag{C3}$$

Let $\{A_i, B_i, C_i, \xi\}$ be defined respectively with equations (C4), (C5), (C6), (C7) as

$$A_i \equiv -\frac{(\Delta l)_{i+1}[2(\Delta l)_i + (\Delta l)_{i+1}]\varepsilon_{i-1} - [(\Delta l)_i + (\Delta l)_{i+1}]^2\varepsilon_i + (\Delta l)_i^2\varepsilon_{i+1}}{(\Delta l)_i(\Delta l)_{i+1}[(\Delta l)_i + (\Delta l)_{i+1}]} \tag{C4}$$

$$B_i \equiv \frac{(\Delta l)_{i+1}\varepsilon_{i-1} - [(\Delta l)_i + (\Delta l)_{i+1}]\varepsilon_i + (\Delta l)_i\varepsilon_{i+1}}{(\Delta l)_i(\Delta l)_{i+1}[(\Delta l)_i + (\Delta l)_{i+1}]} \tag{C5}$$

$$C_i \equiv \frac{c_i - c_{i-1}}{(\Delta l)_i} \tag{C6}$$

$$\xi \equiv (x - x_{i-1}) \tag{C7}$$

then the last three terms of equation (C1) can be written as:

$$\tan\theta(x) = \int_0^{\xi} \frac{\varepsilon_{i-1} + A_i\xi + B_i\xi^2}{c_{i-1} + C_i\xi} d\xi + \tan\theta_{i-1} \quad ; \quad [0 \le \xi \le (\Delta l)_i] \tag{C8}$$

After carrying out integration of equation (C8), one obtains (ref. 15):

$$\begin{aligned}
\tan\theta(x) &= \Bigg[\underbrace{\frac{\varepsilon_{i-1}}{C_i}\log_e(c_{i-1} + C_i\xi)}_{\text{Integration of 1st term in eq. (B-8)}} + \underbrace{A_i\frac{\xi}{C_i} - A_i\frac{c_{i-1}}{C_i^2}\log_e(c_{i-1} + C_i\xi)}_{\text{Integration of 2nd term in eq. (B-8)}} \\
&\qquad \underbrace{+\frac{B_i}{C_i^3}\left[\frac{1}{2}(c_{i-1} + C_i\xi)^2 - 2c_{i-1}(c_{i-1} + C_i\xi) + c_{i-1}^2\log_e(c_{i-1} + C_i\xi)\right]}_{\text{Integration of 3rd term in eq (B-8)}} \Bigg]_0^{\xi} + \tan\theta_{i-1} \\
&= \left(\frac{\varepsilon_{i-1}}{C_i} - A_i\frac{c_{i-1}}{C_i^2} + B_i\frac{c_{i-1}^2}{C_i^3}\right)\log_e(c_{i-1} + C_i\xi) + \frac{A_i}{C_i}\xi + \frac{1}{2}\frac{B_i}{C_i^3}(c_{i-1} + C_i\xi)^2 - 2\frac{B_i}{C_i^3}c_{i-1}(c_{i-1} + C_i\xi) \\
&\quad - \left(\frac{\varepsilon_{i-1}}{C_i} - A_i\frac{c_{i-1}}{C_i^2} + B_i\frac{c_{i-1}^2}{C_i^3}\right)\log_e c_{i-1} - \frac{1}{2}\frac{B_i}{C_i^3}c_{i-1}^2 + 2\frac{B_i}{C_i^3}c_{i-1}^2 + \tan\theta_{i-1} \\
&= \frac{1}{C_i^3}\left[C_i^2\varepsilon_{i-1} - A_iC_ic_{i-1} + B_ic_{i-1}^2\right]\left[\log_e(c_{i-1} + C_i\xi) - \log_e c_{i-1}\right] + \frac{A_i}{C_i}\xi \\
&\quad + \frac{1}{2}\frac{B_i}{C_i^3}\left[(c_{i-1} + C_i\xi)^2 - c_{i-1}^2\right] - 2\frac{B_i}{C_i^3}c_{i-1}\left[(c_{i-1} + C_i\xi) - c_{i-1}\right] + \tan\theta_{i-1} \\
&= \frac{1}{C_i^3}\left[C_i^2\varepsilon_{i-1} - A_iC_ic_{i-1} + B_ic_{i-1}^2\right]\left[\log_e(c_{i-1} + C_i\xi) - \log_e c_{i-1}\right] + \frac{A_i}{C_i}\xi \\
&\quad + \frac{1}{2}\frac{B_i}{C_i^3}\left[(c_{i-1}^2 + 2c_{i-1}C_i\xi + C_i^2\xi)^2 - c_{i-1}^2\right] - 2\frac{B_i}{C_i^3}c_{i-1}\left[(c_{i-1} + C_i\xi) - c_{i-1}\right] + \tan\theta_{i-1} \\
&= \frac{1}{C_i^3}\left[C_i^2\varepsilon_{i-1} - A_iC_ic_{i-1} + B_ic_{i-1}^2\right]\left[\log_e(c_{i-1} + C_i\xi) - \log_e c_{i-1}\right] + \frac{A_i}{C_i}\xi \\
&\quad + \frac{1}{2}\frac{B_i}{C_i^2}(2c_{i-1}\xi + C_i\xi^2) - 2\frac{B_i}{C_i^2}c_{i-1}\xi + \tan\theta_{i-1} \\
&= \frac{1}{C_i^3}\left[C_i^2\varepsilon_{i-1} - A_iC_ic_{i-1} + B_ic_{i-1}^2\right]\left[\log_e(c_{i-1} + C_i\xi) - \log_e c_{i-1}\right] + \frac{A_i}{C_i}\xi \\
&\quad + \frac{B_i}{2C_i^2}(C_i\xi^2 - 2c_{i-1}\xi) + \tan\theta_{i-1}
\end{aligned} \tag{C9}$$

After simplifying, equation (C9) becomes:

$$\tan\theta(x) = \frac{1}{C_i^3}\left[C_i^2\varepsilon_{i-1} - A_iC_ic_{i-1} + B_ic_{i-1}^2\right]\log_e\left(1+\frac{C_i}{c_{i-1}}\xi\right) + \frac{\xi}{C_i}\left[A_i + B_i\left(\frac{\xi}{2} - \frac{c_{i-1}}{C_i}\right)\right] + \tan\theta_{i-1} \tag{C10}$$

At the strain-sensing station, x_i, we have $\xi = x_i - x_{i-1} = (\Delta l)_i$, then equation (C10) gives the slope $\tan\theta_i[\equiv \tan\theta(x_i)]$ at x_i as:

$$\tan\theta_i = \frac{1}{C_i^3}\left[C_i^2\varepsilon_{i-1} - A_iC_ic_{i-1} + B_ic_{i-1}^2\right]\log_e\left(1+\frac{C_i}{c_{i-1}}(\Delta l)_i\right) + \frac{(\Delta l)_i}{C_i}\left[A_i + B_i\left(\frac{(\Delta l)_i}{2} - \frac{c_{i-1}}{C_i}\right)\right] + \tan\theta_{i-1} \tag{C11}$$

In view of $C_i \equiv (c_i - c_{i-1})/(\Delta l)_i$ [eq. (C6)], equation (C11) takes on the form:

$$\begin{aligned}\tan\theta_i &= \frac{(\Delta l)_i^3}{(c_i-c_{i-1})^3}\left[\frac{(c_i-c_{i-1})^2}{(\Delta l)_i^2}\varepsilon_{i-1} - A_i\frac{c_i-c_{i-1}}{(\Delta l)_i}c_{i-1} + B_ic_{i-1}^2\right]\log_e\left(1+\frac{c_i-c_{i-1}}{(\Delta l)_i}\frac{(\Delta l)_i}{c_{i-1}}\right) \\ &\quad + \frac{(\Delta l)_i^2}{c_i-c_{i-1}}\left[A_i + B_i\left(\frac{(\Delta l)_i}{2} - \frac{c_{i-1}(\Delta l)_i}{c_i-c_{i-1}}\right)\right] + \tan\theta_{i-1} \\ &= \frac{(\Delta l)_i^3}{(c_i-c_{i-1})^3}\left[\frac{(c_i-c_{i-1})^2}{(\Delta l)_i^2}\varepsilon_{i-1} - A_i\frac{c_i-c_{i-1}}{(\Delta l)_i}c_{i-1} + B_ic_{i-1}^2\right]\log_e\frac{c_i}{c_{i-1}} \\ &\quad + \frac{(\Delta l)_i^2}{c_i-c_{i-1}}\left[A_i + B_i(\Delta l)_i\frac{c_i-3c_{i-1}}{2(c_i-c_{i-1})}\right] + \tan\theta_{i-1}\end{aligned} \tag{C12}$$

After grouping terms, equation (C12) becomes:

$$\begin{aligned}\tan\theta_i &= \frac{(\Delta l)_i}{(c_i-c_{i-1})^3}\left[(c_i-c_{i-1})^2\varepsilon_{i-1} - A_i(\Delta l)_ic_{i-1}(c_i-c_{i-1}) + B_i(\Delta l)_i^2c_{i-1}^2\right]\log_e\frac{c_i}{c_{i-1}} \\ &\quad + \frac{(\Delta l)_i}{2(c_i-c_{i-1})^2}\left[2A_i(\Delta l)_i(c_i-c_{i-1}) + B_i(\Delta l)_i^2(c_i-3c_{i-1})\right] + \tan\theta_{i-1}\end{aligned} \tag{C13}$$

$$(i = 1,2,3,....,n)$$

Equation (C13) is identical to equation (17a) in the text, the *variable-domain improved slope equation* for nonuniform beams in recursive form based on nonlinear strain representations.

Improved Deflection Equations

The deflection, $y(x)$, can be obtained by integrating the slope equation (C10) as (ref. 15).

$$
\begin{aligned}
y(x) &= \int_{x_{i-1}}^{x} \tan(x)\,dx + \underbrace{y_{i-1}}_{\substack{\text{Deflection} \\ \text{at } x_{i-1}}} = \int_0^{\xi} \tan(\xi)\,d\xi + y_{i-1} \\
&= \int_0^{\xi} \left\{ \begin{array}{c} \dfrac{1}{C_i^3}\left[C_i^2\varepsilon_{i-1} - A_iC_ic_{i-1} + B_ic_{i-1}^2\right]\log_e\left(1+\dfrac{C_i}{c_{i-1}}\xi\right) \\ + \dfrac{\xi}{C_i}\left[A + B_i\left(\dfrac{\xi}{2} - \dfrac{c_{i-1}}{C_i}\right)\right] + \tan\theta_{i-1} \end{array} \right\} d\xi + y_{i-1} \\
&= \left[\begin{array}{c} \dfrac{1}{C_i^3}\left[C_i^2\varepsilon_{i-1} - A_iC_ic_{i-1} + B_ic_{i-1}^2\right]\left[\dfrac{c_{i-1}}{C_i}\left(1+\dfrac{C_i}{c_{i-1}}\xi\right)\log_e\left(1+\dfrac{C_i}{c_{i-1}}\xi\right) - \xi\right] \\ + \dfrac{1}{C_i}\left[A_i\dfrac{\xi^2}{2} + B_i\left(\dfrac{\xi^3}{6} - \dfrac{c_{i-1}}{C_i}\dfrac{\xi^2}{2}\right)\right] + \xi\tan\theta_{i-1} \end{array} \right]_0^{\xi} + y_{i-1} \\
&= \frac{1}{C_i^3}\left[C_i^2\varepsilon_{i-1} - A_iC_ic_{i-1} + B_ic_{i-1}^2\right]\left[\frac{c_{i-1}}{C_i}\left(1+\frac{C_i}{c_{i-1}}\xi\right)\log_e\left(1+\frac{C_i}{c_{i-1}}\xi\right) - \xi\right] \\
&\qquad + \frac{\xi^2}{2C_i}\left[A_i + B_i\left(\frac{\xi}{3} - \frac{c_{i-1}}{C_i}\right)\right] + y_{i-1} + \xi\tan\theta_{i-1}
\end{aligned}
\tag{C14}
$$

At the strain-sensing station, x_i, we have $\xi = x_i - x_{i-1} = (\Delta l)_i$, and equation (C14) gives the deflection $y_i[\equiv y(x_i)]$ as:

$$
\begin{aligned}
y_i = y(x_i) &= \frac{1}{C_i^3}\left[C_i^2\varepsilon_{i-1} - A_iC_ic_{i-1} + B_ic_{i-1}^2\right]\left[\frac{c_{i-1}}{C_i}\left(1+\frac{C_i}{c_{i-1}}(\Delta l)_i\right)\log_e\left(1+\frac{C_i}{c_{i-1}}(\Delta l)_i\right) - (\Delta l)_i\right] \\
&\qquad + \frac{(\Delta l)_i^2}{2C_i}\left[A_i + B_i\left(\frac{(\Delta l)_i}{3} - \frac{c_{i-1}}{C_i}\right)\right] + y_{i-1} + (\Delta l)_i\tan\theta_{i-1}
\end{aligned}
\tag{C15}
$$

In view of $C_i \equiv (c_i - c_{i-1})/(\Delta l)_i$ [eq. (C6)], equation (C15) becomes:

$$
\begin{aligned}
y_i &= \frac{(\Delta l)_i^4}{(c_i - c_{i-1})^3}\left[\frac{(c_i - c_{i-1})^2}{(\Delta l)_i^2}\varepsilon_{i-1} - A_i\frac{c_i - c_{i-1}}{(\Delta l)_i}c_{i-1} + B_ic_{i-1}^2\right]\left(\frac{1}{c_i - c_{i-1}}\right)\left[c_i\log_e\frac{c_i}{c_{i-1}} - (c_i - c_{i-1})\right] \\
&\quad + \frac{(\Delta l)_i^3}{2(c_i - c_{i-1})}\left[A_i + B_i\left(\frac{(\Delta l)_i}{3} - \frac{c_{i-1}(\Delta l)_i}{(c_i - c_{i-1})}\right)\right] + y_{i-1} + (\Delta l)_i\tan\theta_{i-1}
\end{aligned}
\tag{C16}
$$

After grouping terms, equation (C16) becomes:

$$y_i = \frac{(\Delta l)_i^2}{(c_i - c_{i-1})^4}\Big[(c_i - c_{i-1})^2 \varepsilon_{i-1} - A_i(\Delta l)_i(c_i - c_{i-1})c_{i-1} + B_i(\Delta l)_i^2 c_{i-1}^2\Big]\left[c_i \log_e \frac{c_i}{c_{i-1}} - (c_i - c_{i-1})\right]$$
$$+ \frac{(\Delta l)_i^2}{6(c_i - c_{i-1})^2}\Big[3A(\Delta l)_i(c_i - c_{i-1}) + B_i(\Delta l)_i^2(c_i - 4c_{i-1})_i\Big] + y_{i-1} + (\Delta l)_i \tan\theta_{i-1} \qquad \text{(C17)}$$
$$(i = 1,2,3,....,n)$$

Equation (C17) is identical to equation (17b) in the text, the *variable-domain improved deflection equation* for nonuniform beams in recursive form based on nonlinear strain representations.

Improved Displacement Transfer Function

Substitution of slope equation (C13) into deflection equation (C17), and using similar mathematical steps of Appendix B, one can write the deflection equation in dual summation form as:

$$y_i = \underbrace{\sum_{j=1}^{i}\left\{\begin{array}{l}\dfrac{(\Delta l)_j^2}{(c_j - c_{j-1})^4}\Big[(c_j - c_{j-1})^2 \varepsilon_{j-1} - A_j(\Delta l)_j(c_j - c_{j-1})c_{j-1} + B_j(\Delta l)_j^2 c_{j-1}^2\Big]\times \\ \qquad\qquad \times\left[c_j \log_e \dfrac{c_j}{c_{j-1}} - (c_j - c_{j-1})\right] \\ + \dfrac{(\Delta l)_j^2}{6(c_j - c_{j-1})^2}\Big[3A_j(\Delta l)_j(c_j - c_{j-1}) + B_j(\Delta l)_j^2(c_j - 4c_{j-1})\Big]\end{array}\right\}}_{\text{Contributions from deflection terms}} + y_0$$
$$+ \underbrace{\sum_{j=1}^{i-1}\left\{\left[\sum_{k=j+1}^{i}(\Delta l)_k\right]\left[\begin{array}{l}\dfrac{(\Delta l)_j}{(c_j - c_{j-1})^3}\Big\langle (c_j - c_{j-1})^2 \varepsilon_{j-1} - A_j(\Delta l)_j c_{j-1}(c_j - c_{j-1}) \\ \qquad + B_j(\Delta l)_j^2 c_{j-1}^2 \Big\rangle \log_e \dfrac{c_j}{c_{j-1}} \\ + \dfrac{(\Delta l)_i}{2(c_j - c_{j-1})^2}\Big\langle 2A_j(\Delta l)_j(c_j - c_{j-1}) + B_j(\Delta l)_j^2(c_j - 3c_{j-1})\Big\rangle\end{array}\right]\right\}}_{\text{Contributions from slope terms}}$$
$$+ \underbrace{\left[\sum_{j=1}^{i}(\Delta l)_j\right]\tan\theta_0}_{\text{Contributiohjs from slope terms}} \qquad \text{(C18)}$$
$$(i = 1,2,3,....,n)$$

Equation (C18) is identical to equation (17c) in the text, and is called the *Variable-Domain Improved Displacement Transfer Function* in dual summation form for nonuniform embedded beams based on piecewise-nonlinear strain representations.

Degeneration into Constant-Domain Case

This section is to prove that when the variable-domain lengths become constant, the variable-domain slope and deflection equations [(C13), (C17)] will degenerate respectively into the constant-domain slope and deflection equations [(5a), (5b)].

For the constant-domain case, $(\Delta l)_1 = (\Delta l)_2 = (\Delta l)_3 = ... = \Delta l$, the coefficients, A_i [eq. (C4)] and B_i [eq. (C5)] become equations (C19) and (C20) respectively:

$$A_i \equiv -\frac{(\Delta l)_{i+1}[2(\Delta l)_i + (\Delta l)_{i+1}]\varepsilon_{i-1} - [(\Delta l)_i + (\Delta l)_{i+1}]^2 \varepsilon_i + (\Delta l)_i^2 \varepsilon_{i+1}}{(\Delta l)_i (\Delta l)_{i+1}[(\Delta l)_i + (\Delta l)_{i+1}]} = -\frac{3\varepsilon_{i-1} - 4\varepsilon_i + \varepsilon_{i+1}}{2\Delta l} \tag{C19}$$

$$B_i \equiv \frac{(\Delta l)_{i+1}\varepsilon_{i-1} - [(\Delta l)_i + (\Delta l)_{i+1}]\varepsilon_i + (\Delta l)_i \varepsilon_{i+1}}{(\Delta l)_i (\Delta l)_{i+1}[(\Delta l)_i + (\Delta l)_{i+1}]} = \frac{\varepsilon_{i-1} - 2\varepsilon_i + \varepsilon_{i+1}}{2(\Delta l)^2} \tag{C20}$$

Slope Equations

In view of equations [(C19), (C20)], the slope equation (C13) can be written as:

$$\begin{aligned}
\tan\theta_i &= \frac{(\Delta l)_i}{(c_i - c_{i-1})^3}\left[(c_i - c_{i-1})^2 \varepsilon_{i-1} - A_i (\Delta l)_i c_{i-1}(c_i - c_{i-1}) + B_i (\Delta l)_i^2 c_{i-1}^2\right]\log_e \frac{c_i}{c_{i-1}} \\
&\quad + \frac{(\Delta l)_i}{2(c_i - c_{i-1})^2}\left[2A_i (\Delta l)_i (c_i - c_{i-1}) + B_i (\Delta l)_i^2 (c_i - 3c_{i-1})\right] + \tan\theta_{i-1} \\
&= \frac{\Delta l}{(c_i - c_{i-1})^3}\left[(c_i - c_{i-1})^2 \varepsilon_{i-1} - \underbrace{\left(-\frac{3\varepsilon_{i-1} - 4\varepsilon_i + \varepsilon_{i+1}}{2}\right)}_{A_i(\Delta l)} c_{i-1}(c_i - c_{i-1}) + \underbrace{\left(\frac{\varepsilon_{i-1} - 2\varepsilon_i + \varepsilon_{i+1}}{2}\right)}_{B_i(\Delta l)^2} c_{i-1}^2\right]\log_e \frac{c_i}{c_{i-1}} \\
&\quad + \frac{(\Delta l)}{2(c_i - c_{i-1})^2}\left[\underbrace{2\left(-\frac{3\varepsilon_{i-1} - 4\varepsilon_i + \varepsilon_{i+1}}{2}\right)}_{A_i(\Delta l)}(c_i - c_{i-1}) + \underbrace{\left(\frac{\varepsilon_{i-1} - 2\varepsilon_i + \varepsilon_{i+1}}{2}\right)}_{B_i(\Delta l)^2}(c_i - 3c_{i-1})\right] + \tan\theta_{i-1} \\
&= \frac{\Delta l}{2(c_i - c_{i-1})^3}\left[\begin{array}{l} 2(c_i - c_{i-1})^2 \varepsilon_{i-1} + (3\varepsilon_{i-1} - 4\varepsilon_i + \varepsilon_{i+1})(c_i - c_{i-1})c_{i-1} \\ +(\varepsilon_{i-1} - 2\varepsilon_i + \varepsilon_{i+1})c_{i-1}^2 \end{array}\right]\log_e \frac{c_i}{c_{i-1}} \\
&\quad + \frac{\Delta l}{4(c_i - c_{i-1})^2}\left[-2(3\varepsilon_{i-1} - 4\varepsilon_i + \varepsilon_{i+1})(c_i - c_{i-1}) + (\varepsilon_{i-1} - 2\varepsilon_i + \varepsilon_{i+1})(c_i - 3c_{i-1})\right] + \tan\theta_{i-1} \\
&= \frac{\Delta l}{2(c_i - c_{i-1})^3}\left[\begin{array}{l} (2c_i^2 - 4c_i c_{i-1} + 2c_{i-1}^2)\varepsilon_{i-1} + (3\varepsilon_{i-1} - 4\varepsilon_i + \varepsilon_{i+1})(c_i - c_{i-1})c_{i-1} \\ +(\varepsilon_{i-1} - 2\varepsilon_i + \varepsilon_{i+1})c_{i-1}^2 \end{array}\right]\log_e \frac{c_i}{c_{i-1}} \\
&\qquad + \frac{\Delta l}{4(c_i - c_{i-1})^2}\left[-(6\varepsilon_{i-1} - 8\varepsilon_i + 2\varepsilon_{i+1})(c_i - c_{i-1}) + (\varepsilon_{i-1} - 2\varepsilon_i + \varepsilon_{i+1})(c_i - 3c_{i-1})\right] + \tan\theta_{i-1}
\end{aligned}$$

$$
\begin{aligned}
&= \frac{\Delta l}{2(c_i - c_{i-1})^3}\begin{bmatrix} \left\langle (2c_i^2 - 4c_i c_{i-1} + 2c_{i-1}^2) + (3c_i - 3c_{i-1})c_{i-1} + c_{i-1}^2 \right\rangle \varepsilon_{i-1} \\ -\left\langle (4c_i - 4c_{i-1})c_{i-1} + 2c_{i-1}^2 \right\rangle \varepsilon_i \\ +\left\langle (c_i - c_{i-1})c_{i-1} + c_{i-1}^2 \right\rangle \varepsilon_{i+1} \end{bmatrix} \log_e \frac{c_i}{c_{i-1}} \\
&+ \frac{\Delta l}{4(c_i - c_{i-1})^2}\begin{bmatrix} \left\langle -(6c_i - 6c_{i-1}) + (c_i - 3c_{i-1}) \right\rangle \varepsilon_{i-1} \\ +\left\langle (8c_i - 8c_{i-1}) - (2c_i - 6c_{i-1}) \right\rangle \varepsilon_i \\ \left\langle -(2c_i - 2c_{i-1}) + (c_i - 3c_{i-1}) \right\rangle \varepsilon_{i+1} \end{bmatrix} + \tan\theta_{i-1} \\
&= \frac{\Delta l}{2(c_i - c_{i-1})^3}\begin{bmatrix} (2c_i^2 - c_i c_{i-1})\varepsilon_{i-1} \\ -(4c_i c_{i-1} - 2c_{i-1}^2)\varepsilon_i \\ +c_i c_{i-1}\varepsilon_{i+1} \end{bmatrix} \log_e \frac{c_i}{c_{i-1}} + \frac{\Delta l}{4(c_i - c_{i-1})^2}\begin{bmatrix} (-5c_i + 3c_{i-1})\varepsilon_{i-1} \\ +2(3c_i - c_{i-1})\varepsilon_i \\ (-c_i - c_{i-1})\varepsilon_{i+1} \end{bmatrix} + \tan\theta_{i-1} \\
&= \frac{\Delta l}{2(c_i - c_{i-1})^3}\left[(2c_i - c_{i-1})c_i\varepsilon_{i-1} - 2(2c_i - c_{i-1})c_{i-1}\varepsilon_i + c_i c_{i-1}\varepsilon_{i+1}\right]\log_e \frac{c_i}{c_{i-1}} \\
&\quad + \frac{\Delta l}{4(c_i - c_{i-1})^2}\left[-(5c_i - 3c_{i-1})\varepsilon_{i-1} + 2(3c_i - c_{i-1})\varepsilon_i - (c_i + c_{i-1})\varepsilon_{i+1}\right] + \tan\theta_{i-1}
\end{aligned}
\tag{C21}
$$

After grouping terms, equation (C21) becomes:

$$
\begin{aligned}
\tan\theta_i &= \frac{\Delta l}{2(c_i - c_{i-1})^3}\left[(2c_i - c_{i-1})(c_i\varepsilon_{i-1} - 2c_{i-1}\varepsilon_i) + c_i c_{i-1}\varepsilon_{i+1}\right]\log_e \frac{c_i}{c_{i-1}} \\
&\quad - \frac{\Delta l}{4(c_i - c_{i-1})^2}\left[(5c_i - 3c_{i-1})\varepsilon_{i-1} - 2(3c_i - c_{i-1})\varepsilon_i + (c_i + c_{i-1})\varepsilon_{i+1}\right] + \tan\theta_{i-1}
\end{aligned}
\tag{C22}
$$

Equation (C22) is identical to the improved slope equation (7a) for the constant-domain case.

Deflection Equations

In view of equations [(C19), (C20)], the deflection equation (C17) can be written as:

$$
\begin{aligned}
y_i &= \frac{(\Delta l)_i^2}{(c_i - c_{i-1})^4}\left[(c_i - c_{i-1})^2\varepsilon_{i-1} - A_i(\Delta l)_i(c_i - c_{i-1})c_{i-1} + B_i(\Delta l)_i^2 c_{i-1}^2\right]\left[c_i \log_e \frac{c_i}{c_{i-1}} - (c_i - c_{i-1})\right] \\
&\quad + \frac{(\Delta l)_i^2}{6(c_i - c_{i-1})^2}\left[3A(\Delta l)_i(c_i - c_{i-1}) + B_i(\Delta l)_i^2(c_i - 4c_{i-1})_i\right] + y_{i-1} + (\Delta l)_i \tan\theta_{i-1}
\end{aligned}
$$

$$
\begin{aligned}
&= \frac{(\Delta l)^2}{(c_i - c_{i-1})^4}\left[(c_i - c_{i-1})^2\,\varepsilon_{i-1} - \underbrace{\left(-\frac{3\varepsilon_{i-1} - 4\varepsilon_i + \varepsilon_{i+1}}{2}\right)}_{A_i(\Delta l)} (c_i - c_{i-1})\,c_{i-1} + \underbrace{\left(\frac{\varepsilon_{i-1} - 2\varepsilon_i + \varepsilon_{i+1}}{2}\right)}_{B_i(\Delta l)^2} c_{i-1}^2 \right] \times \\
&\qquad \times \left[c_i \log_e\left(\frac{c_i}{c_{i-1}}\right) - (c_i - c_{i-1}) \right] \\
&\quad + \frac{(\Delta l)^2}{2(c_i - c_{i-1})}\left[\underbrace{\left(-\frac{3\varepsilon_{i-1} - 4\varepsilon_i + \varepsilon_{i+1}}{2}\right)}_{A_i(\Delta l)} + \underbrace{\left(\frac{\varepsilon_{i-1} - 2\varepsilon_i + \varepsilon_{i+1}}{2}\right)}_{B_i(\Delta l)^2} \frac{c_i - 4c_{i-1}}{3(c_i - c_{i-1})} \right] + y_{i-1} + (\Delta l)_i \tan\theta_{i-1} \\
&= \frac{(\Delta l)^2}{2(c_i - c_{i-1})^4}\begin{bmatrix} 2(c_i - c_{i-1})^2 \varepsilon_{i-1} + (3\varepsilon_{i-1} - 4\varepsilon_i + \varepsilon_{i+1}) c_{i-1}(c_i - c_{i-1}) \\ +(\varepsilon_{i-1} - 2\varepsilon_i + \varepsilon_{i+1}) c_{i-1}^2 \end{bmatrix}\left[c_i \log_e \frac{c_i}{c_{i-1}} - (c_i - c_{i-1}) \right] \\
&\qquad + \frac{(\Delta l)^2}{12(c_i - c_{i-1})^2}\begin{bmatrix} -3(3\varepsilon_{i-1} - 4\varepsilon_i + \varepsilon_{i+1})(c_i - c_{i-1}) \\ +(\varepsilon_{i-1} - 2\varepsilon_i + \varepsilon_{i+1})(c_i - 4c_{i-1}) \end{bmatrix} + y_{i-1} + (\Delta l)_i \tan\theta_{i-1} \\
&= \frac{(\Delta l)^2}{2(c_i - c_{i-1})^4}\begin{bmatrix} \left\langle (2c_i^2 - 4c_i c_{i-1} + 2c_{i-1}^2) + 3(c_i - c_{i-1})c_{i-1} + c_{i-1}^2 \right\rangle \varepsilon_{i-1} \\ +\left\langle -4(c_i - c_{i-1})c_{i-1} - 2c_{i-1}^2 \right\rangle \varepsilon_i \\ +\left\langle (c_i - c_{i-1})c_{i-1} + c_{i-1}^2 \right\rangle \varepsilon_{i+1} \end{bmatrix}\left[c_i \log_e \frac{c_i}{c_{i-1}} - (c_i - c_{i-1}) \right] \\
&\qquad + \frac{(\Delta l)^2}{12(c_i - c_{i-1})^2}\begin{bmatrix} \left\langle -9(c_i - c_{i-1}) + (c_i - 4c_{i-1}) \right\rangle \varepsilon_{i-1} \\ +\left\langle 12(c_i - c_{i-1}) - 2(c_i - 4c_{i-1}) \right\rangle \varepsilon_i \\ \left\langle -3(c_i - c_{i-1}) + (c_i - 4c_{i-1}) \right\rangle \varepsilon_{i+1} \end{bmatrix} + y_{i-1} + (\Delta l)_i \tan\theta_{i-1} \\
&= \frac{(\Delta l)^2}{2(c_i - c_{i-1})^4}\left[(2c_i^2 - c_i c_{i-1})\varepsilon_{i-1} - 2(2c_i c_{i-1} - c_{i-1}^2)\varepsilon_i + c_i c_{i-1}\varepsilon_{i+1} \right]\left[c_i \log_e \frac{c_i}{c_{i-1}} - (c_i - c_{i-1}) \right] \\
&\quad + \frac{(\Delta l)^2}{12(c_i - c_{i-1})^2}\left[-(8c_i - 5c_{i-1})\varepsilon_{i-1} + 2(5c_i - 2c_{i-1})\varepsilon_i - (2c_i + c_{i-1})\varepsilon_{i+1} \right] + y_{i-1} + (\Delta l)_i \tan\theta_{i-1}
\end{aligned}
\tag{C23}
$$

After grouping terms, equation (C23) becomes:

$$
\begin{aligned}
y_i &= \frac{(\Delta l)^2}{2(c_i - c_{i-1})^4}\left[(2c_i - c_{i-1})(c_i\varepsilon_{i-1} - 2c_{i-1}\varepsilon_i) + c_i c_{i-1}\varepsilon_{i+1} \right]\left[c_i \log_e \frac{c_i}{c_{i-1}} - (c_i - c_{i-1}) \right] \\
&\quad - \frac{(\Delta l)^2}{12(c_i - c_{i-1})^2}\left[(8c_i - 5c_{i-1})\varepsilon_{i-1} - 2(5c_i - 2c_{i-1})\varepsilon_i + (2c_i + c_{i-1})\varepsilon_{i+1} \right] + y_{i-1} + (\Delta l)_i \tan\theta_{i-1}
\end{aligned}
\tag{C24}
$$

Equation (C24) is identical to the improved deflection equation (7b) for the constant-domain case.

Displacement Transfer Function

Combining equations (C22), (C24), and after grouping terms, one obtains the deflection equation in dual summation form as:

$$
\begin{aligned}
y_i = (\Delta l)^2 \sum_{j=1}^{i} \underbrace{\left\{ \begin{array}{l} \dfrac{1}{2(c_j - c_{j-1})^4}\left[(2c_j - c_{j-1})(c_j\varepsilon_{j-1} - 2c_{j-1}\varepsilon_j) + c_j c_{j-1}\varepsilon_{j+1}\right]\times \\ \qquad \times\left[c_j \log_e \dfrac{c_j}{c_{j-1}} - (c_j - c_{j-1})\right] \\ -\dfrac{1}{12(c_j - c_{j-1})^2}\left[(8c_j - 5c_{j-1})\varepsilon_{j-1} - 2(5c_j - 2c_{j-1})\varepsilon_j + (2c_j + c_{j-1})\varepsilon_{j+1}\right] \end{array} \right\}}_{\text{Contribution from deflection terms}} + \mathrm{y}_0 \\
+(\Delta l)^2 \sum_{j=1}^{i-1} (i-j) \underbrace{\left\{ \begin{array}{l} \dfrac{1}{2(c_j - c_{j-1})^3}\left[(2c_j - c_{j-1})(c_j\varepsilon_{j-1} - 2c_{j-1}\varepsilon_j) + c_j c_{j-1}\varepsilon_{j+1}\right]\log_e \dfrac{c_j}{c_{j-1}} \\ -\dfrac{1}{4(c_j - c_{j-1})^2}\left[(5c_j - 3c_{j-1})\varepsilon_{j-1} - 2(3c_j - c_{j-1})\varepsilon_j + (c_j + c_{j-1})\varepsilon_{j+1}\right] \end{array} \right\}}_{+(i)\Delta l \tan\theta_0 \quad \text{Contributions from slope terms}} \\
(i = 1,2,3,....,n)
\end{aligned}
\tag{C25}
$$

Equation (C25) is identical to equation (7c), the *Constant-Domain Improved Displacement Transfer Function* in dual summation form for nonuniform beams based on piecewise-nonlinear strain representations.

APPENDIX D
DERIVATIONS OF THE VARIABLE-DOMAIN LOG-EXPANDED DISPLACEMENT TRANSFER FUNCTION FOR SLIGHTLY NONUNIFORM EMBEDDED BEAMS

(Based on Piecewise-Nonlinear Strain Representations)

Appendix D presents the mathematical derivations of the slope equation (18a), deflection equation (18b), and Displacement Transfer Function (18c) for slightly nonuniform beams through expansions of logarithmic functions.

Log-Expanded Slope Equations

The slope equation (17a) is duplicated below as equation (D1).

$$\tan\theta_i = \frac{(\Delta l)_i}{(c_i - c_{i-1})^3}\left[(c_i - c_{i-1})^2 \varepsilon_{i-1} - A_i(\Delta l)_i c_{i-1}(c_i - c_{i-1}) + B_i(\Delta l)_i^2 c_{i-1}^2\right]\log_e \frac{c_i}{c_{i-1}} + \frac{(\Delta l)_i}{2(c_i - c_{i-1})^2}\left[2A_i(\Delta l)_i(c_i - c_{i-1}) + B_i(\Delta l)_i^2(c_i - 3c_{i-1})\right] + \tan\theta_{i-1} \tag{D1}$$

For slowly changing $c(x)$ [that is, $(c_i/c_{i-1}) \to 1$], the logarithm term, $\log_e(c_i / c_{i-1})$, in the slope equation (D1) can be expanded in series form up to the third order term as (ref. 15):

$$\begin{aligned}
\log_e \frac{c_i}{c_{i-1}} &= \left(\frac{c_i}{c_{i-1}} - 1\right) - \frac{1}{2}\left(\frac{c_i}{c_{i-1}} - 1\right)^2 + \frac{1}{3}\left(\frac{c_i}{c_{i-1}} - 1\right)^3 - .... \\
&= \frac{c_i - c_{i-1}}{c_{i-1}}\left[1 - \frac{c_i - c_{i-1}}{2c_{i-1}} + \frac{(c_i - c_{i-1})^2}{3c_{i-1}^2} - ....\right] \\
&= \frac{c_i - c_{i-1}}{6c_{i-1}^3}\left[6c_{i-1}^2 - 3c_{i-1}(c_i - c_{i-1}) + 2(c_i - c_{i-1})^2 - ....\right] \\
&= \frac{c_i - c_{i-1}}{6c_{i-1}^3}\left[6c_{i-1}^2 - (c_i - c_{i-1})\langle 3c_{i-1} - 2(c_i - c_{i-1})\rangle - ....\right] \\
&= \frac{c_i - c_{i-1}}{6c_{i-1}^3}\left[6c_{i-1}^2 + (c_i - c_{i-1})(2c_i - 5c_{i-1}) - ....\right]
\end{aligned} \tag{D2}$$

In view of equation (D2), equation (D1) can be written as:

$$\tan\theta_i = \frac{(\Delta l)_i}{(c_i - c_{i-1})^3}\Big[(c_i - c_{i-1})^2\varepsilon_{i-1} - A_i(\Delta l)_i c_{i-1}(c_i - c_{i-1}) + B_i(\Delta l)_i^2 c_{i-1}^2\Big]\times$$

$$\times\frac{c_i - c_{i-1}}{6c_{i-1}^3}\Big[6c_{i-1}^2 + (c_i - c_{i-1})(2c_i - 5c_{i-1}) - ....\Big]$$

$$+\frac{(\Delta l)_i}{2(c_i - c_{i-1})^2}\Big[2A_i(\Delta l)_i(c_i - c_{i-1}) + B_i(\Delta l)_i^2(c_i - 3c_{i-1})\Big] + \tan\theta_{i-1}$$

$$= \frac{(\Delta l)_i}{6c_{i-1}^3(c_i - c_{i-1})^2}\begin{Bmatrix}(c_i - c_{i-1})^2\Big[6c_{i-1}^2 + (c_i - c_{i-1})(2c_i - 5c_{i-1}) - ....\Big]\varepsilon_{i-1}\\ -A_i(\Delta l)_i c_{i-1}(c_i - c_{i-1})\Big[6c_{i-1}^2 + (c_i - c_{i-1})(2c_i - 5c_{i-1}) - ....\Big]\\ +B_i(\Delta l)_i^2 c_{i-1}^2\Big[6c_{i-1}^2 + (c_i - c_{i-1})(2c_i - 5c_{i-1}) - ....\Big]\end{Bmatrix}$$

$$+\frac{(\Delta l)_i}{6c_{i-1}^3(c_i - c_{i-1})^2}\Big[6A_i(\Delta l)_i c_{i-1}^3(c_i - c_{i-1}) + 3B_i(\Delta l)_i^2 c_{i-1}^3(c_i - 3c_{i-1})\Big] + \tan\theta_{i-1}$$

$$= \frac{(\Delta l)_i}{6c_{i-1}^3(c_i - c_{i-1})^2}\begin{Bmatrix}(c_i - c_{i-1})^2\Big[6c_{i-1}^2 + (c_i - c_{i-1})(2c_i - 5c_{i-1}) - ....\Big]\varepsilon_{i-1}\\ -A_i(\Delta l)_i c_{i-1}(c_i - c_{i-1})\Big[6c_{i-1}^2 + (c_i - c_{i-1})(2c_i - 5c_{i-1}) - ....\Big]\\ +B_i(\Delta l)_i^2 c_{i-1}^2\Big[6c_{i-1}^2 + (c_i - c_{i-1})(2c_i - 5c_{i-1}) - ....\Big]\\ \Big[6A_i(\Delta l)_i c_{i-1}^3(c_i - c_{i-1}) + 3B_i(\Delta l)_i^2 c_{i-1}^3(c_i - 3c_{i-1})\Big]\end{Bmatrix} + \tan\theta_{i-1}$$

$$= \frac{(\Delta l)_i}{6c_{i-1}^3(c_i - c_{i-1})^2}\begin{Bmatrix}(c_i - c_{i-1})^2\Big[6c_{i-1}^2 + (c_i - c_{i-1})(2c_i - 5c_{i-1}) - ....\Big]\varepsilon_{i-1}\\ -6A_i(\Delta l)_i c_{i-1}^3(c_i - c_{i-1}) - A_i(\Delta l)_i c_{i-1}(c_i - c_{i-1})^2(2c_i - 5c_{i-1}) - ....\\ +6B_i(\Delta l)_i^2 c_{i-1}^4 + B_i(\Delta l)_i^2 c_{i-1}^2(c_i - c_{i-1})\big\langle 2c_i - 2c_{i-1}\big) - 3c_{i-1}\big\rangle - ....\\ 6A_i(\Delta l)_i c_{i-1}^3(c_i - c_{i-1}) + 3B_i(\Delta l)_i^2 c_{i-1}^3\big\langle(c_i - c_{i-1}) - 2c_{i-1}\big\rangle\end{Bmatrix} + \tan\theta_{i-1}$$

$$= \frac{(\Delta l)_i}{6c_{i-1}^3(c_i - c_{i-1})^2}\begin{Bmatrix}(c_i - c_{i-1})^2\Big[6c_{i-1}^2 + (c_i - c_{i-1})(2c_i - 5c_{i-1})....\Big]\varepsilon_{i-1}\\ -A_i(\Delta l)_i c_{i-1}(c_i - c_{i-1})^2(2c_i - 5c_{i-1})....\\ +2B_i(\Delta l)_i^2 c_{i-1}^2(c_i - c_{i-1})^2....\end{Bmatrix} + \tan\theta_{i-1} \qquad \text{(D3)}$$

After cancelling $(c_i - c_{i-1})^2$ terms, equation (D3) becomes:

$$\tan\theta_i = \frac{(\Delta l)_i}{6c_{i-1}^3}\begin{bmatrix}\big\langle 6c_{i-1}^2 + (c_i - c_{i-1})(2c_i - 5c_{i-1})\big\rangle\varepsilon_{i-1}\\ -A_i(\Delta l)_i c_{i-1}(2c_i - 5c_{i-1}) + 2B_i(\Delta l)_i^2 c_{i-1}^2\end{bmatrix} + \tan\theta_{i-1} \qquad \text{(D4)}$$

Equation (D4) is the Log-expanded slope equation (18a) in the text.

For uniform beam ($c_{i-1} = c_i = c$), equation (D4) becomes:

$$\tan\theta_i = \frac{(\Delta l)_i}{c}\left[\varepsilon_{i-1} + \frac{A_i}{2}(\Delta l)_i + \frac{B_i}{3}(\Delta l)_i^2\right] + \tan\theta_{i-1} \tag{D5}$$

which is identical to equation (E8) in Appendix E.

Log-Expanded Deflection Equations

The deflection equation (17b) is duplicated below as equation (D6).

$$\begin{aligned} y_i = {} & \frac{(\Delta l)_i^2}{(c_i - c_{i-1})^4}\left[(c_i - c_{i-1})^2\varepsilon_{i-1} - A_i(\Delta l)_i(c_i - c_{i-1})c_{i-1} + B_i(\Delta l)_i^2 c_{i-1}^2\right]\left[c_i \log_e\frac{c_i}{c_{i-1}} - (c_i - c_{i-1})\right] \\ & + \frac{(\Delta l)_i^2}{6(c_i - c_{i-1})^2}\left[3A(\Delta l)_i(c_i - c_{i-1}) + B_i(\Delta l)_i^2(c_i - 4c_{i-1})_i\right] + y_{i-1} + (\Delta l)_i \tan\theta_{i-1} \end{aligned} \tag{D6}$$

For slowly changing $c(x)$ [that is, $(c_i/c_{i-1}) \to 1$], the logarithm term, $\log_e(c_i/c_{i-1})$, in the deflection equation (18b) can be expanded in series form up to the fourth order term as equation (D7) (ref. 15):

$$\begin{aligned} \log_e\frac{c_i}{c_{i-1}} &= \left(\frac{c_i}{c_{i-1}} - 1\right) - \frac{1}{2}\left(\frac{c_i}{c_{i-1}} - 1\right)^2 + \frac{1}{3}\left(\frac{c_i}{c_{i-1}} - 1\right)^3 - \frac{1}{4}\left(\frac{c_i}{c_{i-1}} - 1\right)^4 + ... \\ &= \frac{c_i - c_{i-1}}{12c_{i-1}^4}\left[12c_{i-1}^3 - 6c_{i-1}^2(c_i - c_{i-1}) + 4c_{i-1}(c_i - c_{i-1})^2 - 3((c_i - c_{i-1})^3 + ...\right] \end{aligned} \tag{D7}$$

Then the term, $\left[c_i \log_e(c_i/c_{i-1}) - (c_i - c_{i-1})\right]$, in equation (D6) can then be written as:

$$\begin{aligned} & c_i\log_e\frac{c_i}{c_{i-1}} - (c_i - c_{i-1}) \\ & = \frac{c_i(c_i - c_{i-1})}{12c_{i-1}^4}\left[12c_{i-1}^3 - 6c_{i-1}^2(c_i - c_{i-1}) + 4c_{i-1}(c_i - c_{i-1})^2 - 3((c_i - c_{i-1})^3 + ...\right] - (c_i - c_{i-1}) \\ & = \frac{c_i(c_i - c_{i-1})}{12c_{i-1}^4}\left[12c_{i-1}^3 - 6c_{i-1}^2(c_i - c_{i-1}) + 4c_{i-1}(c_i - c_{i-1})^2 - 3((c_i - c_{i-1})^3 - \frac{12c_{i-1}^4}{c_i}\right] \\ & = \frac{c_i(c_i - c_{i-1})}{12c_{i-1}^4}\left[\frac{12c_{i-1}^3}{c_i}(c_i - c_{i-1}) - 6c_{i-1}^2(c_i - c_{i-1}) + 4c_{i-1}(c_i - c_{i-1})^2 - 3(c_i - c_{i-1})^3\right] \\ & = \frac{(c_i - c_{i-1})^2}{12c_{i-1}^4}\left[12c_{i-1}^3 - 6c_ic_{i-1}^2 + 4c_ic_{i-1}(c_i - c_{i-1}) - 3c_i(c_i - c_{i-1})^2\right] \\ & = \frac{(c_i - c_{i-1})^2}{12c_{i-1}^4}\left[6c_{i-1}^3 - 6c_{i-1}^2(c_i - c_{i-1}) + 4c_ic_{i-1}(c_i - c_{i-1}) - 3c_i(c_i - c_{i-1})^2\right] \\ & = \frac{(c_i - c_{i-1})^2}{12c_{i-1}^4}\left[6c_{i-1}^3 + (4c_ic_{i-1} - 6c_{i-1}^2)(c_i - c_{i-1}) - 3c_i(c_i - c_{i-1})^2\right] \end{aligned} \tag{D8}$$

In view of equation (D8), equation (D6) can be rewritten as:

$$
\begin{aligned}
y_i &= \frac{(\Delta l)_i^2}{(c_i - c_{i-1})^4}\Big[(c_i - c_{i-1})^2 \varepsilon_{i-1} - A_i (\Delta l)_i c_{i-1}(c_i - c_{i-1}) + B_i (\Delta l)_i^2 c_{i-1}^2\Big] \times \\
&\qquad \times \frac{(c_i - c_{i-1})^2}{12 c_{i-1}^4}\Big[6c_{i-1}^3 + c_{i-1}(4c_i - 6c_{i-1})(c_i - c_{i-1}) - 3c_i (c_i - c_{i-1})^2\Big] \\
&\quad + \frac{(\Delta l)_i^2}{6(c_i - c_{i-1})^2}\Big[3A(\Delta l)_i (c_i - c_{i-1}) + B_i (\Delta l)_i^2 (c_i - 4c_{i-1})\Big] + y_{i-1} + (\Delta l)_i \tan\theta_{i-1} \\
&= \frac{(\Delta l)_i^2}{12 c_{i-1}^4 (c_i - c_{i-1})^2}\left\{\begin{array}{l}
(c_i - c_{i-1})^2\Big[6c_{i-1}^3 + c_{i-1}(4c_i - 6c_{i-1})(c_i - c_{i-1}) - 3c_i (c_i - c_{i-1})^2\Big]\varepsilon_{i-1} \\
-A_i (\Delta l)_i c_{i-1}(c_i - c_{i-1})\Big[6c_{i-1}^3 + c_{i-1}(4c_i - 6c_{i-1})(c_i - c_{i-1}) - 3c_i (c_i - c_{i-1})^2\Big] \\
+B_i (\Delta l)_i^2 c_{i-1}^2\Big[6c_{i-1}^3 + c_{i-1}(4c_i - 6c_{i-1})(c_i - c_{i-1}) - 3c_i (c_i - c_{i-1})^2\Big]
\end{array}\right\} \\
&\qquad + \frac{(\Delta l)_i^2}{12 c_{i-1}^4 (c_i - c_{i-1})^2}\Big[6A_i (\Delta l)_i c_{i-1}^4 + 2B_i (\Delta l)_i^2 c_{i-1}^4 (c_i - 3c_{i-1})\Big] + y_{i-1} + (\Delta l)_i \tan\theta_{i-1} \\
&= \frac{(\Delta l)_i^2}{12 c_{i-1}^4 (c_i - c_{i-1})^2}\left\{\begin{array}{l}
(c_i - c_{i-1})^2\Big[6c_{i-1}^3 + c_{i-1}(4c_i - 6c_{i-1})(c_i - c_{i-1}) - 3c_i (c_i - c_{i-1})^2\Big]\varepsilon_{i-1} \\
-A_i (\Delta l)_i (c_i - c_{i-1}) c_{i-1}\Big[6c_{i-1}^3 + c_{i-1}(4c_i - 6c_{i-1})(c_i - c_{i-1}) - 3c_i (c_i - c_{i-1})^2\Big] \\
+6A_i (\Delta l)_i c_{i-1}^4 (c_i - c_{i-1}) \\
+B_i (\Delta l)_i^2 c_{i-1}^2\Big[6c_{i-1}^3 + c_{i-1}(4c_i - 6c_{i-1})(c_i - c_{i-1}) - 3c_i (c_i - c_{i-1})^2\Big] \\
+2B_i (\Delta l)_i^2 c_{i-1}^4\Big[(c_i - c_{i-1}) - 3c_{i-1}\Big]
\end{array}\right\} \\
&\qquad + y_{i-1} + (\Delta l)_i \tan\theta_{i-1} \\
&= \frac{(\Delta l)_i^2}{12 c_{i-1}^4 (c_i - c_{i-1})^2}\left\{\begin{array}{l}
(c_i - c_{i-1})^2\Big[6c_{i-1}^3 + c_{i-1}(4c_i - 6c_{i-1})(c_i - c_{i-1}) - 3c_i (c_i - c_{i-1})^2\Big]\varepsilon_{i-1} \\
-A_i (\Delta l)_i (c_i - c_{i-1}) c_{i-1}\left[\begin{array}{l}6c_{i-1}^3 + c_{i-1}(4c_i - 6c_{i-1})(c_i - c_{i-1}) - 3c_i (c_i - c_{i-1})^2 \\ -6c_{i-1}^3\end{array}\right] \\
+B_i (\Delta l)_i^2 c_{i-1}^2\left[\begin{array}{l}6c_{i-1}^3 + c_{i-1}(4c_i - 4c_{i-1} - 2c_{i-1})(c_i - c_{i-1}) - 3c_i (c_i - c_{i-1})^2 \\ +2c_{i-1}^2 (c_i - c_{i-1}) - 6c_{i-1}^3\end{array}\right]
\end{array}\right\} \\
&\qquad + y_{i-1} + (\Delta l)_i \tan\theta_{i-1} \\
&= \frac{(\Delta l)_i^2}{12 c_{i-1}^4 (c_i - c_{i-1})^2}\left\{\begin{array}{l}
(c_i - c_{i-1})^2\Big[6c_{i-1}^3 + c_{i-1}(4c_i - 6c_{i-1})(c_i - c_{i-1}) - 3c_i (c_i - c_{i-1})^2\Big]\varepsilon_{i-1} \\
-A_i (\Delta l)_i (c_i - c_{i-1}) c_{i-1}\Big[c_{i-1}(4c_i - 6c_{i-1})(c_i - c_{i-1}) - 3c_i (c_i - c_{i-1})^2\Big] \\
+B_i (\Delta l)_i^2 c_{i-1}^2\Big[4c_{i-1}(c_i - c_{i-1})^2 - 3c_i (c_i - c_{i-1})^2\Big]
\end{array}\right\} \\
&\qquad + y_{i-1} + (\Delta l)_i \tan\theta_{i-1} \\
&= \frac{(\Delta l)_i^2}{12 c_{i-1}^4}\left\{\begin{array}{l}
\Big[6c_{i-1}^3 + c_{i-1}(4c_i - 6c_{i-1})(c_i - c_{i-1}) - 3c_i (c_i - c_{i-1})^2\Big]\varepsilon_{i-1} \\
-A_i (\Delta l)_i c_{i-1}\Big[c_{i-1}(4c_i - 6c_{i-1}) - 3c_i (c_i - c_{i-1})\Big] \\
+B_i (\Delta l)_i^2 c_{i-1}^2 (4c_{i-1} - 3c_i)
\end{array}\right\} + y_{i-1} + (\Delta l)_i \tan\theta_{i-1}
\end{aligned}
$$

$$
\begin{aligned}
&= \frac{(\Delta l)_i^2}{12c_{i-1}^4}\left\{\begin{array}{l}\left[6c_{i-1}^3 + c_{i-1}(4c_i - 6c_{i-1})(c_i - c_{i-1}) - 3c_i(c_i - c_{i-1})^2\right]\varepsilon_{i-1} \\ -A_i(\Delta l)_i c_{i-1}\left[c_{i-1}(4c_i - 4c_{i-1} - 2c_{i-1}) - 3c_i(c_i - c_{i-1})\right] \\ +B_i(\Delta l)_i^2 c_{i-1}^2(4c_{i-1} - 3c_i)\end{array}\right\} + y_{i-1} + (\Delta l)_i \tan\theta_{i-1} \\
&= \frac{(\Delta l)_i^2}{12c_{i-1}^4}\left\{\begin{array}{l}\left[6c_{i-1}^3 + c_{i-1}(4c_i - 6c_{i-1})(c_i - c_{i-1}) - 3c_i(c_i - c_{i-1})^2\right]\varepsilon_{i-1} \\ -A_i(\Delta l)_i c_{i-1}\left[4c_{i-1}(c_i - c_{i-1}) - 2c_{i-1}^2 - 3c_i(c_i - c_{i-1})\right] \\ +B_i(\Delta l)_i^2 c_{i-1}^2(4c_{i-1} - 3c_i)\end{array}\right\} + y_{i-1} + (\Delta l)_i \tan\theta_{i-1} \\
&= \frac{(\Delta l)_i^2}{12c_{i-1}^4}\left\{\begin{array}{l}\overbrace{\left[6c_{i-1}^3 + c_{i-1}(4c_i - 6c_{i-1})(c_i - c_{i-1}) - 3c_i(c_i - c_{i-1})^2\right]}^{L}\varepsilon_{i-1} \\ +A_i(\Delta l)_i c_{i-1}\left[2c_{i-1}^2 + (3c_i - 4c_{i-1})(c_i - c_{i-1})\right] \\ +B_i(\Delta l)_i^2 c_{i-1}^2(4c_{i-1} - 3c_i)\end{array}\right\} + y_{i-1} + (\Delta l)_i \tan\theta_{i-1}
\end{aligned}
\tag{D9}
$$

Term L in equation (D9) can be rewritten as:

$$
\begin{aligned}
L &\equiv \left[6c_{i-1}^3 + c_{i-1}(4c_i - 6c_{i-1})(c_i - c_{i-1}) - 3c_i(c_i - c_{i-1})^2\right] \\
&= \left[6c_{i-1}^3 + \left\langle 4c_i c_{i-1} - 6c_{i-1}^2 - 3c_i(c_i - c_{i-1})\right\rangle(c_i - c_{i-1})\right] \\
&= \left[6c_{i-1}^3 + \left\langle 4c_i c_{i-1} - 6c_{i-1}^2 - 3c_i^2 + 3c_i c_{i-1})\right\rangle(c_i - c_{i-1})\right] \\
&= \left[6c_{i-1}^3 + \left\langle 7c_i c_{i-1} - 6c_{i-1}^2 - 3c_i^2\right\rangle(c_i - c_{i-1})\right] \\
&= \left[6c_{i-1}^3 + \left\langle 7c_i^2 c_{i-1} - 6c_i c_{i-1}^2 - 3c_i^3 - 7c_i c_{i-1}^2 + 6c_{i-1}^3 + 3c_i^2 c_{i-1}\right\rangle\right] \\
&= \left[6c_{i-1}^3 + \left\langle 10c_i^2 c_{i-1} - 13c_i c_{i-1}^2 - 3c_i^3 + 3c_{i-1}^3 + 3c_{i-1}^3\right\rangle\right] \\
&= \left[6c_{i-1}^3 + \left\langle 10c_i^2 c_{i-1} - 13c_i c_{i-1}^2 + 3c_{i-1}^3 - 3(c_i^3 - c_{i-1}^3)\right\rangle\right] \\
&= \left[6c_{i-1}^3 + \left\langle 10c_i^2 c_{i-1} - 10c_i c_{i-1}^2 - 3c_i c_{i-1}^2 + 3c_{i-1}^3 - 3(c_i^3 - c_{i-1}^3)\right\rangle\right] \\
&= \left[6c_{i-1}^3 + \left\langle 10c_i c_{i-1}(c_i - c_{i-1}) - 3c_{i-1}^2(c_i - c_{i-1}) - 3(c_i^3 - c_{i-1}^3)\right\rangle\right] \\
&= \left[6c_{i-1}^3 + c_{i-1}(10c_i - 3c_{i-1})(c_i - c_{i-1}) - 3(c_i^3 - c_{i-1}^3)\right]
\end{aligned}
\tag{D10}
$$

In light of equation (D10), equation (D9) takes on the final form as:

$$y_i = \frac{(\Delta l)_i^2}{12c_{i-1}^4}\begin{Bmatrix}\left[6c_{i-1}^3 + c_{i-1}(10c_i - 3c_{i-1})(c_i - c_{i-1}) - 3(c_i^3 - c_{i-1}^3)\right]\varepsilon_{i-1} \\ +A_i(\Delta l)_i c_{i-1}\left[2c_{i-1}^2 + (3c_i - 4c_{i-1})(c_i - c_{i-1})\right] \\ +B_i(\Delta l)_i^2 c_{i-1}^2\left[c_{i-1} - 3(c_i - c_{i-1})\right]\end{Bmatrix} + y_{i-1} + (\Delta l)_i \tan\theta_{i-1} \qquad \text{(D11)}$$

Equation (D11) is the Log-expanded deflection equation (18b) in the text.
For uniform beam ($c_{i-1} = c_i = c$), equation (D11) becomes equation (D12):

$$y_i = \frac{(\Delta l)_i^2}{2c}\left[\varepsilon_{i-1} + \frac{A_i}{3}(\Delta l)_i + \frac{B_i}{6}(\Delta l)_i^2\right] + y_{i-1} + (\Delta l)_i \tan\theta_{i-1} \qquad \text{(D12)}$$

which is identical to equation (E11) in Appendix E.

Log-Expanded Displacement Transfer Function

Combining equations (D4) and (D11) and using similar mathematical steps to Appendix B, one can write:

$$y_i = \underbrace{\frac{1}{12}\sum_{j=1}^{i}\frac{(\Delta l)_j^2}{c_{j-1}^4}\begin{Bmatrix}\left[6c_{j-1}^3 + c_{j-1}(10c_j - 3c_{i-1})(c_j - c_{j-1}) - 3(c_j^3 - c_{j-1}^3)\right]\varepsilon_{j-1} \\ +A_j(\Delta l)_j\left[2c_{j-1}^2 + c_{i-1}(c_j - c_{j-1})(3c_j - 4c_{j-1})\right] \\ +B_j(\Delta l)_j^2 c_{i-1}^2\left[c_{j-1} - 3(c_j - c_{j-1})\right]\end{Bmatrix}}_{\text{Contributions from deflection terms}} + y_0$$

$$+ \underbrace{\frac{1}{6}\sum_{j=1}^{i-1}\left\{\left[\sum_{k=j+1}^{i}(\Delta l)_k\right]\frac{(\Delta l)_j}{c_{j-1}^3}\begin{bmatrix}\left\langle 6c_{j-1}^2 + (c_j - c_{j-1})(2c_j - 5c_{j-1})\right\rangle\varepsilon_{j-1} \\ -A_j(\Delta l)_j c_{j-1}(2c_j - 5c_{j-1}) + 2B_j(\Delta l)_j^2 c_{j-1}^2\end{bmatrix} + \left[\sum_{j=1}^{i}(\Delta l)_j\right]\tan\theta_0\right\}}_{\text{Contributions from slope terms}} \qquad \text{(D13)}$$

Equation (D13) is equation (18c) in the text, the Variable-Domain Log-expanded Displacement Transfer Functions in dual summation form for slightly nonuniform (including uniform) embedded beams based on piecewise-nonlinear strain representations.

Degeneration into Constant Domain Cases

For constant-domain length, $(\Delta l)_1 = (\Delta l)_2 = (\Delta l)_3 = ... = \Delta l$, coefficients A_i [eq. (C4)] and B_i [(eq. (C5)] become equations (D14) and (D15):

$$A_i \equiv -\frac{(\Delta l)_{i+1}[2(\Delta l)_i + (\Delta l)_{i+1}]\varepsilon_{i-1} - [(\Delta l)_i + (\Delta l)_{i+1}]^2\varepsilon_i + (\Delta l)_i^2\varepsilon_{i+1}}{(\Delta l)_i(\Delta l)_{i+1}[(\Delta l)_i + (\Delta l)_{i+1}]} = -\frac{3\varepsilon_{i-1} - 4\varepsilon_i + \varepsilon_{i+1}}{2\Delta l} \qquad \text{(D14)}$$

$$B_i \equiv \frac{(\Delta l)_{i+1}\varepsilon_{i-1} - [(\Delta l)_i + (\Delta l)_{i+1}]\varepsilon_i + (\Delta l)_i\varepsilon_{i+1}}{(\Delta l)_i(\Delta l)_{i+1}[(\Delta l)_i + (\Delta l)_{i+1}]} = \frac{\varepsilon_{i-1} - 2\varepsilon_i + \varepsilon_{i+1}}{2(\Delta l)^2} \qquad \text{(D15)}$$

Slope Equation $[(\Delta l)_i \to \Delta l]$

In view of equations (D14) and (D15), slope equation (D4) can be written as:

$$\tan\theta_i = \frac{(\Delta l)_i}{12c_{i-1}^3}\begin{bmatrix}12c_{i-1}^2\varepsilon_{i-1}+2(c_i-c_{i-1})(2c_i-5c_{i-1})\varepsilon_{i-1}\\ +6A_ic_{i-1}^2(\Delta l)_i-4A_i(\Delta l)_ic_{i-1}(c_i-c_{i-1})+4B_ic_{i-1}^2(\Delta l)_i^2\end{bmatrix}+\tan\theta_{i-1}$$

$$=\frac{(\Delta l)_i}{c_{i-1}}\begin{bmatrix}\varepsilon_{i-1}+\dfrac{(c_i-c_{i-1})}{6c_{i-1}^2}(2c_i-5c_{i-1})\varepsilon_{i-1}\\ +\dfrac{A_i}{2}(\Delta l)_i-\dfrac{A_i(\Delta l)_i}{3c_{i-1}}(c_i-c_{i-1})+\dfrac{B_i}{3}(\Delta l)_i^2\end{bmatrix}+\tan\theta_{i-1}$$

$$=\frac{\Delta l}{c_{i-1}}\begin{bmatrix}\varepsilon_{i-1}+\dfrac{(c_i-c_{i-1})}{6c_{i-1}^2}(2c_i-2c_{i-1}-3c_{i-1})\varepsilon_{i-1}\\ -\dfrac{3\varepsilon_{i-1}-4\varepsilon_i+\varepsilon_{i+1}}{4}+\dfrac{3\varepsilon_{i-1}-4\varepsilon_i+\varepsilon_{i+1}}{6c_{i-1}}(c_i-c_{i-1})+\dfrac{\varepsilon_{i-1}-2\varepsilon_i+\varepsilon_{i+1}}{6}\end{bmatrix}+\tan\theta_{i-1}$$

$$=\frac{\Delta l}{c_{i-1}}\begin{bmatrix}\varepsilon_{i-1}+\dfrac{2(c_i-c_{i-1})^2}{6c_{i-1}^2}\varepsilon_{i-1}-\dfrac{3(c_i-c_{i-1})}{6c_{i-1}}\varepsilon_{i-1}\\ -\dfrac{3\varepsilon_{i-1}-4\varepsilon_i+\varepsilon_{i+1}}{4}+\dfrac{3\varepsilon_{i-1}-4\varepsilon_i+\varepsilon_{i+1}}{6c_{i-1}}c_i-\dfrac{3\varepsilon_{i-1}-4\varepsilon_i+\varepsilon_{i+1}}{6}\\ +\dfrac{\varepsilon_{i-1}-2\varepsilon_i+\varepsilon_{i+1}}{6}\end{bmatrix}+\tan\theta_{i-1}$$

$$=\frac{\Delta l}{c_{i-1}}\begin{bmatrix}\varepsilon_{i-1}+\dfrac{(c_i-c_{i-1})^2}{3c_{i-1}^2}\varepsilon_{i-1}-\dfrac{c_i}{2c_{i-1}}\varepsilon_{i-1}+\dfrac{1}{2}\varepsilon_{i-1}-\dfrac{3}{4}\varepsilon_{i-1}+\dfrac{c_i}{2c_{i-1}}\varepsilon_{i-1}-\dfrac{1}{2}\varepsilon_{i-1}+\dfrac{1}{6}\varepsilon_{i-1}\\ -\dfrac{-4\varepsilon_i}{4}+\dfrac{-4\varepsilon_i}{6c_{i-1}}c_i-\dfrac{-4\varepsilon_i}{6}+\dfrac{-2\varepsilon_i}{6}\\ -\dfrac{\varepsilon_{i+1}}{4}+\dfrac{\varepsilon_{i+1}}{6c_{i-1}}c_i-\dfrac{\varepsilon_{i+1}}{6}+\dfrac{\varepsilon_{i+1}}{6}\end{bmatrix}+\tan\theta_{i-1}$$

$$=\frac{\Delta l}{c_{i-1}}\left[\left(1+\frac{(c_i-c_{i-1})^2}{3c_{i-1}^2}-\frac{3}{4}+\frac{1}{6}\right)\varepsilon_{i-1}+\left(1+\frac{2}{3}-\frac{1}{3}-\frac{2c_i}{3c_{i-1}}\right)\varepsilon_i+\left(-\frac{1}{4}+\frac{c_i}{6c_{i-1}}\right)\varepsilon_{i+1}\right]+\tan\theta_{i-1}$$

$$=\frac{\Delta l}{c_{i-1}}\left[\left(\frac{5}{12}+\frac{4(c_i-c_{i-1})^2}{12c_{i-1}^2}\right)\varepsilon_{i-1}+\left(\frac{4}{3}-\frac{2c_i}{3c_{i-1}}\right)\varepsilon_i+\left(-\frac{3}{12}+\frac{2c_i}{12c_{i-1}}\right)\varepsilon_{i+1}\right]+\tan\theta_{i-1} \qquad \text{(D16)}$$

After grouping terms, equation (D16) becomes:

$$\tan\theta_i=\frac{\Delta l}{12c_{i-1}^3}\left\{\left[5c_{i-1}^2+4(c_i-c_{i-1})^2\right]\varepsilon_{i-1}-8c_{i-1}\left(c_i-2c_{i-1}\right)\varepsilon_i+c_{i-1}(2c_i-3c_{i-1})\varepsilon_{i+1}\right\}+\tan\theta_{i-1} \qquad \text{(D17)}$$

Equation (D17) is identical to equation (8a) in the text, and thus confirming the mathematical accuracy of the Log-expanded slope equation (D4).

Deflection Equation $[(\Delta l)_i \to \Delta l]$

In view of equations (D14) and (D15), deflection equation (D11) can be written as:

$$y_i = \frac{(\Delta l)_i^2}{12c_{i-1}^4}\begin{Bmatrix}\left[6c_{i-1}^3+(10c_ic_{i-1}-3c_{i-1}^2)(c_i-c_{i-1})-3(c_i^3-c_{i-1}^3)\right]\varepsilon_{i-1}\\ +A_i(\Delta l)_i c_{i-1}\left[2c_{i-1}^2+(3c_i-4c_{i-1})(c_i-c_{i-1})\right]\\ +B_i(\Delta l)_i^2 c_{i-1}^2\left[c_{i-1}-3(c_i-c_{i-1})\right]\end{Bmatrix}$$

$$+ y_{i-1} + (\Delta l)_i \tan\theta_{i-1}$$

$$= \frac{(\Delta l)^2}{12c_{i-1}^4}\begin{Bmatrix}\left[6c_{i-1}^3+(10c_ic_{i-1}-3c_{i-1}^2)(c_i-c_{i-1})-3(c_i^3-c_{i-1}^3)\right]\varepsilon_{i-1}\\ -\left(\frac{3\varepsilon_{i-1}-4\varepsilon_i+\varepsilon_{i+1}}{2}\right)c_{i-1}\left[2c_{i-1}^2+(3c_i-4c_{i-1})(c_i-c_{i-1})\right]\\ +\left(\frac{\varepsilon_{i-1}-2\varepsilon_i+\varepsilon_{i+1}}{2}\right)c_{i-1}^2\left[c_{i-1}-3(c_i-c_{i-1})\right]\end{Bmatrix} + y_{i-1} + (\Delta l)\tan\theta_{i-1}$$

$$= \frac{(\Delta l)^2}{12c_{i-1}^4}\begin{Bmatrix}\left[6c_{i-1}^3+(10c_ic_{i-1}-3c_{i-1}^2)(c_i-c_{i-1})-3(c_i^3-c_{i-1}^3)\right]\varepsilon_{i-1}\\ -\left(\frac{3\varepsilon_{i-1}}{2}\right)c_{i-1}\left[2c_{i-1}^2+(3c_i-4c_{i-1})(c_i-c_{i-1})\right]\\ -\left(\frac{-4\varepsilon_i}{2}\right)c_{i-1}\left[2c_{i-1}^2+(3c_i-4c_{i-1})(c_i-c_{i-1})\right]\\ -\left(\frac{\varepsilon_{i+1}}{2}\right)c_{i-1}\left[2c_{i-1}^2+(3c_i-4c_{i-1})(c_i-c_{i-1})\right]\\ +\left(\frac{\varepsilon_{i-1}}{2}\right)c_{i-1}^2\left[c_{i-1}-3(c_i-c_{i-1})\right]\\ +\left(\frac{-2\varepsilon_i}{2}\right)c_{i-1}^2\left[c_{i-1}-3(c_i-c_{i-1})\right]\\ +\left(\frac{\varepsilon_{i+1}}{2}\right)c_{i-1}^2\left[c_{i-1}-3(c_i-c_{i-1})\right]\end{Bmatrix} + y_{i-1} + (\Delta l)\tan\theta_{i-1}$$

$$= \frac{(\Delta l)^2}{24c_{i-1}^4}\begin{Bmatrix}\left[12c_{i-1}^3+(20c_ic_{i-1}-6c_{i-1}^2)(c_i-c_{i-1})-6(c_i^3-c_{i-1}^3)\right]\varepsilon_{i-1}\\ -3\varepsilon_{i-1}c_{i-1}\left[2c_{i-1}^2+(3c_i-4c_{i-1})(c_i-c_{i-1})\right]+\varepsilon_{i-1}c_{i-1}^2\left[c_{i-1}-3(c_i-c_{i-1})\right]\\ +4\varepsilon_i c_{i-1}\left[2c_{i-1}^2+(3c_i-4c_{i-1})(c_i-c_{i-1})\right]-2\varepsilon_i c_{i-1}^2\left[c_{i-1}-3(c_i-c_{i-1})\right]\\ -\varepsilon_{i+1}c_{i-1}\left[+2c_{i-1}^2+(3c_i-4c_{i-1})(c_i-c_{i-1})\right]+\varepsilon_{i+1}c_{i-1}^2\left[c_{i-1}-3(c_i-c_{i-1})\right]\end{Bmatrix} + y_{i-1} + (\Delta l)\tan\theta_{i-1}$$

$$= \frac{(\Delta l)^2}{24c_{i-1}^4}\begin{Bmatrix}\left[12c_{i-1}^3+c_{i-1}(20c_i-6c_{i-1})(c_i-c_{i-1})-6(c_i^3-c_{i-1}^3)\right.\\ \left.-6c_{i-1}^3-c_{i-1}(9c_i-12c_{i-1})(c_i-c_{i-1})+c_{i-1}^3-3c_{i-1}^2(c_i-c_{i-1})\right]\varepsilon_{i-1}\\ +c_{i-1}\left[8c_{i-1}^2+(12c_i-16c_{i-1})(c_i-c_{i-1})-2c_{i-1}^2+6c_{i-1}(c_i-c_{i-1})\right]\varepsilon_i\\ -c_{i-1}\left[2c_{i-1}^2+(3c_i-4c_{i-1})(c_i-c_{i-1})-c_{i-1}^2+3c_{i-1}(c_i-c_{i-1})\right]\varepsilon_{i+1}\end{Bmatrix} + y_{i-1} + (\Delta l)\tan\theta_{i-1}$$

$$= \frac{(\Delta l)^2}{24 c_{i-1}^4} \left\{ \begin{array}{l} \underbrace{\left[7c_{i-1}^3 + c_{i-1}(11c_i + 3c_{i-1})(c_i - c_{i-1}) - 6(c_i^3 - c_{i-1}^3) \right]}_{F_1} \varepsilon_{i-1} \\ + \underbrace{c_{i-1}\left[6c_{i-1}^2 + (12c_i - 10c_{i-1})(c_i - c_{i-1}) \right]}_{F_2} \varepsilon_i \\ \underbrace{-c_{i-1}\left[c_{i-1}^2 + (3c_i - c_{i-1})(c_i - c_{i-1}) \right]}_{F_3} \varepsilon_{i+1} \end{array} \right\} + y_{i-1} + (\Delta l)\tan\theta_{i-1} \tag{D18}$$

Ther terms $\{F_1, F_2, F_3\}$ in equation (D18) can be rewritten as:

$$\begin{aligned} F_1 &= \left[7c_{i-1}^3 + c_{i-1}(11c_i + 3c_{i-1})(c_i - c_{i-1}) - 6(c_i^3 - c_{i-1}^3) \right] \\ &= \left[7c_{i-1}^3 + 11c_i^2 c_{i-1} - 11c_i c_{i-1}^2 + 3c_i c_{i-1}^2 - 3c_{i-1}^3 - 3c_i^3 + 3c_{i-1}^3) - 3(c_i^3 - c_{i-1}^3) \right] \\ &= \left[7c_{i-1}^3 + 8c_i^2 c_{i-1} + 3c_i^2 c_{i-1} - 8c_i c_{i-1}^2 - 3c_i^3 - 3(c_i^3 - c_{i-1}^3) \right] \\ &= \left[7c_{i-1}^3 + 8c_i c_{i-1}(c_i - c_{i-1}) - 3c_i^2(c_i - c_{i-1}) - 3(c_i^3 - c_{i-1}^3) \right] \\ &= \left[7c_{i-1}^3 + (c_i - c_{i-1})(8c_i c_{i-1} - 3c_i^2) - 3(c_i^3 - c_{i-1}^3) \right] \end{aligned} \tag{D19}$$

$$\begin{aligned} F_2 &= c_{i-1}\left[6c_{i-1}^2 + (12c_i - 10c_{i-1})(c_i - c_{i-1}) \right] \\ &= 2c_{i-1}\left[3c_{i-1}^2 + 6c_i^2 - 5c_i c_{i-1} - 6c_i c_{i-1} + 5c_{i-1}^2 \right] \\ &= 2c_{i-1}\left[8c_{i-1}^2 + 6c_i^2 - 11c_i c_{i-1} \right] \\ &= 2c_{i-1}\left[8c_{i-1}^2 + 3c_i^2 + 3c_i^2 - 8c_i c_{i-1} - 3c_i c_{i-1} \right] \\ &= 2c_{i-1}\left[3c_i^2 + (3c_i - 8c_{i-1})(c_i - c_{i-1}) \right] \end{aligned} \tag{D20}$$

$$\begin{aligned} F_3 &= -c_{i-1}\left[c_{i-1}^2 + (3c_i - c_{i-1})(c_i - c_{i-1}) \right] \\ &= -c_{i-1}\left[c_{i-1}^2 + (3c_i^2 - c_i c_{i-1} - 3c_i c_{i-1} + c_{i-1}^2) \right] \\ &= -c_{i-1}\left[c_i^2 + (2c_i^2 - 4c_i c_{i-1} + 2c_{i-1}^2) \right] \\ &= -c_{i-1}\left[c_i^2 + 2(c_i - c_{i-1})^2 \right] \end{aligned} \tag{D21}$$

Substitutions of equations (D19), (D20) (D21) into equation (D18) yields:

$$\begin{aligned} y_i = \frac{(\Delta l)^2}{24 c_{i-1}^4} \Big\{ & \left[7c_{i-1}^3 + (c_i - c_{i-1})(8c_i c_{i-1} - 3c_i^2) - 3(c_i^3 - c_{i-1}^3) \right] \varepsilon_{i-1} \\ & + 2c_{i-1}\left[(3c_i^2 + (c_i - c_{i-1})(3c_i - 8c_{i-1}) \right] \varepsilon_i - c_{i-1}\left[c_i^2 + 2(c_i - c_{i-1})^2 \right] \varepsilon_{i+1} \Big\} \\ & + y_{i-1} + \Delta l \tan\theta_{i-1} \end{aligned} \tag{D22}$$

Equation (D22) is identical to equation (8b) in the text, and thus confirming the mathematical accuracy of the Log expanded deflection equation (D11).

Displacement Transfer Function $[(\Delta l)_i \rightarrow \Delta l]$

Combining equations (D17) and (D22), and after grouping terms, one obtains the displacement transfer function in dual summation form as:

$$y_i = \underbrace{\frac{(\Delta l)^2}{24}\sum_{j=1}^{i}\frac{1}{c_{j-1}^4}\begin{Bmatrix}\left[7c_{j-1}^3+(c_j-c_{j-1})(8c_jc_{j-1}-3c_j^2)-3(c_j^3-c_{j-1}^3)\right]\varepsilon_{j-1}\\ +2c_{j-1}\left[(3c_j^2+(c_j-c_{j-1})(3c_j-8c_{j-1})\right]\varepsilon_j\\ -c_{j-1}\left[c_j^2+2(c_j-c_{j-1})^2\right]\varepsilon_{j+1}\end{Bmatrix}+y_0}_{\text{Contributions from deflection terms}}$$

$$+\underbrace{\frac{(\Delta l)^2}{12}\sum_{j=1}^{i-1}\frac{(i-j)}{c_{j-1}^3}\begin{Bmatrix}\left[5c_{j-1}^2+4(c_j-c_{j-1})^2\right]\varepsilon_{j-1}-8c_{j-1}(c_j-2c_{j-1})\varepsilon_j\\ +c_{j-1}(2c_j-3c_{j-1})\varepsilon_{j+1}\end{Bmatrix}+(i)\Delta l\tan\theta_0}_{\text{Contributions from slope terms}} \qquad \text{(D23)}$$

Equation (D23) is identical to equation (8c) in the text, the Constant-Domain Log-expanded Displacement Transfer Functions in dual summation form for slightly nonuniform (including uniform) embedded beams based on piecewise-nonlinear strain representations.

APPENDIX E
DERIVATIONS OF VARIABLE-DOMAIN IMPROVED DISPLACE TRANSFER FUNCTIONS FOR UNIFORM BEAMS

(Based on Piecewise-Nonlinear Strain Representations)

Appendix E presents the derivations of the slope and deflection equations for the special case of the uniform beam based on piecewise-nonlinear strain representations.

Slope Equations $[c(x)=c]$

The slope, $\tan\theta(x)$, of the uniform beam $[c(x)=c]$ in the small domain, $x_{i-1} \le x \le x_i$, between the two adjacent strain-sensing stations, $\{x_{i-1}, x_i\}$, can be obtained by integrating both sides of equation (E1):

$$\underbrace{\int_{x_{i-1}}^{x} \frac{d^2y}{dx^2}dx = \frac{dy}{dx} - \underbrace{\left(\frac{dy}{dx}\right)_{i-1}}_{\text{Slope at } x_{i-1}} \equiv \tan\theta(x) - \underbrace{\tan\theta_{i-1}}_{\text{Slope at } x_{i-1}}}_{\text{Intergation of left hand side of equation (1)}} = \underbrace{\int_{x_{i-1}}^{x} \frac{\varepsilon(x)}{c}dx}_{\text{Integration of right hand side of equation (1)}} \quad ; \quad (x_{i-1} \le x \le x_i) \qquad \text{(E1)}$$

The piecewise-nonlinear equation (16) representing the bending strain, $\varepsilon(x)$, within the small domain, $x_{i-1} \le x \le x_i$, between the two adjacent strain-sensing stations, $\{x_{i-1}, x_i\}$, is duplicated below as equations (E2) –(E5):

$$\begin{aligned}\varepsilon(x) = \varepsilon_{i-1} &- \frac{(\Delta l)_{i+1}[2(\Delta l)_i + (\Delta l)_{i+1}]\varepsilon_{i-1} - [(\Delta l)_i + (\Delta l)_{i+1}]^2\varepsilon_i + (\Delta l)_i^2\varepsilon_{i+1}}{(\Delta l)_i(\Delta l)_{i+1}[(\Delta l)_i + (\Delta l)_{i+1}]}(x - x_{i-1}) \\ &+ \frac{(\Delta l)_{i+1}\varepsilon_{i-1} - [(\Delta l)_i + (\Delta l)_{i+1}]\varepsilon_i + (\Delta l)_i\varepsilon_{i+1}}{(\Delta l)_i(\Delta l)_{i+1}[(\Delta l)_i + (\Delta l)_{i+1}]}(x - x_{i-1})^2 \\ &\qquad\qquad (x_{i-1} \le x \le x_i)\end{aligned} \qquad \text{(E2)}$$

Let,

$$A_i \equiv -\frac{(\Delta l)_{i+1}[2(\Delta l)_i + (\Delta l)_{i+1}]\varepsilon_{i-1} - [(\Delta l)_i + (\Delta l)_{i+1}]^2\varepsilon_i + (\Delta l)_i^2\varepsilon_{i+1}}{(\Delta l)_i(\Delta l)_{i+1}[(\Delta l)_i + (\Delta l)_{i+1}]} \qquad \text{(E3)}$$

$$B_i \equiv \frac{(\Delta l)_{i+1}\varepsilon_{i-1} - [(\Delta l)_i + (\Delta l)_{i+1}]\varepsilon_i + (\Delta l)_i\varepsilon_{i+1}}{(\Delta l)_i(\Delta l)_{i+1}[(\Delta l)_i + (\Delta l)_{i+1}]} \qquad \text{(E4)}$$

$$\xi \equiv (x - x_{i-1}) \qquad \text{(E5)}$$

In view of equation (E2), (E3), (E4), and (E5), the last three terms of equation (E1) can be written as:

$$\tan\theta(x) = \frac{1}{c}\int_0^{\xi}(\varepsilon_{i-1} + A_i\xi + B_i\xi^2)d\xi + \tan\theta_{i-1} \quad ; \quad [0 \le \xi \le (\Delta l)_i] \tag{E6}$$

After carrying out integration of equation (E6), one obtains (ref. 15):

$$\tan\theta(x) = \frac{\xi}{c}\left[\varepsilon_{i-1} + \frac{A_i}{2}\xi + \frac{B_i}{3}\xi^2\right] + \tan\theta_{i-1} \quad ; \quad [0 \le \xi \le (\Delta l)_i] \tag{E7}$$

At the strain-sensing station, x_i, we have $\xi = x_i - x_{i-1} = (\Delta l)_i$, then equation (E7) gives the slope, $\tan\theta_i[\equiv \tan\theta(x_i)]$ at x_i as:

$$\tan\theta_i = \frac{(\Delta l)_i}{c}\left[\varepsilon_{i-1} + \frac{A_i}{2}(\Delta l)_i + \frac{B_i}{3}(\Delta l)_i^2\right] + \tan\theta_{i-1} \quad ; \quad (i = 1,2,3,....,n) \tag{E8}$$

Equation (E8) is the slope equation in recursion form.

Deflection Equation $[c(x) = c]$

Deflection can be obtained by integrating the slope equation (E7) as:

$$y(x) = \int_0^{\xi}\tan\theta(\xi)d\xi + y_{i-1} = \frac{1}{c}\int_0^{\xi}\left\{\left[\varepsilon_{i-1}\xi + \frac{A_i}{2}\xi^2 + \frac{B_i}{3}\xi^3\right] + \tan\theta_{i-1}\right\}d\xi + y_{i-1} \tag{E9}$$

$$[0 \le \xi \le (\Delta l)_i]$$

Carrying out integration of equation (E9), one obtains:

$$y(x) = \frac{\xi^2}{2c}\left[\varepsilon_{i-1} + \frac{A_i}{3}\xi + \frac{B_i}{6}\xi^2\right] + y_{i-1} + \xi\tan\theta_{i-1} \quad ; \quad [0 \le \xi \le (\Delta l)_i] \tag{E10}$$

At the strain-sensing station, x_i, we have $\xi = x_i - x_{i-1} = (\Delta l)_i$, and the deflection, $y_i[\equiv y(x_i)]$ at x_i, is given by equation (E10) in the form:

$$y_i = \frac{(\Delta l)_i^2}{2c}\left[\varepsilon_{i-1} + \frac{A_i}{3}(\Delta l)_i + \frac{B_i}{6}(\Delta l)_i^2\right] + y_{i-1} + (\Delta l)_i\tan\theta_{i-1} \quad ; \quad (i = 1,2,3,....,n) \tag{E11}$$

Equation (E11) is the deflection equation in recursion form.

Displacement Transfer Function $[c(x) = c]$

Substitution of slope equation (E8) into deflection equation (E11), and following the mathematical steps presented in Appendix B, one obtains the deflection equation written in dual summation form as:

$$y_i = \underbrace{\frac{1}{2c}\sum_{j=1}^{i}\left\{(\Delta l)_j^2\left[\varepsilon_{j-1} + \frac{A_j}{3}(\Delta l)_j + \frac{B_j}{6}(\Delta l)_j^2\right]\right\}}_{\text{Contribution from deflection terms}}$$
$$+ \underbrace{\frac{1}{c}\sum_{j}^{i-1}\left\{\left[\sum_{k=j+1}^{i}(\Delta l)_k\right](\Delta l)_j^2\left[\varepsilon_{j-1} + \frac{A_j}{2}(\Delta l)_j + \frac{B_j}{3}(\Delta l)_j^2\right]\right\}}_{\text{Contributions from slope terms}} + \underbrace{y_0 + \left[\sum_{j=1}^{i}(\Delta l)_j\right]}_{=0 \text{ for cantilever beams}}\tan\theta_0 \qquad (E12)$$
$$(i = 1,2,3,....,n)$$

Equation (E12) is called the variable-domain Improved Displacement Transfer Function in dual summation form for uniform beams based on piecewise-nonlinear strain representations.

Degeneration into Constant-Domain Cases

For constant-domain length, $(\Delta l)_1 = (\Delta l)_2 = (\Delta l)_3 = ... = \Delta l$, coefficients A_i [eq. (E3)] and B_i [(eq. (E4)] become equations (E13) and (E14):

$$A_i \equiv -\frac{(\Delta l)_{i+1}[2(\Delta l)_i + (\Delta l)_{i+1}]\varepsilon_{i-1} - [(\Delta l)_i + (\Delta l)_{i+1}]^2\varepsilon_i + (\Delta l)_i^2\varepsilon_{i+1}}{(\Delta l)_i(\Delta l)_{i+1}[(\Delta l)_i + (\Delta l)_{i+1}]} = -\frac{3\varepsilon_{i-1} - 4\varepsilon_i + \varepsilon_{i+1}}{2\Delta l} \qquad (E13)$$

$$B_i \equiv \frac{(\Delta l)_{i+1}\varepsilon_{i-1} - [(\Delta l)_i + (\Delta l)_{i+1}]\varepsilon_i + (\Delta l)_i\varepsilon_{i+1}}{(\Delta l)_i(\Delta l)_{i+1}[(\Delta l)_i + (\Delta l)_{i+1}]} = \frac{\varepsilon_{i-1} - 2\varepsilon_i + \varepsilon_{i+1}}{2(\Delta l)^2} \qquad (E14)$$

Slope equation $[c(x) = c]$**:**

In view of equations (E13) and (E14), slope equation (E8) can be written as:

$$\tan\theta_i = \frac{(\Delta l)_i}{c}\left[\varepsilon_{i-1} + \frac{A_i}{2}(\Delta l)_i + \frac{B_i}{3}(\Delta l)_i^2\right] + \tan\theta_{i-1}$$
$$= \frac{\Delta l}{c}\left[\varepsilon_{i-1} + \underbrace{\left(-\frac{3\varepsilon_{i-1} - 4\varepsilon_i + \varepsilon_{i+1}}{2\Delta l}\right)}_{A_i}\frac{\Delta l}{2} + \underbrace{\left(\frac{\varepsilon_{i-1} - 2\varepsilon_i + \varepsilon_{i+1}}{2(\Delta l)^2}\right)}_{B_i}\frac{(\Delta l)^2}{3}\right] + \tan\theta_{i-1}$$
$$= \frac{\Delta l}{12c}\left[12\varepsilon_{i-1} - 3(3\varepsilon_{i-1} - 4\varepsilon_i + \varepsilon_{i+1}) + 2(\varepsilon_{i-1} - 2\varepsilon_i + \varepsilon_{i+1})\right] + \tan\theta_{i-1}$$
$$= \frac{\Delta l}{12c}(12\varepsilon_{i-1} - 9\varepsilon_{i-1} + 12\varepsilon_i - 3\varepsilon_{i+1} + 2\varepsilon_{i-1} - 4\varepsilon_i + 2\varepsilon_{i+1}) + \tan\theta_{i-1} \qquad (E15)$$

After grouping terms, equation (E15) becomes:

$$\tan\theta_i = \frac{\Delta l}{12c}(5\varepsilon_{i-1} + 8\varepsilon_i - \varepsilon_{i+1}) + \tan\theta_{i-1} \quad ; \quad (i = 1,2,3,....,n) \qquad (E16)$$

Equation (E16) is the degenerated form of equation (8a) in the text for $c_{i-1} = c_i = c$.

Deflection Equation $[c(x)=c]$

In view of equations (E13) and (E14), deflection equation (E11) becomes:

$$
\begin{aligned}
y_i &= \frac{(\Delta l)_i^2}{2c}\left[\varepsilon_{i-1}+\frac{A_i}{3}(\Delta l)_i+\frac{B_i}{6}(\Delta l)_i^2\right]+y_{i-1}+(\Delta l)_i\tan\theta_{i-1}\\
&= \frac{(\Delta l)^2}{2c}\left[\varepsilon_{i-1}+\underbrace{\left(-\frac{3\varepsilon_{i-1}-4\varepsilon_i+\varepsilon_{i+1}}{2\Delta l}\right)}_{A_i}\frac{\Delta l}{3}+\underbrace{\left(\frac{\varepsilon_{i-1}-2\varepsilon_i+\varepsilon_{i+1}}{2(\Delta l)^2}\right)}_{B_i}\frac{(\Delta l)^2}{6}\right]+y_{i-1}+\Delta l\tan\theta_{i-1}\\
&= \frac{(\Delta l)^2}{24c}\left[12\varepsilon_{i-1}-2(3\varepsilon_{i-1}-4\varepsilon_i+\varepsilon_{i+1})+(\varepsilon_{i-1}-2\varepsilon_i+\varepsilon_{i+1})\right]+y_{i-1}+\Delta l\tan\theta_{i-1}\\
&= \frac{(\Delta l)^2}{24c}\left[12\varepsilon_{i-1}-6\varepsilon_{i-1}+8\varepsilon_i-2\varepsilon_{i+1}+\varepsilon_{i-1}-2\varepsilon_i+\varepsilon_{i+1}\right]+y_{i-1}+\Delta l\tan\theta_{i-1}
\end{aligned}
\qquad \text{(E17)}
$$

After grouping terms, equation (E17) becomes:

$$
y_i=\frac{(\Delta l)^2}{24c}(7\varepsilon_{i-1}+6\varepsilon_i-\varepsilon_{i+1})+y_{i-1}+\Delta l\tan\theta_{i-1}\quad;\quad(i=1,2,3,....,n) \qquad \text{(E18)}
$$

Equation (E18) is the degenerated form of equation (8b) in the text for $c_{i-1}=c_i=c$.

Displacement Transfer Function $[c(x)=c]$

Combining equations (E16) and (E18) into one equation, and after grouping terms, one obtains:

$$
y_i=\underbrace{\frac{(\Delta l)^2}{24c}\sum_{j=1}^{i}(7\varepsilon_{j-1}+6\varepsilon_j-\varepsilon_{j+1})+y_0}_{\text{Contributions from deflection terms}}+\underbrace{\frac{(\Delta l)^2}{12c}\sum_{j=1}^{i-1}\left[(i-j)(5\varepsilon_{j-1}+8\varepsilon_j-\varepsilon_{j+1})\right]+(i)\Delta l\tan\theta_0}_{\text{Contributions from slope terms}} \qquad \text{(E19)}
$$

$$(i=1,2,3,....,n)$$

Equation (E19) is the degenerated form of equation (8c) in the text for $c_{i-1}=c_i=c$.

Special Case

For a special case when the strain distribution along the uniform beam is linear, one can write equation (E20),

$$
\varepsilon_{i+1}-\varepsilon_i=\varepsilon_i-\varepsilon_{i-1} \qquad \text{(E20)}
$$

or equation (E21),

$$
\varepsilon_{i+1}=2\varepsilon_i-\varepsilon_{i-1} \qquad \text{(E21)}
$$

In light of equation (E21), the slope equation (E16) becomes:

$$\begin{aligned}\tan\theta_i &= \frac{\Delta l}{12c}(5\varepsilon_{i-1} + 8\varepsilon_i - \varepsilon_{i+1}) + \tan\theta_{i-1} \\ &= \frac{\Delta l}{12c}[5\varepsilon_{i-1} + 8\varepsilon_i - (2\varepsilon_i - \varepsilon_{i-1})] + \tan\theta_{i-1}\end{aligned} \tag{E22}$$

After grouping terms, equation (E22) becomes:

$$\tan\theta_i = \frac{\Delta l}{2c}(\varepsilon_{i-1} + \varepsilon_i) + \tan\theta_{i-1} \quad ; \quad (i = 1,2,3,....,n) \tag{E23}$$

Equation (E23) is the degenerated form of equation (6a) for $c_{i-1} = c_i = c$.

Also, in view of equation (E21), the deflection equation (E18) becomes:

$$\begin{aligned}y_i &= \frac{(\Delta l)^2}{24c}(7\varepsilon_{i-1} + 6\varepsilon_i - \varepsilon_{i+1}) + y_{i-1} + \Delta l \tan\theta_{i-1} \\ &= \frac{(\Delta l)^2}{24c}[7\varepsilon_{i-1} + 6\varepsilon_i - (2\varepsilon_i - \varepsilon_{i-1})] + y_{i-1} + \Delta l \tan\theta_{i-1}\end{aligned} \tag{E24}$$

After grouping terms, equation (E24) becomes:

$$y_i = \frac{(\Delta l)^2}{6c}(2\varepsilon_{i-1} + \varepsilon_i) + y_{i-1} + \Delta l \tan\theta_{i-1} \quad ; \quad (i = 1,2,3,....,n) \tag{E25}$$

Equation (E25) is the degenerated form of equation (6b) for $c_{i-1} = c_i = c$.

Finally, in view of equation (E21), the deflection equation (E19) becomes:

$$\begin{aligned}y_i &= \underbrace{\frac{(\Delta l)^2}{24c}\sum_{j=1}^{i}(7\varepsilon_{j-1} + 6\varepsilon_j - \varepsilon_{j+1}) + y_0}_{\text{Contributions from deflection terms}} + \underbrace{\frac{(\Delta l)^2}{12c}\sum_{j=1}^{i-1}\Big[(i-j)(5\varepsilon_{j-1} + 8\varepsilon_j - \varepsilon_{j+1})\Big] + (i)\Delta l \tan\theta_0}_{\text{Contributions from slope terms}} \\ &= \frac{(\Delta l)^2}{24c}\sum_{j=1}^{i}\Big[7\varepsilon_{j-1} + 6\varepsilon_j - (2\varepsilon_j - \varepsilon_{j-1})\Big] + y_0 \\ &+ \frac{(\Delta l)^2}{12c}\sum_{j=1}^{i-1}\Big[(i-j)[5\varepsilon_{j-1} + 8\varepsilon_j - (2\varepsilon_j - \varepsilon_{j-1})]\Big] + (i)\Delta l \tan\theta_0\end{aligned} \tag{E26}$$

After grouping terms, equation (E26) becomes:

$$y_i = \underbrace{\frac{(\Delta l)^2}{6c}\sum_{j=1}^{i}(2\varepsilon_{j-1}+\varepsilon_j)+y_0}_{\text{Contributions from deflection terms}} + \underbrace{\frac{(\Delta l)^2}{2c}\sum_{j=1}^{i}\Big[(i-j)(\varepsilon_{j-1}+\varepsilon_j)\Big]+(i)\Delta l\tan\theta_0}_{\text{Contributions from slope terms}} \qquad (E27)$$

$$(i=1,2,3,....,n)$$

Equation (E27) is the degenerated form of equation (6c) for $c_{i-1}=c_i=c$.

REFERENCES

1. Ko, William L., W. L. Richards, and Van T. Tran, *Displacement Theories for In-Flight Deformed Shape Predictions of Aerospace Structures*, NASA/TP-2007-214612, October 2007.

2. Ko, William L., *Collection of Memoranda on Applications of Ko Displacement Theory to Deformed Shape Predictions of Aerospace Structures*, NASA/BR-119, April 2008.

3. Ko, William L., and Van Tran Fleischer, *Further Development of Ko Displacement Theory for Deformed Shape Predictions of Non-Uniform Aerospace Structures*, NASA/TP-2009-214643, September 2009.

4. Ko, William L., W. L. Richards, and Van Tran Fleischer, *Applications of Ko Displacement Theory to the Deformed Shape Predictions of Doubly Tapered Ikhana Wing*, NASA/TP-2009-214652, November 2009.

5. Ko, William L., and Van Tran Fleischer, *Methods for In-Flight Wing Shape Predictions of Highly Flexible Aerospace Structures: Formulation of Ko Displacement Theory*, NASA/TP-2010-214656, August 2010.

6. Ko, William L., and W. Lance Richards, *Method for Real-Time Structure Shape-Sensing*, U.S. Patent No. 7,520,176, issued April 21, 2009.

7. Ko, William L., and Van Tran Fleischer, *First and Second Order Displacement Transfer Functions for Structure Shape Calculations Using Analytically Predicted Surface Strains*, NASA/TP-2012-215976, March 2012.

8. Ko, William L., and Van Tran Fleischer, *Improved Displacement Transfer Functions for Structure Deformed Shape Predictions Using Discreetly Distributed Surface Strains*, NASA/TP-2012-216060, November 2012.

9. Ko, William L., and Van Tran Fleischer, *Large-Deformation Displacement Transfer Functions for Shape Predictions of Highly Flexible Slender Aerospace Structures*, NASA/TP-2013-216550, November 2013.

10. Ko, William L., and Van Tran Fleischer, *Extension of Ko Straight-Beam Displacement Theory to Deformed Shape Predictions of Slender Curved Structures*, NASA/TP-2011-214567, April 2011.

11. Kopmaz, Osman, and Omer Gundogdu, "On the Curvature of an Euler-Bernoulli Beam," *International Journal of Mechanical Engineering Education*, Vol. 31, No. 2, p. 132-142, 2004.

12. Hodges, Dewey H., "Proper Definition of Curvature in Nonlinear Beam Kinematics," *AIAA Journal*, Vol. 22, No. 12, pp. 1825-1827, December 1984.

13. Jutte, Christine, William L. Ko, Craig Stephens, John Bakalyar, Lance Richards, and Allen Parker, *Deformed Shape Calculations of a Full-Scale Wing Using Fiber Optic Strain Data from a Ground Loads Test*, NASA/TP-2011-215975, December 2011.

14. Whetstone, W. D., *SPAR Structural Analysis System Reference Manual, System Level 13A,Volume 1, Program Execution*, NASA CR-158970-1, December 1978.

15. Hodgeman, Charles D., *Standard Mathematical Tables*, 7th edition, Chemical Rubber Publishing Co. Cleveland, Ohio, 1957.